Nuclear translocation of RNA binding proteins links accelerated cytoplasmic mRNA decay and transcription

By

Sarah Gilbertson

A dissertation submitted in partial satisfaction of the

requirements for the degree of

Doctor of Philosophy

in

Molecular and Cell Biology

in the

Graduate Division

of the

University of California, Berkeley

Committee in charge:

Professor Britt Glaunsinger, Chair
Professor Laurent Coscoy
Professor Donald Rio
Professor Steven Brenner

Fall 2018

Abstract

Nuclear translocation of RNA binding proteins links accelerated cytoplasmic mRNA decay and transcription

By Sarah Gilbertson

Doctor of Philosophy in Molecular and Cell Biology

University of California, Berkeley

Professor Britt Glaunsinger, Chair

Alterations in global mRNA decay broadly impact upstream and downstream stages of gene expression, although signals that connect these processes are incompletely defined. Here, we used tandem mass tag labeling coupled with mass spectrometry to reveal that changing the mRNA decay landscape, as frequently occurs during viral infection, results in subcellular redistribution of RNA binding proteins. Accelerating Xrn1-dependent mRNA decay through expression of a gammaherpesviral endonuclease drove nuclear translocation of many RBPs, including poly(A) tail-associated proteins. Conversely, cells lacking Xrn1 exhibited changes in the localization or abundance of numerous factors linked to mRNA turnover. Using these data, we uncovered a new role for cytoplasmic poly(A) binding protein in repressing mammalian TATA-binding protein and RNA polymerase II transcription upon its mRNA decay-induced translocation to the nucleus.

We identified PABPC nuclear-specific protein-protein interactions, and found a number of interactions with proteins involved in the ubiquitin-proteasome system. Two of these protein partners were required to maintain the mRNA decay-transcription feedback pathway. Furthermore, mRNA decay initiated using the decapping enzyme, D10 from vaccinia virus, revealed that this system did not depend on the process by which the accelerated mRNA decay was initiated and instead is responsive to broad changes in mRNA abundance. In addition, we found that PABPC nuclear translocation was not affected by Dis3L2. Together with the finding that PABPC nuclear accumulation alone was not sufficient to repress nascent mRNA synthesis by RNAPII, these data provide evidence that another unknown factor is required, along with PABPC, to fulfill the feedback loop.

Collectively, our results show that changes in cytoplasmic mRNA decay can directly impact protein subcellular localization, providing a mechanism to connect seemingly distal stages of gene expression.

Dedication

This work is dedicated to my little girl.
I can’t wait to meet you in June.

Table of Contents

Acknowledgements

I could not have accomplished this work without my best friend and husband, Evan. He moved to Berkeley so I could pursue my dream of being a scientist, sacrificing his job and leaving his family in Redmond. We had an amazing five years together, just the two of us, exploring the world and drinking wine. He picked me up every day from lab so I wouldn't have to take the bus. He even came with me to lab in the middle of the night the few times I needed to do time course experiments, wanting to make sure I was safe and knowing it would help me finish my project. I only hope that I can do as much for him someday.

I am extremely fortunate to have had the opportunity to work for Britt Glaunsinger. She is the best scientist I know, and she is a shining light at Berkeley, as well as in the fields of virology and RNA biology. I have learned so much from her, both scientifically and personally, and could not have asked for a better mentor. I think it is rare to love graduate school as much as I did, and I know I have her to thank for that. She creates a lab environment where everyone learns to thrive at the bench, while also encouraging us to remain enriched in activities outside of science. She has a great sense of humor that permeates the lab. I am especially lucky to have been able to observe how she balances her life as a female scientist and a mother. It is inspiring to see her handle it all with such grace and flexibility. I can not thank her enough for giving me a chance to do my PhD work with her.

To everyone in the Glaunsinger lab, thanks for making me a better scientist. It was so much fun coming to work everyday with such a diverse and fun group of people. I especially want to thank everyone who worked on the feedback loop project with me, Emma Abernathy, Ella Hartenian, Chris Duncan-Lewis, and Michael Ly. Thank you for all of your insight and support through the ups and the downs (especially with ChIP!). Good luck to each of you and I cannot wait to see what you discover next. Thanks also to Matt Gardner who has been in the lab with me from the time I joined to the time I left. You were always the first person I came to with questions and I aspire to be a better scientist because of you. Thank you to Jennifer Blancas for being such an amazing guide in the lab. You take care of all of our needs and we are incredibly spoiled to have you by our sides. To everyone, I will especially miss all the balcony parties, monkey head nights, conferences, and happy hours with you all!

Thanks to the Coscoy Lab for all of your helpful comments in lab meetings. I did not enjoy lab meetings in any of my previous labs, but when I joined the Glaunsinger lab I realized how helpful and fun they can be. I was surprised to find that I actually relished the opportunity to share my work in round table and formal presentations. I truly looked forward to it every week.

Lastly, to all my friends in the MCB department, I can not imagine graduate school without you. Kelsey Van Dalfsen, Ella and Joe (and later Luna) Ireland, you were our family in Berkeley. Thank you for sharing your lives with us! We were so lucky to have spent so much time together for 5 years, it feels like we have been friends forever. Thank you to Rebecca Lamothe, Madeleine Jensen, and Amy Tresenrider. It was so much fun baking together and relaxing at the house on California street, I learned so much from you and I will really miss you. Good luck with the end of you PhDs, I know you will do amazing things.

Chapter 1: Introduction

Cellular mRNA decay and quality control pathways

The abundance of mRNAs in the cell at a given time is dictated by the rate of mRNA production, processing, and destruction. mRNA half lives are regulated by an abundance of RNA binding proteins and non-coding mRNAs that when bound to the mRNA, coordinate its processing, localization, translation, and decay. mRNAs are produced with a 5' 7-methylguanosine (7mG) cap, and a 3'poly(A) tail that together form a stable closed-loop structure due to interactions between the cap-binding complex and poly(A) tail binding proteins (PABPs). This closed-loop structure not only protects the mRNA ends from exonuclease degradation, it also serves to efficiently recruit translational machinery.

At the end of the translational life of the mRNA, degradation begins with shortening of the poly(A) tail, a process called deadenylation. Deadenylation occurs in two phases and is initiated by the Pan2/Pan3 complex, a non-processive enzyme that slowly shortens the tail by 12-25 adenosine increments (Wolf and Passmore, 2014). The slow progression of Pan2/Pan3 ultimately prevents PABP association with the shortened poly(A) tail, disrupting the mRNA closed-loop structure. This is followed by a second more processive phase in which the Ccr4/Not complex removes the remaining length of tail (Chen and Shyu, 2011; Stubbs and Wahle, 2014). Shortened mRNAs with adenosine extensions serve as a binding site for the Lsm1-7/Pat1 complex, which recruits the decapping complex Dcp1/2, stimulating cap-hydrolysis. Together, this generates an mRNA that is unprotected at both ends. Highly processive cellular exonucleases bind the unprotected mRNA ends and rapidly degrade the mRNA. This occurs primarily in the 5'-3' direction by Xrn1, but also in the 3'-5' direction by the cytoplasmic exosome, or Dis3L2 (Lubas et al., 2013; Schoenberg and Maquat, 2012).

Basal mRNA decay is circumvented by quality control pathways which serve to maintain transcriptome fidelity and clear aberrant transcripts. In contrast to the slow, regulated process of basal mRNA decay, these pathways release the closed-loop structure through endonucleolytic cleavage and exposure of unprotected mRNA ends. Quality control pathways include non-sense mediated mRNA decay (NMD), which recognizes pre-mature termination codons (PTC), no-go decay (NGD) which resolves stalled ribosomes, and nonstop decay (NSD) which recognizes mRNAs without a termination codon (Łabno et al., 2016; Shoemaker and Green, 2012). Central to each of these pathways is the corresponding endonuclease, which bypasses the regulated, rate-limiting deadenylation step of basal decay, allowing rapid removal of faulty transcripts by exonuclease degradation. For example, in the NMD pathway, a transcript containing an in-frame PTC upstream of the canonical stop codon is bound by the UPF1 protein. UPF1 binding leads to translational repression and degradation of the transcript. The mRNA endonuclease SMG6 is recruited to the site of the PTC where it cleaves the mRNA, leading to rapid degradation of the mRNA fragments by the same cellular exonucleases involved in basal mRNA decay, Xrn1, Dis3L2, and the exosome (Lykke-Andersen et al., 2014). Other quality control pathways also make use of endonucleolytic cleavage to remove transcript errors or mRNAs with stalled ribosomes much more rapidly than could be done with basal mRNA decay.

Viruses manipulate host mRNA decay pathways

Viruses are skilled at co-opting host machinery during infection in order to disrupt cellular gene expression and subvert resources for viral replication. Every step in the cellular gene expression cascade is vulnerable to exploitation by viruses, yet some steps are more vulnerable than others. Not surprisingly, there are many examples of viral manipulation of the cellular mRNA decay pathway, and the subsequent viral induced accelerated mRNA decay is called 'host shutoff'. Diverse viruses, including the DNA viruses alpha and gammaherpesviruses, and poxviruses, as well as the RNA viruses influenza A virus and SARS coronavirus, have all evolved similar mechanisms that are reminiscent of cellular quality control pathways. They bypass the slow, regulated deadenylation step through endonucleolytic cleavage leading to rapid degradation by cellular exonucleases. Despite using unique mechanisms of mRNA recognition, each viral protein targets a majority of cellular transcripts for destruction allowing the virus to efficiently dampen host translation.

The alphaherpesvirus herpes simplex virus 1 (HSV-1) encodes an mRNA endonuclease called virion host shutoff protein (vhs). Packaged and released directly from the virion, vhs is immediately recruited to mRNAs through interactions with the translation initiation factor eIF4F and cleaves mRNAs at unstructured sites within the 5'UTR (Feng et al., 2005; Page and Read, 2010). Gammaherpesviruses also encode an mRNA endonuclease called SOX in Kaposi's sarcoma-associated herpesvirus (KSHV), BGLF5 in Epstein-Barr virus (EBV), and muSOX in murine gammaherpesvirus 68 (MHV68) (Covarrubias et al., 2009). This protein is a member of the PD-(D/E)XK type II restriction endonuclease superfamily, and has evolved mechanistically separable DNase and RNase activities. The RNase activity is specific for translationally competent mRNAs, although active translation is not a requirement, and it cleaves mRNAs at a sequence- and structure- specific RNA element (Gaglia et al., 2015; Mendez et al., 2018). Like vhs, SOX, BGLF5, and muSOX all create unprotected mRNA fragments that are degraded by cellular exonucleases.

Another more divergent DNA virus, vaccinia virus (VACV) from the Poxvirus family, encodes two decapping endonucleases, D9 and D10, that are similar to cellular decapping enzymes (Parrish and Moss, 2007; Parrish et al., 2007). Both D9 and D10 contain a Nudix hydrolase domain that is essential for cleaving the 7mG cap. However, D9 and D10 have different functional requirements related to the length of the RNA substrate, and are thought to be required for different kinetic phases of the viral lifecycle. Removal of the cap leaves the 5' end unprotected, and like the herpesvirus endonucleases, results in degradation of the transcript by Xrn1.

RNA viruses have converged on similar mechanisms of manipulating the cellular mRNA decay machinery. Influenza A virus (IAV) expresses an mRNA endonuclease called PA-X through a ribosomal frameshifting event in the translation of the PA subunit of the viral RNA-dependent RNA polymerase (RdRp) (Khaperskyy et al., 2014; Khaperskyy et al., 2016). PA has an N-terminal endonuclease domain responsible for cap-snatching in the nucleus. PA-X retains the endonuclease domain, but has a unique C-terminal domain termed X-ORF that is important for host shutoff activity. PA-X cleaves mRNAs internally and appears to do so anywhere along the transcript. Cleavage may be coupled to 3'end processing of mRNAs in the nucleus and therefore IAV host shutoff is not linked to translation like it is for the DNA viruses (Khaperskyy

et al., 2016). This provides a mechanism for specificity to RNAPII transcripts, as the processing machinery is not shared among RNA polymerase I or III. In fact, IAV viral mRNAs are not targeted by PA-X, as they are transcribed by the viral RdRp which does not use the same processing machinery as RNAPII. As might be expected from viral mRNA escape, PA-X catalytic mutants have reduced viral protein expression (Rivas et al., 2016). Like the DNA virus examples of host shutoff, however, degradation of host transcripts following PA-X cleavage was found to be completed by Xrn1 (Khaperskyy et al., 2016).

Finally, SARS coronavirus (SARS-CoV), a large positive-sense RNA virus, expresses a viral protein called Nsp1 that when expressed binds to the 40S ribosomal subunit, leading to cleavage of the mRNA as well as inactivation of the ribosome (Huang et al., 2011). As Nsp1 is specific for the 40S ribosome, it results in cleavage of all translationally competent mRNAs for broad cellular repression. However, Nsp1 does not contain nuclease activity and it is thought that it instead activates cleavage of mRNAs through an unknown cellular mRNA surveillance pathway. Like all the viral endonucleases and decapping factors, Nsp1-induced cleavage fragments are fully degraded by Xrn1 (Gaglia et al., 2012).

Importantly, expression of viral mRNAs from all DNA viruses is dependent on host RNA polymerase II (RNAPII). Therefore, viral transcripts are structurally identical to host transcripts and are susceptible to cleavage by the viral host shutoff factors. Despite this seemingly contradictory aspect of host shutoff, gammaherpesviral mutants that lack RNase activity show altered expression of viral proteins and a defect in the establishment of latency *in vivo* (Abernathy et al., 2014; Richner et al., 2011). This supports the model that host shutoff does benefit the virus, although it was unclear how.

Downstream consequences of host shutoff

In addition to decreased translation of host messages, there are other far reaching consequences of host shutoff for the cell. mRNAs that are cleaved during host shutoff are bound at the 3'end by cytoplasmic poly(A) binding protein (PABPC). PABPC normally contributes to mRNA stability and translation by maintaining the stable closed-loop structure of mRNAs (Burgess and Gray, 2010). Following exonucleolytic degradation of mRNAs during host shutoff, PABPC is released from the poly(A) tail, uncovering a noncanonical nuclear localization signal (NLS) previously hidden within its RNA recognition motifs (RRMs). PABPC uses the unmasked NLS motif to interact directly with nuclear import machinery, causing a majority of PABPC to be relocalized to the nucleus (Kumar et al., 2011). This has been shown to occur during expression of SOX, muSOX, BGLF5, vhs, PA-X, and nsp1, suggesting that the mechanism by which accelerated mRNA decay is initiated is inconsequential for PABPC nuclear relocalization (Arias et al., 2009; Khaperskyy et al., 2014; (Kumar and Glaunsinger, 2010; Lee and Glaunsinger, 2009; Park et al., 2014).

Nuclear translocation of PABPC leads to further restriction of gene expression following host shutoff. Nascent mRNAs become aberrantly hyperadenylated by poly(A) polymerase II (PAPII). These hyperadenylated mRNAs are then retained in the nucleus, preventing access to the translational machinery in the cytoplasm (Kumar and Glaunsinger, 2010; Lee and Glaunsinger, 2009). It remains unclear how viral messages are able to escape this PABPC-induced mRNA export block as they are able to be efficiently translated and expressed.

In addition to PABPC nuclear accumulation and mRNA hyperadenylation, accelerated cytoplasmic mRNA decay was also shown to lead to repression of RNAPII transcription (Abernathy et al., 2015). RNAPII occupancy at promoters and production of nascent mRNAs was reduced during infection with the gammaherpesviruses KSHV and MHV68 in a manner that was dependent on host shutoff. This transcriptional repression also occurred during expression of the viral endonucleases alone and was the first characterized example of a connection between mRNA decay and transcription in mammalian cells. The repression of RNAPII promoter occupancy was dependent on the activity of the cellular exonucleases Xrn1 and Dis3L2. Knockdown of either of these exonucleases during muSOX expression was sufficient to restore RNAPII occupancy. This suggested that the initial cleavage and ensuing translational repression of the mRNA was not sufficient to trigger transcriptional repression, and that the full degradation of the cleaved transcripts was critical. Importantly, the virus was able to maintain efficient transcription of the viral genome, despite its dependence on cellular RNAPII. Therefore, the virus benefits from repression of host transcription and is able to outcompete cellular messages for the translational machinery.

Interestingly, a previous example of an mRNA decay-transcription feedback loop had been described in yeast (Haimovich et al., 2013; Sun et al., 2013). Here, a decrease in the rate of cytoplasmic mRNA decay led to a similar decrease mRNA synthesis in the nucleus. In this way, these cells maintain an optimal level of total cellular mRNA, and use the connection between mRNA synthesis and decay to protect the cell from changes to either arm of the pathway. Though it operated in a different direction than the mammalian pathway, the yeast system also depended on Xrn1, suggesting that this factor is particularly important for both feedback pathways. However, in both yeast and mammalian cells, the mechanism(s) by which these cytoplasmic and nuclear events are connected were unknown.

Dissertation overview

The work presented in this dissertation aims to characterize the nature of the link between cytoplasmic mRNA decay and transcription. There is a focus on mRNA decay induced by the gammaherpesviral endonuclease muSOX outside of the context of infection. This is augmented by additional work examining diverse viral endonucleases and decapping enzymes, and is extended further to include infection with MHV68.

It is revealed that in addition to PABPC, many RNA binding proteins are enriched in the nucleus during accelerated cytoplasmic mRNA decay in an Xrn1-dependent manner. Proteins that bind the 3'end of mRNAs are preferentially enriched in the nucleus, conveying mRNA abundance information between the two compartements, including poly(A) and poly(U) binding proteins. We reveal that PABPC is crucial for the feedback loop, and nuclear accumulation of PABPC alone mimics repression of RNAPII promoter occupancy. Promoter recruitment of TATA-binding protein is disrupted and explains the decrease in RNAPII at the promoter, and the concomitant decrease in gene bodies, and further elucidates the nature of the transcriptional repression. We also began identifying the mechanism of transcriptional repression by nuclear PABPC. Nuclear PABPC makes a number of interactions with protein partners involved in the ubiquitin-specific proteasome system. Two proteins, the makorin E3 ubiquitin ligases MKRN1 and MKRN2, are required for the repression of RNAPII promoter recruitment.

The complexities of the mechanism by which nuclear PABPC represses RNAPII are highlighted in Chapter 4. Data presented in the first half of this work suggests that nuclear enrichment of PABPC alone is necessary and sufficient for repression of RNAPII. However, it remained unclear how PABPC movement could be linked to degradation of cleaved mRNAs by the 3'-5' exonuclease Dis3L2, which presumably does not cause release of PABPC from poly(A) tails. Work in Chapter 4 reveals that Dis3L2 activity was dispensable for repression of RNAPII during D10-mediated mRNA decay. These decapped mRNAs are degraded by Xrn1 in the 5'-3' direction without the need of Dis3L2. This led to the conclusion that Dis3L2 may only be required during muSOX-mediated mRNA decay because two fragments are made, which both require degradation. Furthermore, depletion of Dis3L2 did not alter PABPC nuclear translocation during muSOX expression. This suggests that PABPC still translocates to the nucleus, yet RNAPII promoter occupancy is not repressed. This was the first example of nuclear PABPC enrichment without RNAPII repression, and opened the possibility that another factor may be required for this pathway. While this seemed contradictory to evidence from Chapter 2 that artificial enrichment of PABPC in the nucleus alone can recapitulate the effects of accelerated mRNA decay, the nuclear levels of PABPC when overexpressed were much higher than the amount of endogenous PABPC enriched in the nucleus by muSOX. Surprisingly, artificial enrichment of PABPC in the nucleus was unable to recapitulate repression of mRNA synthesis by RNAPII despite the observed reduction in RNAPII promoter occupancy. It may be that these higher nuclear levels of PABPC overcome the need for other factors that may be required for this pathway, and force repression of RNAPII promoter recruitment without complete repression of transcription. Therefore, we present a model in which accelerated cytoplasmic mRNA decay drives nuclear translocation of PABPC and an unknown factor bound to mRNA 5'ends. In the nucleus, these factors together repress RNAPII promoter occupancy as well as transcriptional output.

Chapter 2: Changes in mRNA abundance drive shuttling of RNA binding proteins, linking cytoplasmic RNA degradation to transcription

Introduction

mRNA decay is a critical stage of gene expression that regulates the abundance and lifespan of cellular mRNAs. Many viruses including alpha and gammaherpesviruses, influenza A virus, and SARS coronavirus accelerate host mRNA degradation through the use of viral proteins that trigger endonucleolytic cleavage of mRNAs in the cytoplasm. Each of these viral proteins bypasses the rate-limiting deadenylation step of the basal decay pathway, resulting in cleaved mRNAs that are rapidly degraded by the major cellular 5'-3' exonuclease Xrn1 (Covarrubias et al., 2011; Gaglia et al., 2012). This process, termed 'host shutoff', allows viruses to rapidly restrict cellular gene expression in order to blunt immune responses and liberate resources for viral replication (Abernathy and Glaunsinger, 2015; Burgess and Mohr, 2015; Gaglia and Glaunsinger, 2010; Rivas et al., 2016). Viral endonucleases have also served as tools for deciphering how cells sense and respond to large changes in mRNA abundance.

While mRNA decay is often considered the terminal stage of gene expression, the rate of mRNA decay has recently been shown to influence transcription by RNA polymerase II

(RNAPII) in both yeast and mammalian cells (Abernathy and Glaunsinger, 2015; Braun and Young, 2014; Haimovich et al., 2013; Sun et al., 2013). In yeast, a buffering system exists in which Xrn1 plays a major role in connecting mRNA synthesis and decay, presumably allowing cells to maintain an appropriate overall mRNA abundance. Mammalian cells also have a mechanism to sense mRNA levels, though the pathway appears to operate differently than in yeast. Here, accelerated cytoplasmic mRNA degradation does not lead to a compensatory increase in mRNA synthesis, as might be predicted by the homeostatic model, but instead decreases cellular RNAPII promoter recruitment, thereby amplifying the restrictive gene expression environment (Abernathy et al., 2015). Significant transcriptional repression as measured by nascent mRNA production was reported to occur at approximately 9% of host genes, although validation experiments suggested this number is likely to be an underestimate (Abernathy et al., 2015).

The mRNA decay-transcription feedback pathway is activated in mammalian cells infected with gammaherpesviruses like Kaposi's sarcoma-associated herpesvirus (KSHV) and murine gammaherpesvirus 68 (MHV68), as well as upon expression of virally encoded mRNA endonucleases in uninfected cells. Herpesviral endonucleases, including the muSOX protein of MHV68, cleave mRNA but do not impact the abundance of noncoding RNAs transcribed by RNA polymerase I (RNAPI) or III (RNAPIII) (Covarrubias et al., 2011). Correspondingly, muSOX-induced mRNA decay elicits a significant decrease in RNA polymerase II (RNAPII) recruitment to cellular promoters (Abernathy et al., 2015). Notably, depletion of Xrn1 from muSOX-expressing cells prevents the ensuing RNAPII transcriptional repression. This suggests that the initial mRNA cleavage and translational inactivation are insufficient to restrict RNAPII recruitment, and that subsequent exonucleolytic degradation of the cleaved mRNA fragments is a critical signaling step.

Little is currently known about this pathway linking cytoplasmic mRNA decay to RNAPII activity in mammalian cells, including the nature of the signal that is transmitted between the two cellular compartments. An attractive hypothesis is that one or more RNA binding proteins (RBPs) differentially traffics between the cytoplasm and the nucleus when basal rates of mRNA decay are perturbed, thereby conveying global mRNA abundance information. Recent analyses indicate that mammalian cells contain hundreds of RBPs that bind polyadenylated mature mRNAs, and proteins within this group have been shown to regulate all stages of gene expression (Gerstberger et al., 2014; Mitchell and Parker, 2014; Müller-McNicoll and Neugebauer, 2013; Singh et al., 2015). Furthermore, RBPs frequently display nucleocytoplasmic shuttling behavior.

Here, we charted global alterations in protein localization that occur specifically in response to increased or decreased Xrn1 activity. This revealed a set of mammalian RBPs that preferentially move from the cytoplasm to the nucleus during accelerated mRNA decay, as well as components of the 5'-3' decay machinery and other RBPs whose subcellular distribution is altered in cells lacking Xrn1. Poly(A) tail associated proteins are overrepresented among the RBPs that accumulate in the nucleus under conditions of global mRNA decay, offering an explanation for how RNAPII could be selectively sensitive to mRNA abundance. Indeed, we uncovered a new role for cytoplasmic poly(A) binding protein (PABPC) in mediating mRNA decay-driven repression of RNAPII promoter recruitment. Furthermore, we show that the recruitment of TATA binding protein (TBP) to promoters is also impaired in response to PABPC nuclear translocation, indicating that cytoplasmic mRNA decay impacts early events in preinitiation complex assembly. Our results reveal how mRNA levels exert significant influence

on RBP localization and suggest that select RBPs transmit mRNA abundance information from the cytoplasm to the nucleus to broadly influence gene expression, particularly under conditions of cellular stress.

Results

RNA binding proteins translocate from the cytoplasm to the nucleus in cells undergoing enhanced cytoplasmic mRNA decay.

To chart mRNA decay-driven movement of proteins between the cytoplasm and the nucleus, we used a quantitative liquid chromatography/tandem mass spectrometry (LC/MS-MS)-based approach. Specifically, following subcellular fractionation, proteins from nuclear and cytoplasmic fractions were labeled with isobaric tandem mass tags (TMT). TMT labeling enables multiplexing of up to 11 samples per run and was proven to improve the analytical power for quantitation during viral infections (Beltran et al., 2016; McAlister et al., 2012). We used HEK293T cells expressing the MHV68 muSOX endonuclease to create a condition of accelerated, Xrn1-dependent cytoplasmic mRNA decay. We previously demonstrated that muSOX expression in these cells activates the mRNA decay-RNAPII transcription feedback pathway similar to virally infected fibroblasts (Abernathy et al., 2015). Pure populations of cells expressing either WT muSOX or the catalytically dead D219A muSOX point mutant were generated using Thy1.1-based cell sorting. Here, muSOX was fused to the cell surface glycoprotein Thy1.1 with an intervening self-cleaving 2A protease, causing release of Thy1.1 from muSOX for cell surface expression and selection. Three biological replicates of control, WT, and D219A muSOX expressing cells were then separated into nuclear and cytoplasmic fractions, and trypsin-digested proteins from each fraction were differentially TMT labeled prior to LC/MS-MS (**Figure 2.1A**). Among the 5,994 total quantifiable nuclear proteins (detected in all replicates), 123 displayed significant nuclear enrichment (adjusted P value of ≤ 0.05) in WT muSOX expressing cells relative to the D219A mutant (**Figure 2.1B**). We then removed from further analysis proteins that were simultaneously increased in the cytoplasm in muSOX expressing cells to remove proteins that increase in overall abundance, as well as proteins displaying significant differences between the D219A catalytic mutant and the empty vector control. These filtering steps yielded a final list of 67 proteins that were differentially enriched in the nucleus under conditions of accelerated mRNA decay (**Figure 2.1B, Table 2.12**). Notably, 22 of the 67 proteins (33%) are annotated as RBPs (Pantherdb) in line with the expectation that mRNA-bound proteins in particular should be impacted during widespread mRNA degradation. In addition, 31 of the 67 proteins (46%) are listed as localized both to the cytoplasm and nucleus according to the Database for Annotation, Visualization and Integrated Discovery (DAVID), supporting the idea that they are shuttling factors. As an independent validation of these results, we evaluated 12 of the top hits by western blotting of fractionated cell lysates in control or muSOX-expressing cells, 10 of which recapitulated the MS results (**Figure 2.1C**).

Proteins associated with the poly(A) tail display robust mRNA decay-dependent nuclear translocation.

The poly(A) tail is a defining mRNA feature and during basal mRNA decay, deadenylation is the initiating step that licenses subsequent decapping and exonucleolytic degradation of an mRNA (Schoenberg and Maquat, 2012). Thus, the binding state of poly(A) tail associated proteins could

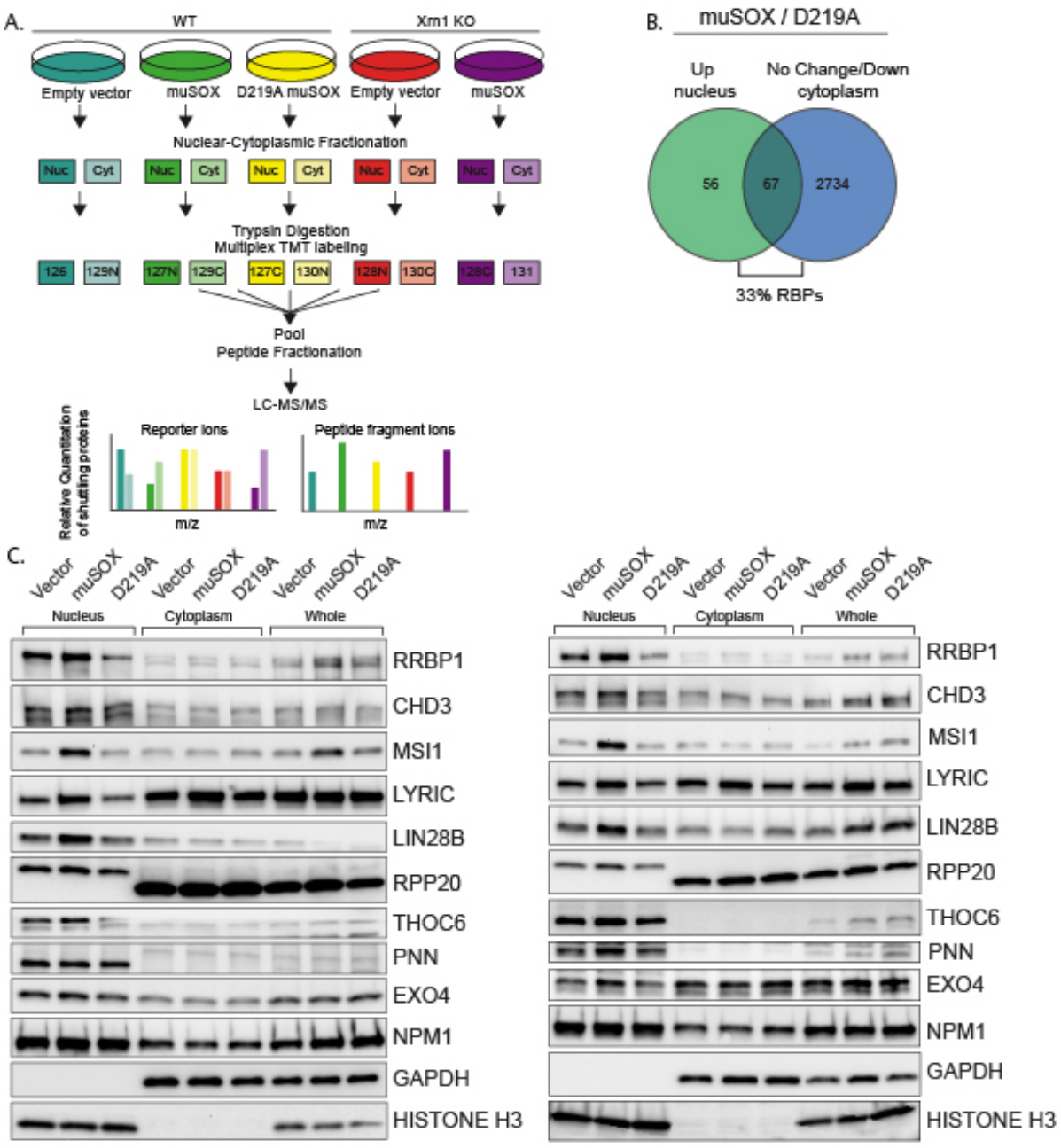

Figure 2.1. RNA binding proteins are translocated from the cytoplasm to the nucleus in cells undergoing enhanced cytoplasmic mRNA decay. (A) Diagram depicting the experimental setup. (B) Venn diagram of nuclear proteins that are specifically and significantly ($p < 0.05$) enriched in muSOX-expressing cells compared to D219A-expressing cells that also show either no change or a decrease in cytoplasmic abundance. (C) Western blots of nuclear, cytoplasmic, and whole cell fractions of HEK293T cells transfected with either empty vector control, WT muSOX, or D219A muSOX. Shown are two independent biological replicates. GAPDH and histone H3 serve as fractionation and loading controls.

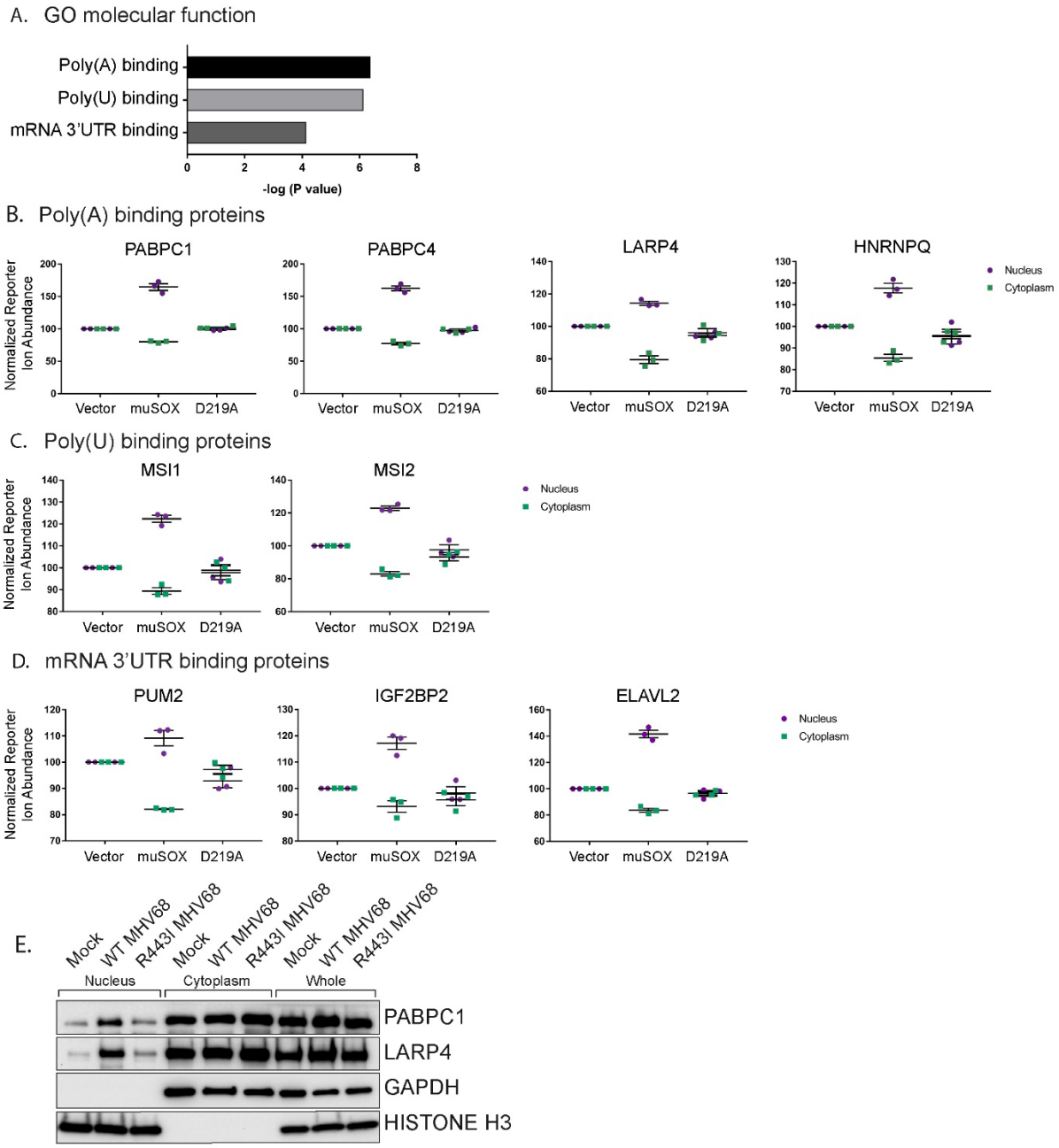

Figure 2.2. Poly(A), Poly(U), and mRNA 3'UTR binding proteins are enriched in the set of translocated proteins. (A) Gene ontology molecular function overrepresentation analysis by Pantherdb, graphed according to their P value. (B-D) Graphs showing the nuclear and cytoplasmic distribution of poly(A) binding proteins (B), poly(U) binding proteins (C), mRNA 3'UTR binding proteins (D) from the TMT-MS/MS data. Graphs display the mean with SEM of 3 biological replicates. (E) Western blot of nuclear, cytoplasmic, and whole cell fractions of NIH3T3 fibroblasts mock infected or infected with WT or R443I MHV68 for 24h. GAPDH and histone H3 serve as fractionation and loading controls. Shown is a representative example of 3 biological replicates.

theoretically serve as a readout to distinguish the overall abundance of mRNA over other forms of RNA in the cytoplasm. Notably, nuclear relocalization of PABPC has been observed during

infection with multiple viruses that promote mRNA decay, supporting the idea that poly(A) tail associated proteins may be particularly sensitive to mRNA abundance (Harb et al., 2008; Lee and Glaunsinger, 2009; Park et al., 2014; Piron et al., 1998; Salaun et al., 2010). Indeed, an overrepresentation analysis using Pantherdb revealed that poly(A) binding proteins, poly(U) binding proteins, and mRNA 3'UTR binding proteins were significantly overrepresented among the 67 differentially expressed proteins (**Figure 2.2A-D**). Proteins linked to the poly(A) tail consistently arose as robust hits in our MS dataset, including PABPC proteins 1 and 4 (PABPC1, PABPC4), LA-related protein 4 (LARP4), and heterogeneous nuclear ribonucleoprotein Q (HNRNPQ) (**Table 2.12**, **Figure 2.2B**). We confirmed that PABPC1 and LARP4 also translocate to the nucleus in NIH3T3 cells infected with WT MHV68, but not in cells infected with an MHV68 muSOX mutant virus (R443I) with impaired mRNA cleavage activity (Adler et al., 2000; Richner et al., 2011) (**Figure 2.2E**). Thus, poly(A) associated proteins preferentially move from the cytoplasm to the nucleus in response to muSOX-activated mRNA decay in both transiently transfected and virally infected cells.

Nuclear translocation of RNA binding proteins is dependent on mRNA degradation by Xrn1.

Xrn1 is the major 5'-3' exonuclease in mammalian cells and is responsible for the degradation of 3' RNA fragments generated upon cleavage by muSOX (Gaglia et al., 2012). In the absence of Xrn1, muSOX-induced repression of RNAPII promoter occupancy does not occur, suggesting that Xrn1 activity should be required for release and subsequent nuclear translocation of RBPs involved in this phenotype (Abernathy et al., 2015). We therefore used Cas9-based genome editing to generate Xrn1 knockout clones in HEK293T cells and confirmed that muSOX expression in these cells failed to reduce RNAPII promoter occupancy (**Figure 2.3-A-B**). The Xrn1 knockout cells exhibited a ~2-fold reduction in growth compared to control Cas9-expressing WT cells (**Figure 2.3C**), in line with observations in yeast (Larimer and Stevens, 1990). Importantly, this did not lead to broad changes in gene expression (see below). Given that Xrn1 is a central component of the mammalian mRNA decay machinery, only low passage versions of these cells were used to decrease the likelihood of compensatory changes occurring in other decay components. Using the same TMT-LC/MS-MS strategy described above, we analyzed nuclear and cytoplasmic fractions from 3 biological replicates of Xrn1 knockout cells expressing muSOX or an empty vector control (**Figure 2.1A**). Comparison of these data to the list of proteins from Table 2.12 indicated that 45 of the 67 hits failed to shuttle in muSOX-expressing Xrn1 knockout cells, confirming that our workflow identified factors that differentially shuttle in response to mRNA degradation (**Figure 2.3D, E**). Poly(A) tail degradation is normally carried out by deadenylases prior to activation of Xrn1-mediated decay from the 5' end, but we previously demonstrated that SOX-cleaved mRNAs are not deadenylated prior to their targeting by Xrn1 (Covarrubias et al., 2011). Indeed, analysis of endogenous PABPC1 and LARP4 localization by confocal microscopy and western blot analysis of fractionated cells confirmed that both proteins translocated from the cytoplasm to the nucleus upon muSOX expression in WT but not Xrn1 knockout cells (**Figure 2.4A, B**).

Xrn1 knockout leads to subcellular redistribution of proteins functionally associated with RNA.

Given that increased Xrn1 activity caused nuclear translocation of mRNA-associated RBPs, we hypothesized that RBPs linked to Xrn1 function might also exhibit altered subcedistribution in cells lacking Xrn1. We first looked broadly for proteins with reproducibly altered abundance in the nucleus or the cytoplasm of Xrn1 knockout cells relative to the vector control cells. There were 149 and 158 proteins differentially expressed in the absence of Xrn1 in the nucleus or cytoplasm, respectively (adjusted P value ≤ 0.05) (**Figure 2.5A, Table 2.13**). Both the oligosaccharyltransferase (OST) complex and RBPs were significantly overrepresented among the set of differentially expressed proteins in each compartment (**Figure 2.5A, B**). The significance of the OST enrichment is currently unknown, although the OST complex has been shown to be critical for infection with flaviviruses, which depend on Xrn1 for the production of a subgenomic viral noncoding RNA (Chapman et al., 2014; Moon et al., 2012). However, the RBP enrichment is in line with Xrn1 function, and it is notable that among the proteins significantly enriched in the nucleus of Xrn1 KO cells were factors that encompass the first steps of 5'-3' mRNA decay. These included all members of the decapping complex (DCP1A, DCP1B and DCP2), factors that promote decapping complex formation (EDC3 and EDC4), and a protein that connects the decapping complex to the deadenylation machinery (PATL1) (**Figure 2.5C**).

We next examined whether the absence of Xrn1 also impacted the relative abundance of its known interaction partners (as listed in the BioGRID database) in the two compartments (**Figure 2.6A**). This did not appear to be the case in the TMT data, as the majority of known Xrn1 protein partners were expressed at normal levels in the absence of Xrn1. However, there was a significant increase in the cytoplasmic levels of UPF1, a mediator of nonsense mediated mRNA decay (NMD). Similarly, DNASE2, a nuclease which contributes to the degradation of DNA in dying cells, had increased cytoplasmic abundance. Secernin-2 (SCRN2), a protein involved in exocytosis, translocated to the nucleus in the absence of Xrn1. Conversely, PABPC4 levels were decreased in both compartments, and two centrosomal proteins CEP152 and CEP128 were reduced in the nucleus.Finally, we considered the possibility that upon loss of Xrn1, cells might upregulate other components of the mRNA decay machinery. Perhaps surprisingly, out of all 5,994 detected proteins, only three were significantly upregulated in both the nucleus and the cytoplasm of Xrn1 knockout cells: GW182, Galectin-3, and BAG1. Among these, GW182 stands out because it is a member of the miRNA-induced silencing complex (miRISC) involved in recruitment of deadenylases to initiate degradation of target mRNAs (**Figure 2.6B**). This increase in GW182 abundance, along with the changes to DCP2, DDX6, and PABPC4, were independently validated by western blot analysis (**Figure 2.6C**). To determine whether the increases in the whole cell protein abundance of GW182 and in the nuclear protein abundance in DDX6 and PATL1 occurred at the mRNA level or were a result of translational regulation, we measured steady-state mRNA expression for each of these factors by RT-qPCR. In each case, the mRNA abundance was increased in Xrn1 knockout cells compared to WT cells (**Figure 2.6D**). Importantly, the increases appeared specific to these transcripts and not due to generalized mRNA abundance changes in the absence of Xrn1, as there was no significant difference in *gapdh* or *actB* mRNA levels (**Figure 2.6D**). Collectively, these data suggest that there are not broad increases in cellular proteins in response to inhibition of 5'-3' mRNA decay. However, there appear to be selective increases in the whole cell or compartment-specific abundance of

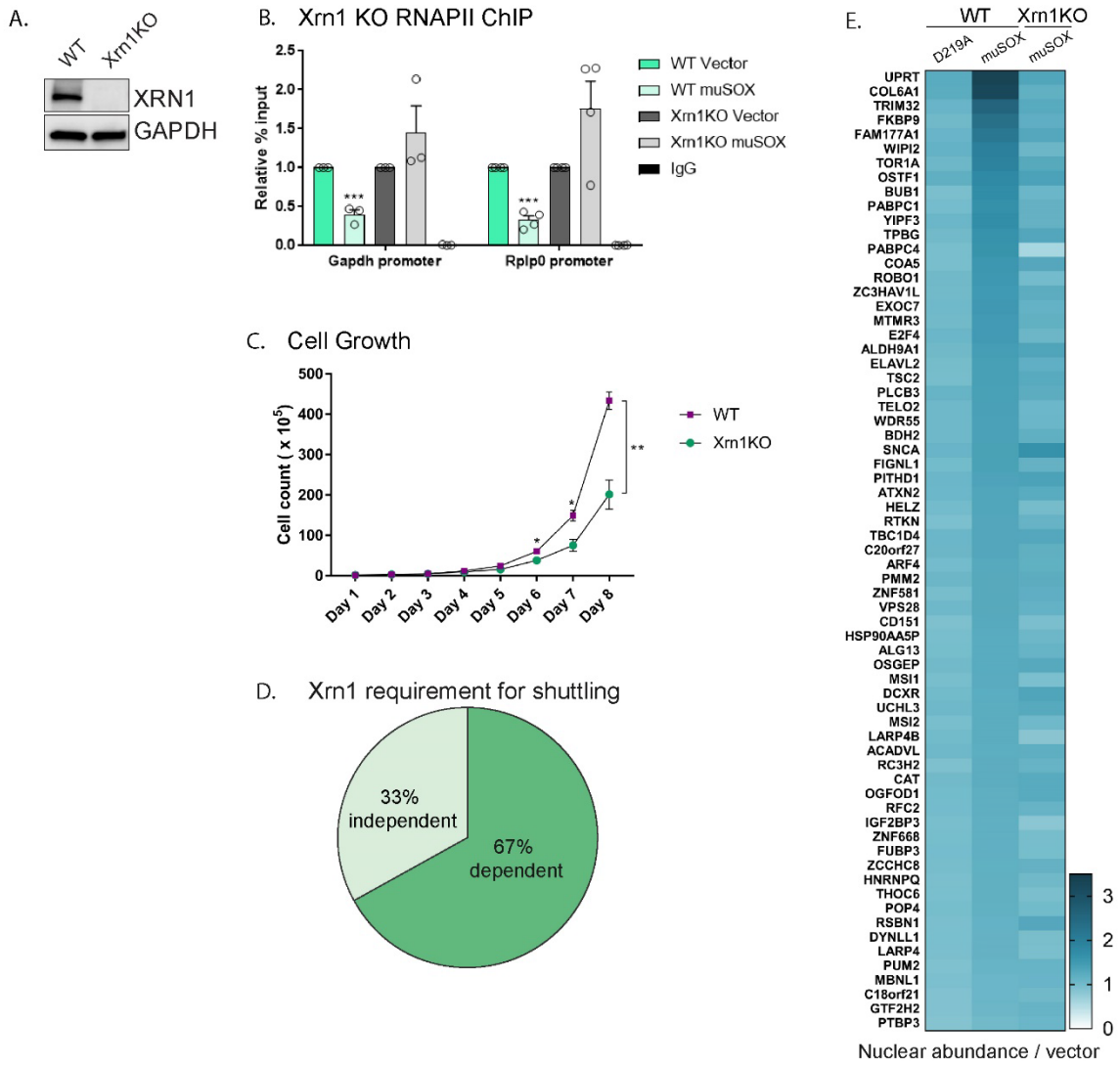

Figure 2.3. Nuclear translocation of RNA binding proteins is dependent on mRNA degradation by Xrn1. (A) Western blots showing the levels of Xrn1 or the GAPDH loading control in WT or Xrn1 KO HEK293T cells. (B) WT or Xrn1 KO HEK293T cells transfected with either empty vector or muSOX were subjected to ChIP using antibodies to RNAPII or IgG. Purified chromatin was quantified by qPCR. Graph displays individual biological replicates as dots, with the mean and SEM. Statistical significance was determined using Student's t test *p <0.05 **p <0.005 ***p <0.0005. (C) Growth curve of WT or Xrn1 KO HEK293T cells. Statistical significance was determined using Student's t test *p <0.05 **p <0.005 ***p <0.0005 (D) Pie chart showing the percent of shuttling proteins that fail to translocate in Xrn1 KO cells. (E) Heat map depicting the average nuclear abundance in WT or Xrn1 KO HEK293T cells of the 67 significantly shifted proteins in samples expressing muSOX or D219A, relative to the empty vector control.

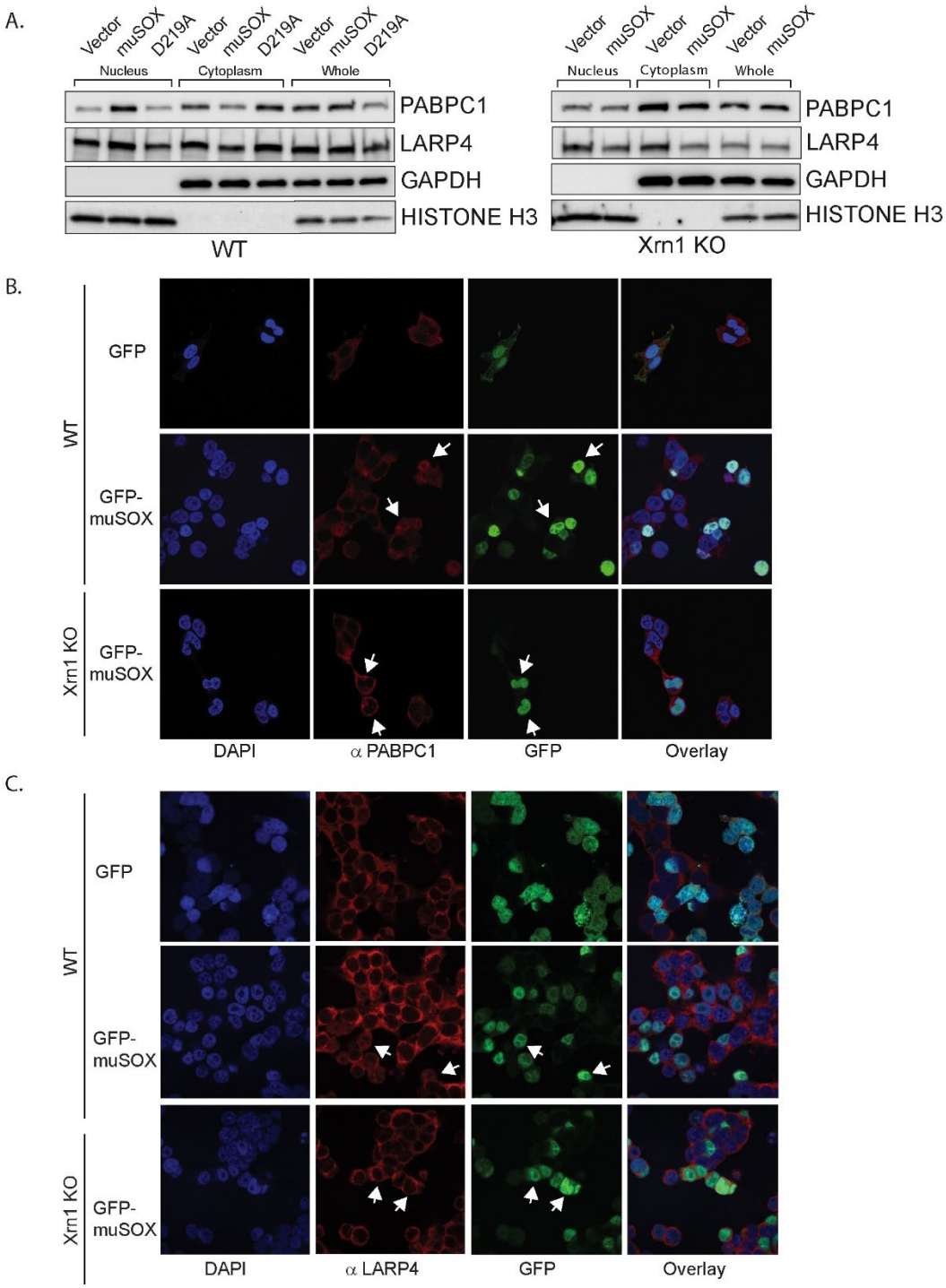

Figure 2.4. Nuclear translocation of PABPC and LARP4 is dependent on mRNA degradation by Xrn1. (A) Western blots of nuclear, cytoplasmic, and whole cell fractions of WT (left panel) or Xrn1 KO (right panel) HEK293T cells transfected with the indicated plasmid. GAPDH and histone H3 serve as fractionation and loading controls. (B, C) Confocal microscopy of WT or Xrn1 KO HEK293T cells transfected with GFP or GFP-muSOX, showing signals for DAPI stained nuclei (blue), PABPC (red, B), LARP4 (red, C), GFP (green), and the merged images (overlay). Arrow heads point to representative GFP-muSOX expressing cells.

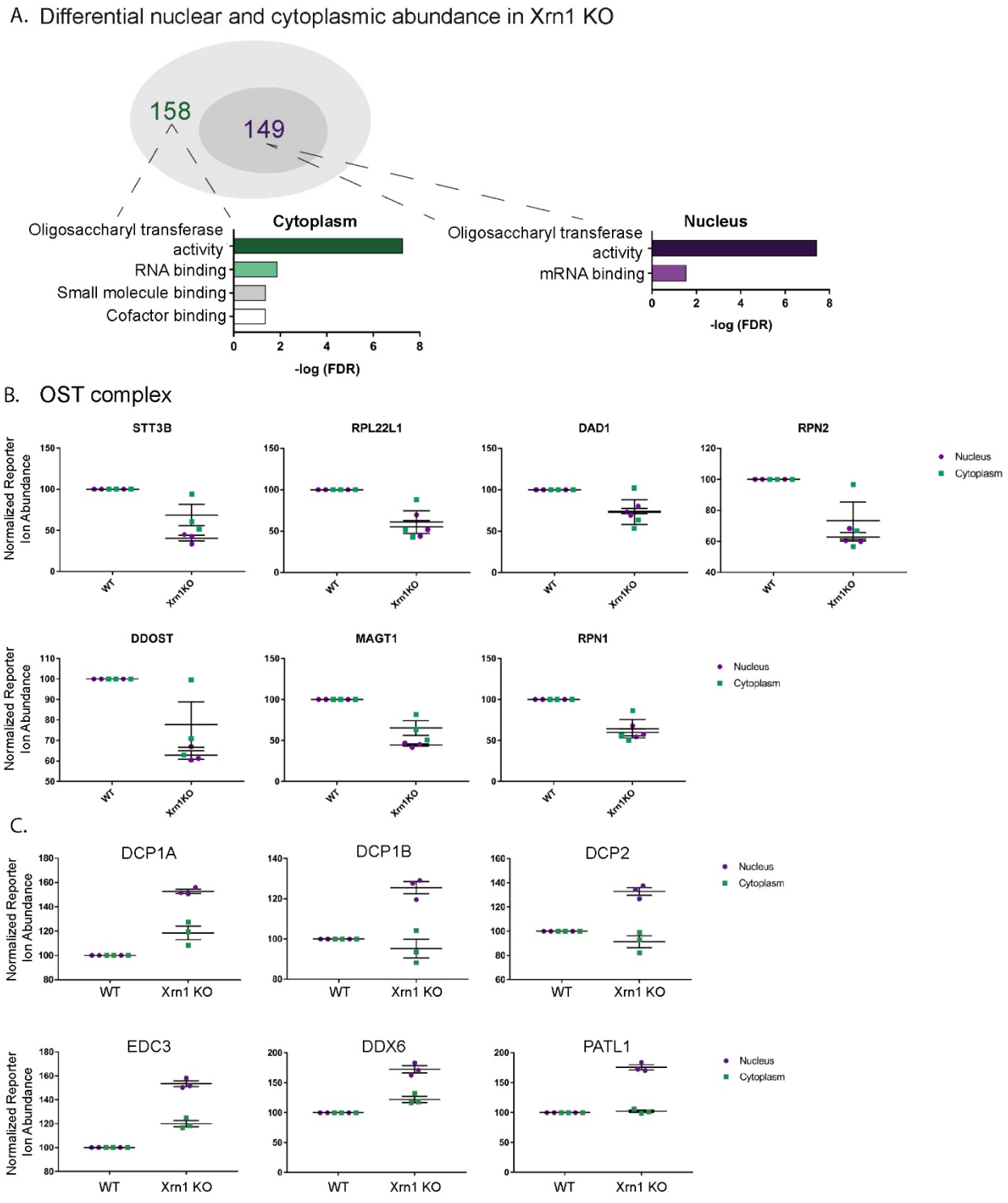

Figure 2.5. Xrn1 knockout leads to subcellular redistribution of the OST complex and mRNA decapping-related proteins. (A) The number of proteins that are differentially expressed in Xrn1 knockout (KO) cells from the nucleus (149) and the cytoplasm (158). Gene ontology molecular function overrepresentation analysis by Pantherdb is shown for each compartment, graphed according to their false discovery rate (FDR). (B) Graphs showing the distribution of proteins of the oligosaccharyltransferase (OST) complex in the nucleus and

cytoplasm from the TMT-LC/MS-MS data. Graphs display the mean with SEM of 3 biological replicates. (C) Graphs showing the nuclear and cytoplasmic distribution of decapping-related proteins from the TMT-LC/MS-MS data. Graphs display the mean with SEM of 3 biological replicates.

select factors associated with mRNA decay, which likely arises from increases in their mRNA levels in Xrn1 knockout cells.

LARP4 shuttles to the nucleus in a PABPC-dependent manner.

Protein relocalization in response to altered cytoplasmic mRNA decay could occur as a consequence of direct interactions with the nuclear transport machinery that are antagonized by mRNA, as has been documented for the PABPC nuclear localization signal (NLS) (Kumar et al., 2011). Alternatively, translocation could occur indirectly via interactions with other proteins that contain nuclear transport signals. To test for this latter possibility, we first plotted the network of known interactions among the list of proteins that relocalized in cells undergoing accelerated mRNA decay using the STRING database (**Figure 2.7A**). There were significantly more interactions among this set of proteins than would be predicted for a random group of proteins of similar size ($p = 0.0496$), with many of the interactions involving PABPC. This enrichment suggests that these proteins are biologically related, confirming what was seen in the GO term analysis. We examined the relocalization mechanism for one of the PABPC interacting proteins, LARP4 (Yang et al., 2011). We reasoned that if LARP4 relocalization involved direct interactions with the nuclear import machinery, then it should relocalize in muSOX-expressing cells in a PABPC independent manner. Conversely, if it was 'escorted' into the nucleus via its interaction with PABPC, then its relocalization should be blocked by PABPC depletion. Depletion of PABPC1 has been shown to lead to compensatory induction of PABPC4, which can function in a redundant manner (Kumar, 2010). Therefore, we co-depleted both PABPC1 and PABPC4 using siRNAs. Upon co-depletion of the PABPC proteins, LARP4 no longer accumulated in the nucleus of muSOX-expressing cells (**Figure 2.7B**). In contrast, siRNA-mediated depletion of LARP4 had no effect on PABPC1 shuttling in these cells (**Figure 2.7C**). These results support a model in which LARP4 is brought into the nucleus in cells undergoing accelerated mRNA decay through its interaction with PABPC.

PABPC depletion abrogates the muSOX-driven decrease in RNAPII promoter occupancy.

Given the nuclear enrichment of many poly(A) and poly(U) associated proteins, we considered these factors to be strong candidates for involvement in the signaling pathway linking accelerated mRNA decay to RNAPII transcriptional repression. To determine if they were required for the mRNA decay-transcription feedback loop, we tested whether depletion of several of these factors individually altered RNAPII occupancy using chromatin immunoprecipitation assays (ChIP). To test the role of PABPC we co-depleted both PABPC1 and PABPC4 using siRNAs, then monitored RNAPII occupancy at two cellular promoters (*gapdh, rplp0*) previously shown to be responsive to mRNA decay-induced transcriptional repression (Abernathy et al., 2015). In cells depleted of PABPC1 and PABPC4, there was no longer a reduction in RNAPII occupancy at the *gapdh* and *rplp0* promoters in muSOX expressing cells relative to vector control cells (**Figure 2.8A**). In contrast, RNAPII promoter

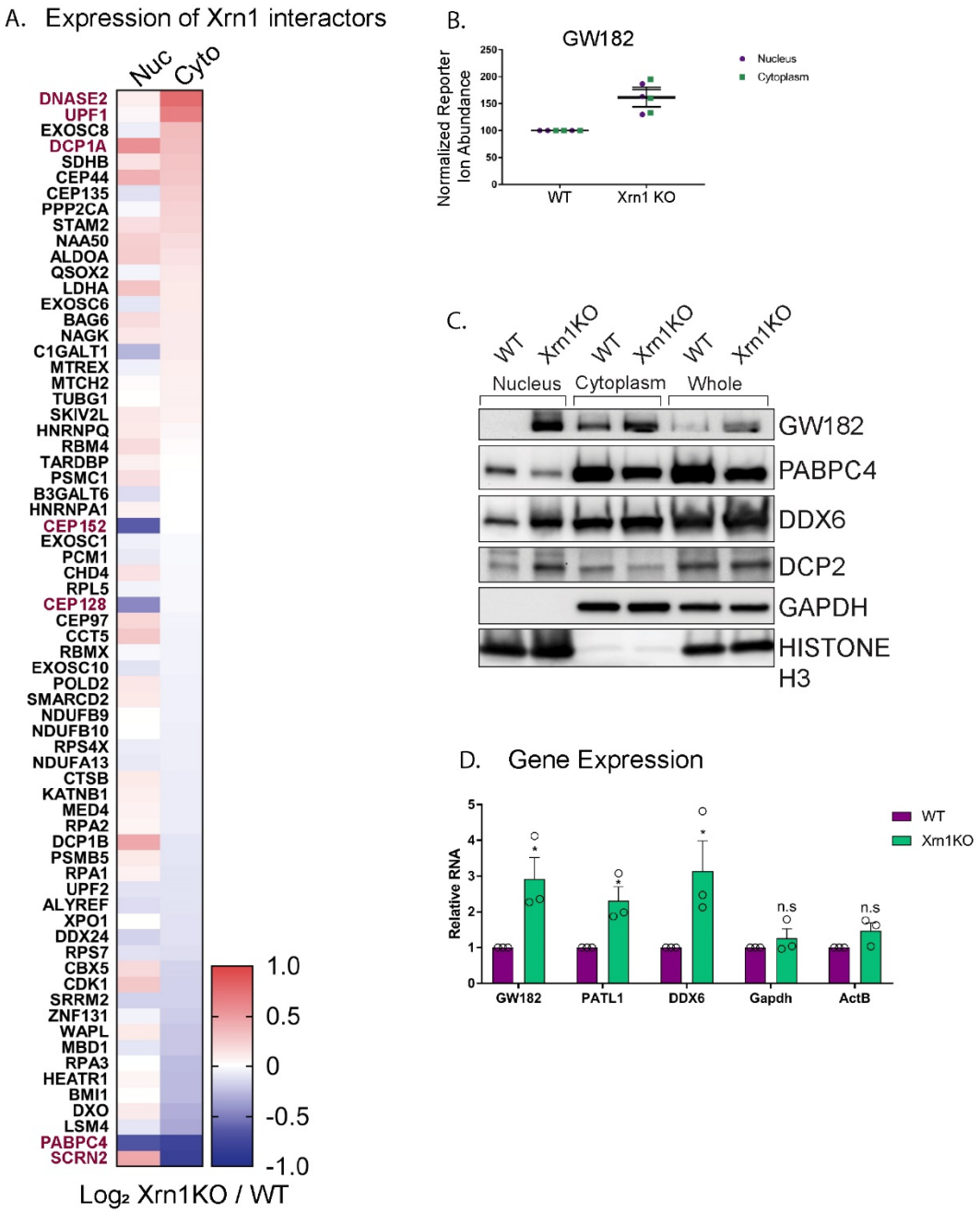

Figure 2.6. Xrn1 knockout leads to subcellular redistribution of proteins functionally associated with RNA. (A) Heatmap depicting the Log_2 abundance ratio in Xrn1 KO HEK293T cells compared to WT HEK293T cells of proteins identified as Xrn1 interactors using the BioGRID database. Proteins with a significant difference in abundance between WT and Xrn1 KO are listed in red. (B) Graph of nuclear and cytoplasmic distribution of GW182 from the TMT-LC/MS-MS data. Graph displays the mean with SEM of 3 biological replicates. (C) Western blot of nuclear, cytoplasmic, and whole cell fractions of WT and Xrn1 KO HEK293T cells. GAPDH and histone H3 serve as fractionation and loading controls. (D) mRNA levels from WT and Xrn1 KO HEK293T cells were measured by RT-qPCR. Graphs display individual biological replicates as dots, with the mean and SEM. Statistical significance was determined using Student's t test *p <0.05 **p <0.005 ***p <0.0005.

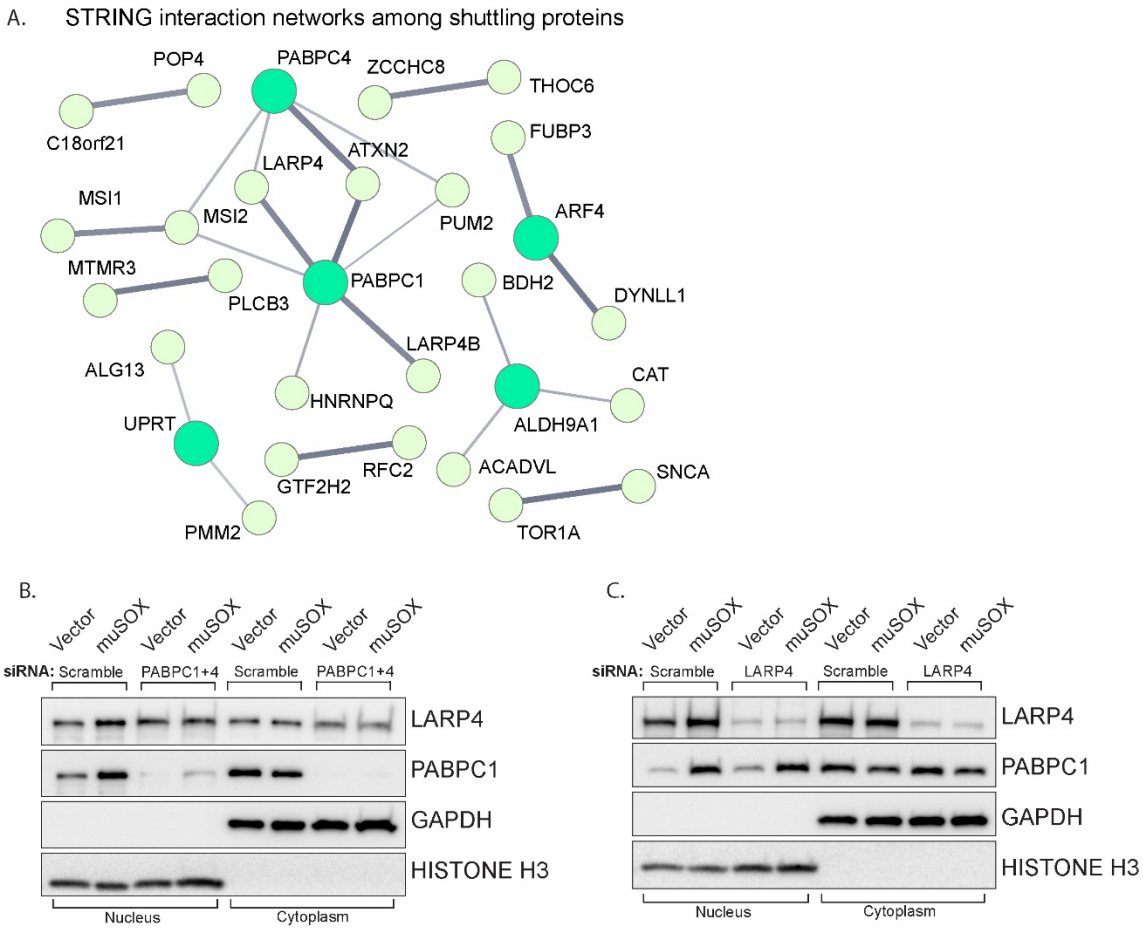

Figure 2.7. LARP4 translocates to the nucleus in a PABPC-dependent manner. (A) STRING network of reported protein-protein interactions between the 67 proteins that shuttle in muSOX-expressing cells. Medium and high confidence interactions are shown with thin and thick connector lines, respectively. (B, C) Western blots of nuclear and cytoplasmic fractions of vector- or muSOX-transfected HEK293T cells treated with the indicated siRNA. GAPDH and histone H3 serve as fractionation and loading controls.

occupancy remained repressed in muSOX expressing cells upon depletion of LARP4 (**Figure 2.8B**). In addition to poly(A) tail associated proteins, we tested the effects of depleting three additional factors that translocated to the nucleus in an mRNA-decay dependent manner: the poly(U) binding protein MSI1, the CHD3 transcriptional regulator, and one of the top scoring hits from the MS data, TRIM32 (**Figure 2.8C-E**). RNAPII occupancy remained reduced in muSOX-expressing cells relative to vector control cells upon depletion of MSI1, CHD3, and TRIM32 (**Figure 2.8C-E**).

It should be noted that when we measured the effect of depleting the above factors on RNAPII occupancy in the absence of muSOX, we unexpectedly observed that their knockdown alone reduced the RNAPII ChIP signal (**Figure 2.9A-E**). However, unlike the case for PABPC, RNAPII levels were further reduced in muSOX expressing cells after depletion of LARP4, MSI1, CHD3, and TRIM32 (**Figure 2.8A-E**). We hypothesize that knockdown of these factors may lead to broad impacts on cellular function, in ways that directly or indirectly influence transcription. Therefore, although PABPC appeared to be selectively involved in suppressing

RNAPII occupancy during enhanced mRNA decay, we sought an alternative strategy to evaluate its connection to this process.

Nuclear accumulation of PABPC1 is sufficient to inhibit RNAPII recruitment to promoters.

Endogenous PABPC is subject to translational autoregulation, and our previous data suggested that the abundance of PABPC in uninfected cells is fine-tuned to match poly(A) tail availability (Kumar and Glaunsinger, 2010; Kumar et al., 2011). In this regard, even modest over-expression of PABPC1 leads to nuclear accumulation of the 'excess' (presumably non-poly(A) bound) protein in cells lacking muSOX (**Figure 2.10A**). This feature enabled us to test whether nuclear accumulation of PABPC1 was sufficient to cause a reduction in RNAPII promoter recruitment in the absence of muSOX-induced mRNA decay. Indeed, FLAG-PABPC1 transfected cells displayed a significant decrease in RNAPII occupancy at the *gapdh and rplp0* promoters (**Figure 2.10B**). These observations suggested that the failure of muSOX to trigger transcriptional repression in Xrn1 knockout cells might be overcome by driving PABPC into the nucleus via overexpression. In agreement with this prediction, muSOX-induced transcriptional repression was restored in Xrn1 knockout cells upon transfection of FLAG-PABPC1, confirming that nuclear translocation of this RBP plays a central role in connecting cytoplasmic mRNA decay to RNAPII promoter recruitment (**Figure 2.10C**).

Nuclear translocation of PABPC selectively impacts early stages of transcription.

To more precisely define the stage(s) of transcription impacted by mRNA decay-induced translocation of PABPC, we began by measuring RNAPII occupancy at both the promoter and the gene body (exon) of the genes *gapdh*, *actB*, and *tlcd1*. In each of the experiments below, we evaluated cells transfected with empty vector control, muSOX (to activate cytoplasmic mRNA decay), or FLAG-PABPC1 (to selectively increase nuclear PABPC levels in the absence of widespread mRNA decay). Cells expressing muSOX or FLAG-PABPC1 exhibited parallel phenotypes, in which RNAPII occupancy was reduced at promoters as well as within the gene body compared to control cells (**Figure 2.11A**). Western blotting confirmed that the reduced ChIP signals were not due to a decrease in the overall levels of RNAPII in these cells (**Figure 2.11B**).

The C-terminal domain (CTD) of the RNAPII Rpb1 subunit has unique phosphorylation patterns associated with each phase of transcription; it initially binds DNA in an unphosphorylated state, but undergoes progressive serine 5-phosphorylation (Ser5P) during initiation, then serine 2-phosphorylation (Ser2P) during elongation (Heidemann et al., 2013). To determine whether mRNA decay-induced PABPC1 translocation impacted RNAPII initiation or elongation in addition to promoter recruitment, we measured the ratio of total RNAPII to either Ser5P or Ser2P RNAPII (**Figure 2.11C, D**). In both muSOX and FLAG-PABPC expressing cells, these ratios were unchanged relative to control cells, suggesting that the primary defect is in promoter recruitment, and that there are not independent impacts on downstream events. These data are consistent with previous observations in MHV68-infected cells (Abernathy et al., 2015).

RNAPII promoter recruitment occurs during assembly of the transcription preinitiation complex (PIC), a multi-step event involving numerous general transcription factors and transcription associated factors (Roeder, 1996). The initial promoter-defining event in PIC

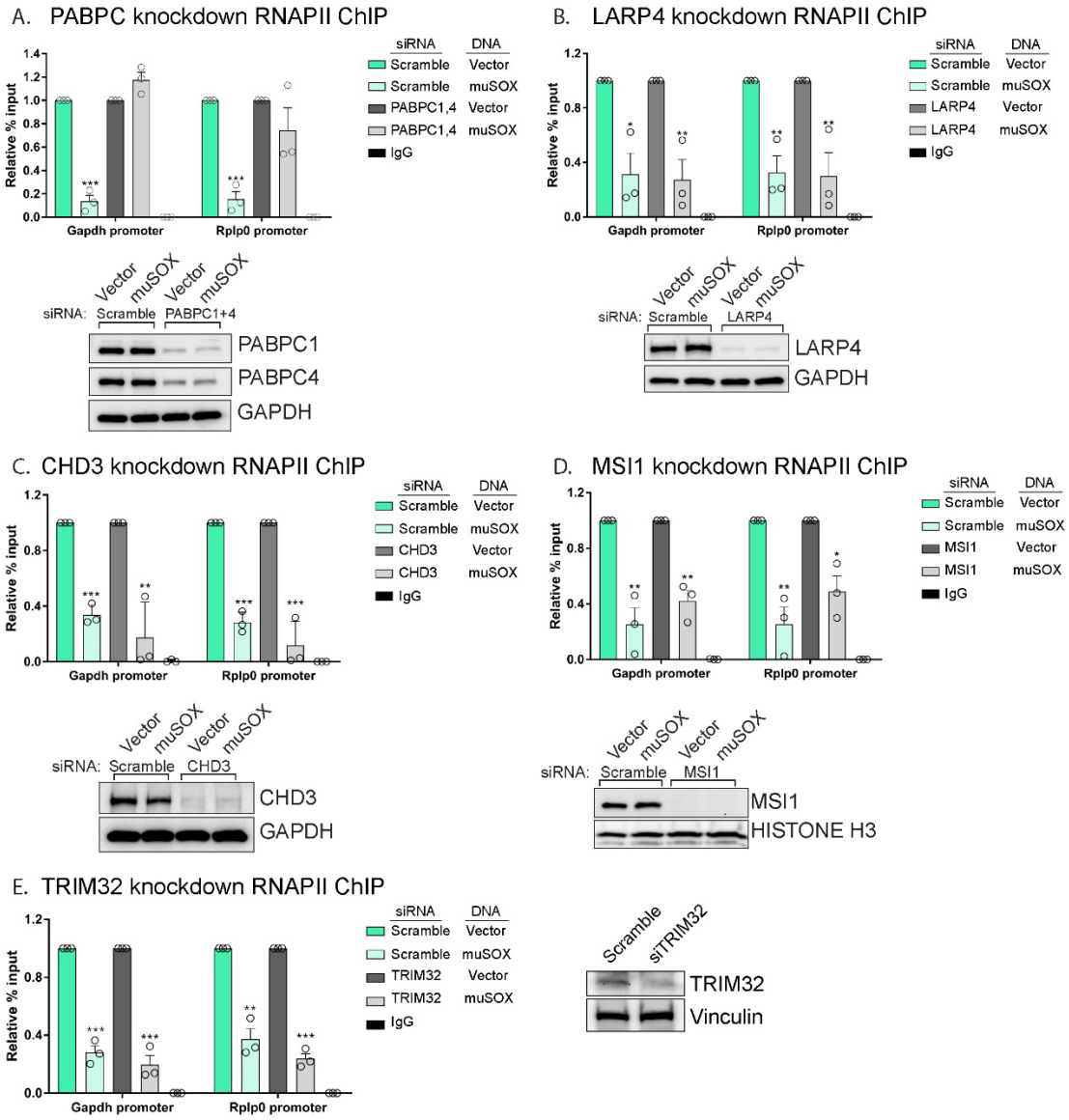

Figure 2.8. PABPC depletion prevents muSOX-induced repression of RNAPII recruitment. (A-E) HEK293T cells treated with siRNAs targeting PABPC1 and 4 (A), LARP4 (B), CHD3 (C), MSI1 (D), TRIM32 (E), or non-targeting scramble siRNAs were subsequently transfected with either empty vector or muSOX, then subjected to chromatin immunoprecipitation (ChIP) using antibodies to RNAPII or IgG. Purified chromatin was quantified by qPCR. Western blots showing protein levels after siRNA depletion are shown, along with a loading control. All graphs display individual biological replicates as dots, with the mean and SEM. Statistical significance was determined using Student's t test *p <0.05 **p <0.005 ***p <0.0005.

assembly that occurs prior to RNAPII recruitment is binding of TATA-binding protein (TBP) as part of the transcription factor TFIID complex, whose recruitment is essential for initiating transcription (Darzacq et al., 2007; Louder et al., 2016). Notably, TBP ChIP revealed that its occupancy at the *gapdh*, *actB*, *tlcd1*, and *rplp0* promoters was significantly reduced in cells expressing either muSOX or FLAG-PABPC1 compared to control cells (**Figure 2.11E**). Similar to RNAPII, western blotting confirmed that this reduction in promoter binding was not due to

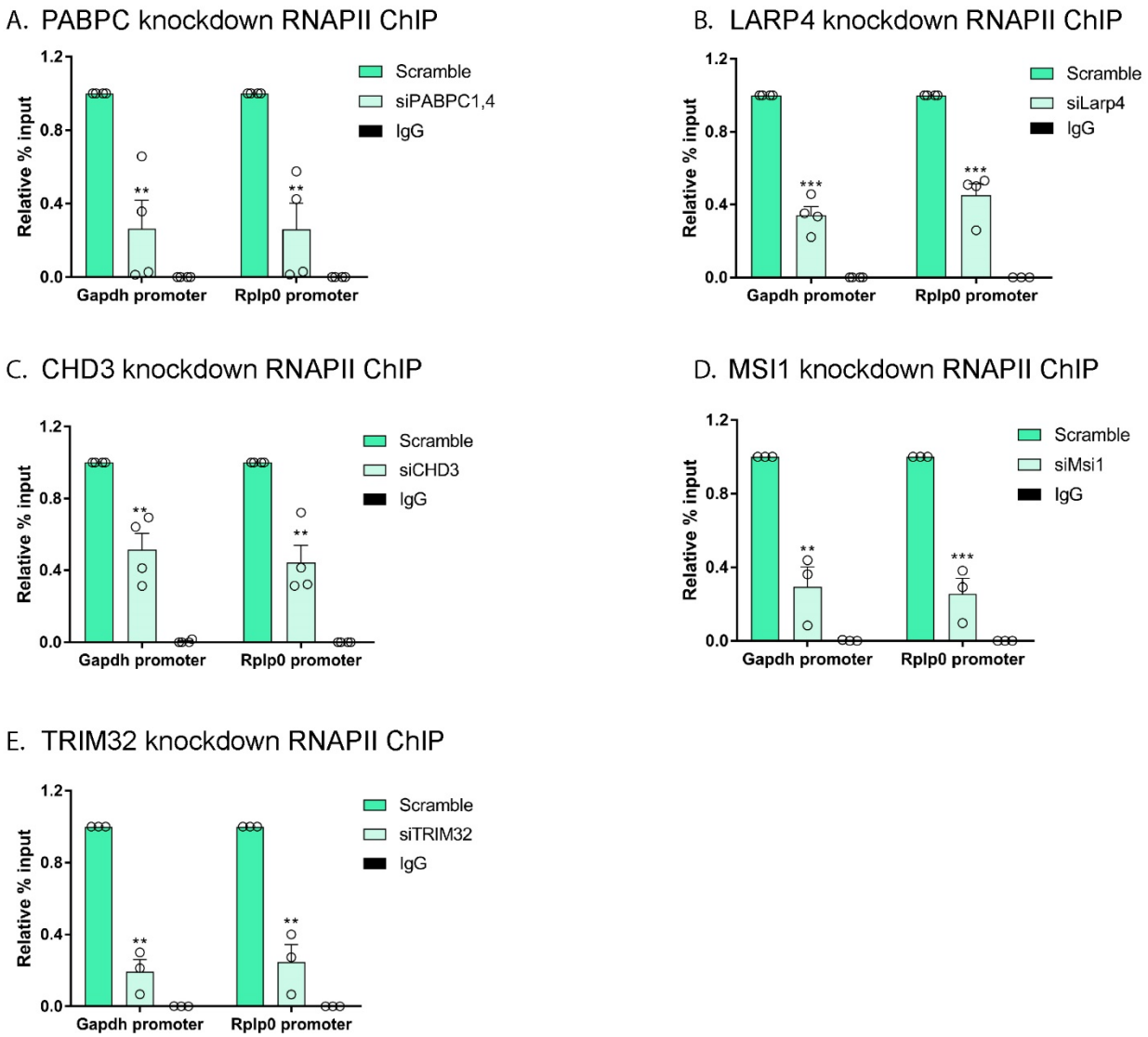

Figure 2.9. Effects of depleting PABPC, LARP4, CHD3, MSI1 and TRIM32 on RNAPII promoter occupancy. (A-E) HEK293T cells were treated with siRNAs targeting PABPC1 and PABPC4 (A), LARP4 (B), CHD3 (C), MSI1 (D), or TRIM32 (E), and subjected to ChIP using antibodies to RNAPII or IgG. Purified chromatin was quantified by qPCR. All graphs display individual biological replicates as dots, with the mean and SEM. Statistical significance was determined using Student's t test *p <0.05 **p <0.005 ***p <0.0005.

altered expression of TBP in these cells (**Figure 2.11B**). Given that TBP is a transcription factor required by cellular polymerases other than just RNAPII, we considered the possibility that all TBP-dependent transcription might be impaired as a consequence of cytoplasmic mRNA decay. This was not the case however, as 7SK and U6 promoter occupancy by RNA polymerase III (RNAPIII), which also requires TBP, was unaltered in cells expressing muSOX or FLAG-PABPC1 compared to control cells (**Figure 2.11F**). We therefore conclude that mRNA decay-driven nuclear accumulation of PABPC1 reduces PIC assembly selectively at the promoters of RNAPII transcribed genes.

Discussion

Cellular mRNA abundance can be dramatically altered in response to a variety of pathogenic and nonpathogenic stresses including both viral and bacterial infections, and early apoptosis (Abernathy and Glaunsinger, 2015; Barry et al., 2017; Thomas et al., 2015). In many of these cases, accelerated cytoplasmic mRNA decay initiates a widespread reduction in transcript levels, often through the engagement of the major mammalian 5'-3' exonuclease Xrn1 (Covarrubias et al., 2011; Gaglia et al., 2012). In addition to altering the translational landscape, depletion of cytoplasmic mRNA elicits changes in upstream components of the mammalian gene expression pathway, including RNAPII transcription, largely by unknown mechanisms (Abernathy et al., 2015). Here, we tested the hypothesis that cellular RNA binding proteins may shift their subcellular localization in response to altered mRNA decay, thus conveying mRNA abundance information between the cytoplasm and the nucleus (**Figure 2.12**). Quantitative proteomics was previously reported to allow the discovery of viral infection-induced protein translocations (Beltran et al., 2017). Indeed, our unbiased TMT-based proteomics approach revealed that among the total cellular protein pool, an RBP-enriched protein subset concentrates in the nucleus specifically in response to increased mRNA decay in an Xrn1 dependent manner. RBPs have critical roles in all stages of gene expression (Müller-McNicoll and Neugebauer, 2013), and our data further emphasize their multifunctional capacity.

We also found that RBPs are enriched in the set of proteins with altered nuclear or cytoplasmic localization in Xrn1 knockout cells. Interestingly, factors involved in decapping, the event that directly precedes Xrn1 attack during basal mRNA decay, were selectively increased in the nuclei of cells lacking Xrn1. Furthermore, we detected increased levels of the NMD factor UPF1 in the cytoplasm and overall elevated levels of GW182 in these cells. One speculative possibility is that these changes occur in response to cellular 'reprogramming' of the mRNA decay network, for example shifting emphasis towards 3' end targeting mechanisms to compensate for the absence of the primary 5' end decay mechanism. This scenario might explain the increase in GW182 levels, as it recruits the cellular deadenylase complexes PAN2-PAN3 and CCR4-NOT to mRNA targets to promote mRNA decay by Xrn1 (Braun et al., 2011). In its absence, the increased GW182 levels may accelerate deadenylation to instead promote 3'-5' decay. Alternatively, the RBP nuclear and/or cytoplasmic enrichment in Xrn1 knockout cells may reflect changes that occur when the cytoplasmic mRNA decay rate is reduced. The fact that we did not observe significant redistribution of the majority of Xrn1 interacting proteins argues against a model in which physical association with Xrn1 helps control decay factor protein localization.

Aside from RBPs, there was a clear overrepresentation of the OST complex, which catalyzes co-translational N-glycosylation, among the set of differentially expressed proteins in Xrn1 knockout cells. Although OST does not have established links to RNA decay or Xrn1, it has been shown to be a critical component of the replication cycle of flaviviruses such as Dengue and Zika (Marceau et al., 2016; Puschnik et al., 2017). Furthermore, these arthropod-borne flaviviruses inhibit Xrn1 activity through a subgenomic viral noncoding RNA that contains an Xrn1 blocking sequence (Chapman et al., 2014; Moon et al., 2012). In this context, it will be exciting to explore possible links between these two processes, especially given that small molecule OST inhibitors are now being tested for their pan-flaviviral inhibition (Puschnik et al., 2017). Among the set of proteins that translocated in cells undergoing accelerated Xrn1-dependent mRNA decay, there was a striking enrichment in factors that bind the 3'end of

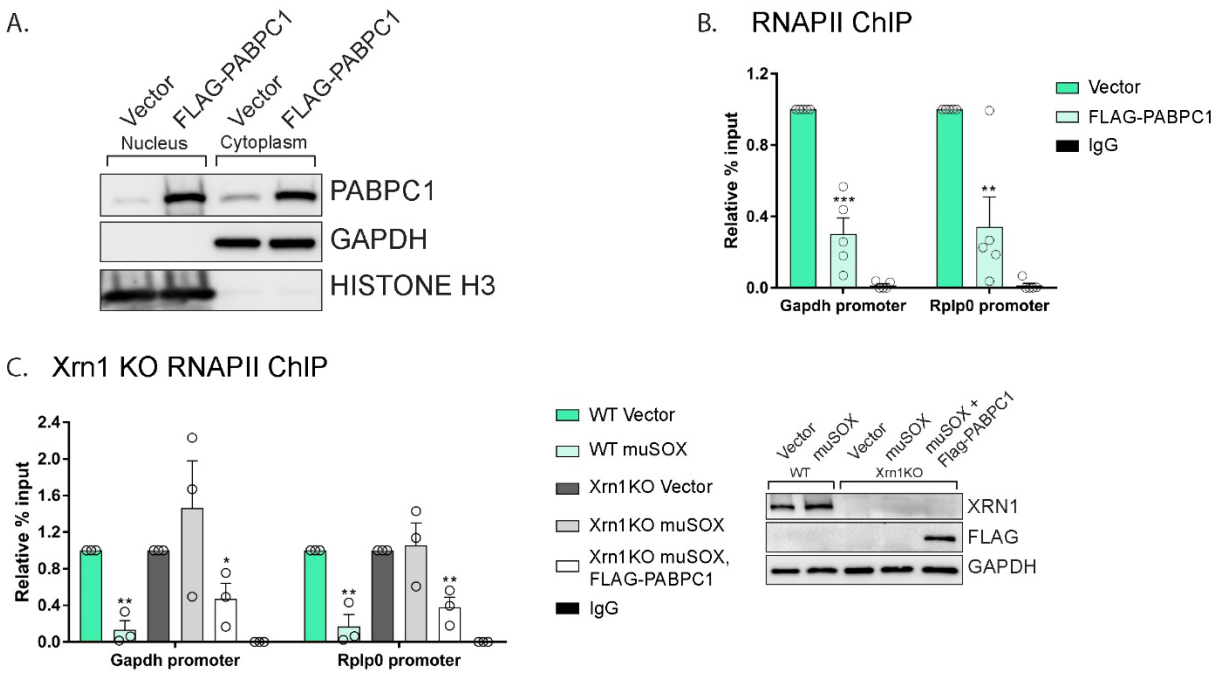

Figure 2.10. Nuclear accumulation of PABPC1 is sufficient to inhibit RNAPII recruitment to promoters. (A) Western blots of nuclear and cytoplasmic fractions of HEK293T cells transfected with an empty vector or a plasmid containing FLAG-PABPC1. GAPDH and histone H3 serve as fractionation and loading controls. (B) HEK293T cells transfected with either empty vector or FLAG-PABPC1 were subjected to ChIP using antibodies to RNAPII or IgG. (C) WT or Xrn1 KO HEK293T cells transfected with either empty vector or muSOX alone or together with FLAG-PABPC1 were subjected to ChIP using antibodies to RNAPII or IgG. Purified chromatin in each of the above experiments was quantified by qPCR. Western blots showing the levels of Xrn1 in WT or Xrn1KO HEK293Ts are shown, along with a GAPDH loading control. All graphs display individual biological replicates as dots, with the mean and SEM. Statistical significance was determined using Student's t test *p <0.05 **p <0.005 ***p <0.0005.

mRNAs. This supports the hypothesis that this class of RBPs would be significantly impacted by the mRNA abundance and availability. PABPC nuclear translocation in particular has been well documented in the context of infection with viruses that drive mRNA decay (Bablanian et al., 1991; Borah et al., 2012; Harb et al., 2008; Lee and Glaunsinger, 2009; Park et al., 2014; Piron et al., 1998; Salaun et al., 2010), and our unbiased proteomics approach establishes it as one of the most robustly relocalized RBPs under these conditions. Several features of PABPC render it an ideal indicator of mRNA abundance. First, its association with poly(A) tails implies that depletion of mRNAs but no other type of abundant non-polyadenylated RNAs should selectively alter the level of PABPC in the RNA bound versus unbound state. Second, nuclear import of PABPC is antagonized by cytoplasmic mRNA abundance. We previously reported that PABPC harbors noncanonical NLSs within its RNA recognition motifs (RRMs); upon poly(A) binding, these elements are masked and the protein is thus retained in the cytosol (Kumar et al., 2011). However, release of PABPC from mRNA exposes the NLSs, enabling its interaction with

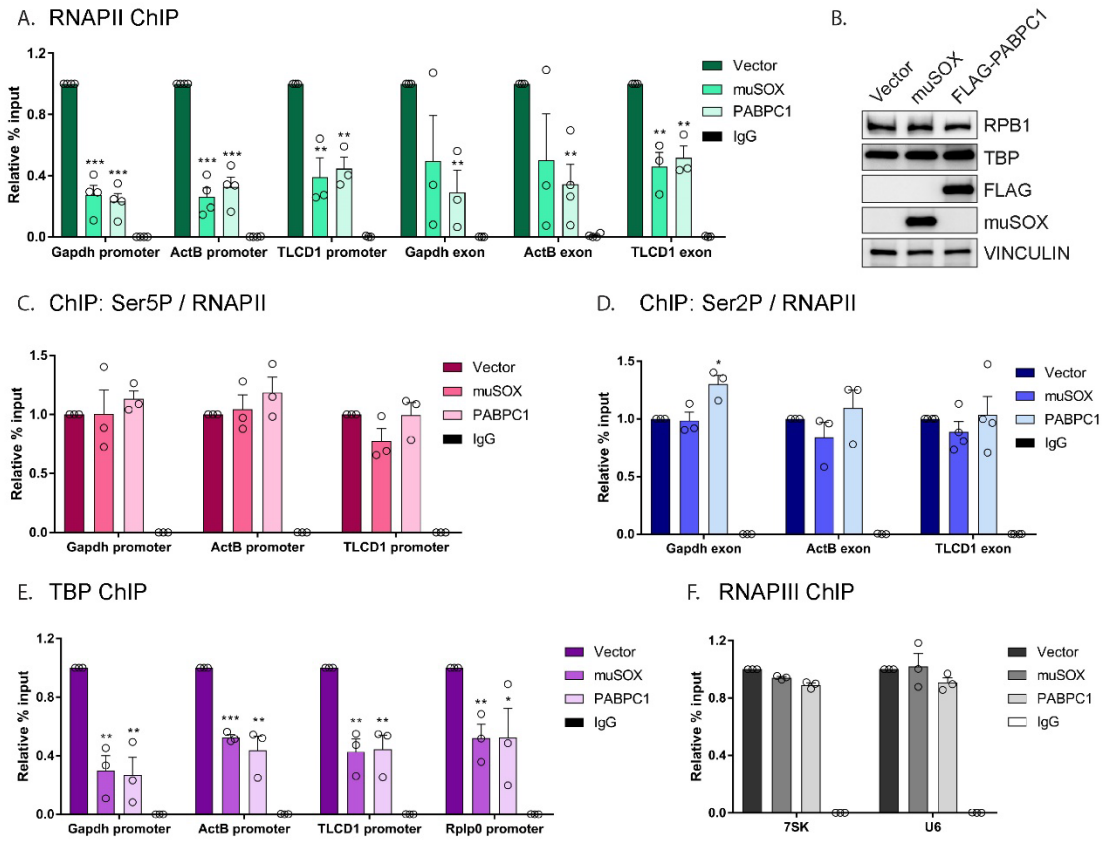

Figure 2.11. Nuclear translocation of PABPC selectively impacts early stages of transcription. (A) HEK293T cells transfected with empty vector, muSOX, or FLAG-PABPC1 were subjected to ChIP using antibodies to RNAPII or IgG at the indicated gene matched promoters and exons. (B) Western blots of RPB1 (RNAPII) and TBP in cells transfected with empty vector, muSOX, or FLAG-PABPC1. VINCULIN serves as a loading control. (C) ChIP using antibodies to serine 5-phosphorylated (Ser5P) RNAPII or IgG at gene promoters. The level of Ser5P RNAPII was determined by dividing the Ser5P values over the total RNAPII values within the same region of the gene in HEK293T cells transfected with empty vector, muSOX, or FLAG-PABPC1. (D) ChIP was performed as described in (B), but using antibodies to serine 2-phosphorylated (Ser2P) RNAPII or IgG at gene exons. The level of Ser2P RNAPII was determined by dividing the Ser2P values over the total RNAPII values within the same region of the gene. (E) ChIP was performed as described in (B), but using antibodies to TATA-binding protein (TBP) or IgG at gene promoters. (F) ChIP was performed as described in (B), but using antibodies to the POLR3A subunit of RNAPIII or IgG. In each experiment, chromatin was quantified by qPCR and all graphs display individual biological replicates as dots, with the mean and SEM. Statistical significance was determined using Student's t test *p <0.05 **p <0.005 ***p <0.0005.

importin α and its subsequent nuclear import. The observation that PABPC localization is directly influenced by mRNA abundance suggest that cells must carefully calibrate the ratio of PABPC to mRNA. Indeed, PABPC protein binds an autoregulatory A-rich sequence in the 5'UTR of its own mRNA to disrupt 40S ribosomal scanning and reduce its translation (Neto et al., 1995; Wu and Bag, 1998).

When bound to poly(A) tails in the cytoplasm, PABPC contributes to mRNA stability and facilitates protein-protein interactions for efficient translation by the ribosome (Burgess and Gray, 2010). However, when concentrated in the nucleus, PABPC functions instead to restrict gene expression. One previously established mechanism by which gene expression is inhibited involves disruption of mRNA processing, where PABPC drives hyperadenylation of nascent mRNAs (Kumar and Glaunsinger, 2010). In this study, we reveal that nuclear accumulation of PABPC phenotypically mimics muSOX-dependent repression of RNAPII promoter binding; it appears necessary and sufficient to repress RNAPII promoter recruitment as a consequence of accelerated mRNA decay. Both muSOX and FLAG-PABPC1 expression target early stages of PIC assembly, as TBP and RNAPII occupancy are reduced at promoters. Interestingly, the *S. cerevisiae* nuclear poly(A) binding protein Nab 2 has been shown to potentiate RNAPIII activity by directly binding RNAPIII and stabilizing TFIIIB with promoter DNA (Reuter et al., 2015), providing a precedent for PABPs influencing transcription. However, although TBP is required for the activity of other polymerases including RNAPIII, we found that the impact of mRNA decay-induced PABPC translocation appears specific to RNAPII responsive promoters. Furthermore, while RNAPII levels are reduced at both promoters and in the gene body, the residual promoter-bound population of RNAPII does not appear to have additional defects in promoter escape or elongation, as measured by polymerase CTD phosphorylation patterns. Collectively, these observations suggest that altered PABPC trafficking primarily impacts the very earliest stages of PIC assembly. Determining which factors govern the specificity for RNAPII responsive promoters during accelerated mRNA decay and their connection to nuclear PABPC remain important challenges for the future.

Although we did not detect a role for LARP4, MSI1, CHD3, or TRIM32 in muSOX-induced transcriptional repression, these findings are complicated by the observation that their depletion alone impaired RNAPII recruitment. In our hands, this phenotype is common to the depletion of a number of different RBPs (though not all), suggesting that their absence may cause secondary effects on gene expression. This also underscores the importance of using alternative assays to evaluate their contributions, as we did for PABPC. Interestingly, some of these proteins are likely to engage in distinct gene regulatory functions in the nucleus that could also be impacted by their altered nuclear-cytoplasmic trafficking. For example, a nuclear role for MSI1 has recently been uncovered during mouse spermatogenesis, when it translocates from the cytoplasm to the nucleus (Sutherland et al., 2015). In the cytoplasm, MSI1 negatively regulates the translation of its target RNAs by competing with eukaryotic initiation factor eIF4G for binding to PABPC (Kawahara et al., 2008). However, upon spermatocyte differentiation, MSI1 relocalizes to the nucleus through direct interaction with importin-5 (IPO5), where it concentrates at the silent XY chromatin domain. This not only releases its repression on translation, but also alters its repertoire of RNA targets in the nucleus. LARP4 also binds PABPC, but unlike MSI1, this interaction promotes mRNA poly(A) tail lengthening and stabilization in the cytoplasm (Yang et al., 2011). Our findings suggest that nuclear accumulation of LARP4 is also dependent on its interaction with PABPC. LARP4 protein levels are controlled post-transcriptionally via an instability determinant within its coding sequence, suggesting that akin to PABPC, its protein abundance is tightly regulated (Mattijssen et al., 2017). The functions of LARP4 in the nucleus, as well as other RBPs identified in this work, are currently unknown. Exploring these roles and how they become manipulated during times of cellular stress are areas ripe for future studies.

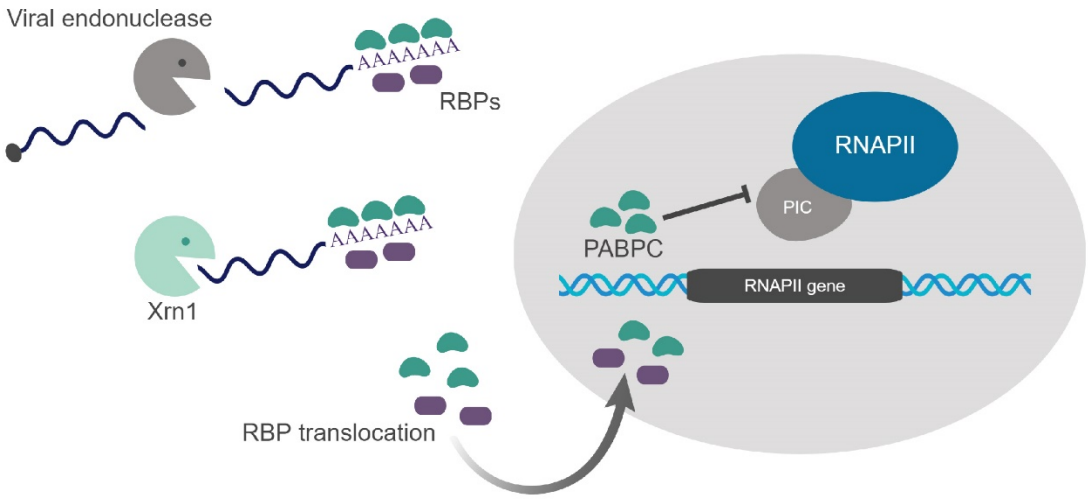

Figure 2.12. Model summarizing the impact of muSOX and Xrn1-driven mRNA degradation on RBP trafficking and RNAPII transcription. See text for details.

Finally, it is notable that connections between Xrn1-driven mRNA decay and RNAPII transcription have also been made in yeast, providing further evidence that these seemingly divergent stages of the gene expression cascade are intimately linked (Haimovich et al., 2013; Sun et al., 2013). However, one key difference between this pathway in yeast and mammalian cells is that in yeast it appears to operate as a compensatory mechanism to maintain optimal mRNA abundance: reduced mRNA decay results in reduced transcription, and vice versa (Haimovich et al., 2013; Sun et al., 2013). This potentially represents an evolutionary divergence in which a unicellular eukaryote 'buffers' its overall gene expression for continued maintenance of the organism. In multicellular eukaryotes like mammals, global mRNA decay (which is induced by numerous pathogens) may instead serve as a stress signal, and the ensuing response is thus geared towards shutdown of major cellular programs.

Acknowledgements
This work was funded by NIH grant CA136367 to B.G., who is also an investigator of the Howard Hughes Medical Institute, and by NIH GM114141 to I.M.C. We thank all members of the Glaunsinger and Coscoy labs for helpful comments and suggestions.

Table 2.1 Proteins enriched in the nucleus in muSOX expressing cells. Proteins significantly ($p < 0.05$) enriched in the nucleus in muSOX expressing cells compared to D219A expressing cells that also show either no change or a decrease in cytoplasmic abundance. Listed from left to right: Accession number, gene symbol, nuclear abundance ratio, muSOX compared to D219A muSOX, subcellular localization, and gene ontology (GO) Molecular Function. The Database for Annotation, Visualization, and Integrated Discovery (DAVID v6.8) was used for subcellular localization and GO molecular function information.

Accession	Gene Symbol	muSOX/ D219A	Localization	GO Molecular Function
Q96BW1	UPRT	2.70	Both	Uridine kinase activity

P12109	COL6A1	2.63	Cytoplasm	Platelet-derived growth factor binding
Q13049	TRIM32	2.35	Both	RNA binding
O95302	FKBP9	2.24	Cytoplasm	PPIase activity
Q8N128	FAM177A1	1.93		
O43683	BUB1	1.86	Both	Protein kinase activity
O14656	TOR1A	1.81	Both	ATP binding
Q9Y4P8	WIPI2	1.70	Both	Phosphatidylinositol-5-phosphate binding
P11940	PABPC1	1.69	Both	Poly(A) / Poly(U) binding, mRNA 3'UTR binding
Q13310	PABPC4	1.69	Both	Poly(A) / Poly(U) binding
Q86WW8	COA5	1.63	Cytoplasm	Protein binding, Mitochondrial respiration
Q13641	TPBG	1.61	Cytoplasm	Cell adhesion
Q9GZM5	YIPF3	1.57	Both	Protein binding
Q92882	OSTF1	1.48	Cytoplasm	Protein binding, SH3 domain binding
Q96H79	ZC3HAV1L	1.48	Both	Metal ion binding
Q13615	MTMR3	1.47	Both	Phosphatidylinositol-3-phosphatase activity
Q9Y6N7	ROBO1	1.47	Cytoplasm	Protein binding
Q9UPT5	EXOC7	1.46	Cytoplasm	Protein binding, exocytosis
P49815	TSC2	1.46	Both	GTPase activator activity
Q12926	ELAVL2	1.44	Nucleus	mRNA 3'UTR binding
Q9BST9	RTKN	1.40	Cytoplasm	GTPase inhibitor activity
P49189	ALDH9A1	1.39	Cytoplasm	3-chloroallyl aldehyde dehydrogenase activity
Q6PIW4	FIGNL1	1.37	Both	Magnesium ion binding
P48509	CD151	1.37	Cytoplasm	Integrin binding
Q16254	E2F4	1.37	Nucleus	Nucleic Acid binding
Q9Y4R8	TELO2	1.34	Both	Protein binding
Q9H6Y2	WDR55	1.33	Both	WD40 domain protein
Q9BUT1	BDH2	1.33	Cytoplasm	3-hydroxybutyrate dehydrogenase activity
P42694	HELZ	1.32	Nucleus	Helicase activity, RNA binding
Q9HBD1	RC3H2	1.32	Both	RNA binding
Q9P0T4	ZNF581	1.31	Nucleus	Nucleic Acid binding
Q58FG0	HSP90AA5P	1.30	Cytoplasm	ATP binding
P18085	ARF4	1.29	Cytoplasm	Protein ADP-ribosylation
O43347	MSI1	1.29	Both	Poly(U) binding
Q9NP73	ALG13	1.28	Cytoplasm	N,N'-diacetylchitobiosylpyrophosphoryldolichol synthase activity, RNA binding
Q96DH6	MSI2	1.27	Cytoplasm	Poly(U) binding
P37840	SNCA	1.26	Both	Magnesium ion binding, Nucleic Acid binding
O60506	HNRNPQ	1.26	Both	Poly(A) binding
Q01970	PLCB3	1.26	Both	Phosphoinositidase C activity

O00425	IGF2BP3	1.24	Both	mRNA 3'UTR binding
Q8TB72	PUM2	1.24	Both	mRNA 3'UTR binding
Q9GZP4	PITHD1	1.23	Nucleus	Galactose binding domain-like
Q5VWQ0	RSBN1	1.23	Nucleus	
Q86W42	THOC6	1.23	Nucleus	RNA binding
Q99700	ATXN2	1.23	Both	RNA binding
Q7Z4W1	DCXR	1.23	Both	Oxidoreductase activity
Q96K58	ZNF668	1.23	Nucleus	Nucleic Acid binding
Q6NZY4	ZCCHC8	1.23	Nucleus	RNA binding
Q9GZN8	C20orf27	1.22		
Q32NC0	C18orf21	1.22		
Q9NPF4	OSGEP	1.22	Both	Metal ion binding
Q9UK41	VPS28	1.21	Cytoplasm	Protein binding
Q96I24	FUBP3	1.21	Both	RNA binding, transcription factor
P35250	RFC2	1.21	Nucleus	DNA binding
Q13888	GTF2H2	1.21	Nucleus	Nucleic acid binding, RNA binding
Q92615	LARP4B	1.21	Both	RNA binding
Q71RC2	LARP4	1.20	Cytoplasm	Poly(A) binding
Q8N543	OGFOD1	1.20	Both	Iron ion binding
O15305	PMM2	1.20	Cytoplasm	Protein binding
O95707	POP4	1.19	Nucleus	RNA binding
P63167	DYNLL1	1.19	Both	Motor activity
O60343	TBC1D4	1.19	Cytoplasm	GTPase activation
P04040	CAT	1.18	Cytoplasm	Aminoacylase activity
O95758	PTBP3	1.18	Nucleus	RNA binding
P15374	UCHL3	1.17	Both	Deubiquitinase
Q9NR56	MBNL1	1.16	Both	RNA binding
P49748	ACADVL	1.16	Both	Fatty-acyl-CoA binding

Table 2.2 Proteins differentially expressed in Xrn1 knockout cells. Proteins that are differentially expressed in Xrn1 knockout cells in the nucleus (left) and the cytoplasm (right). Listed are the protein accession numbers and the corresponding gene symbol.

Nuclear		Cytoplasmic	
Accession	Gene symbol	Accession	Gene symbol
Q9Y375	NDUFAF1	Q96IU4	ABHD14B
P61218	POLR2F	P16403	HIST1H1C
Q9UPP1	PHF8	P31937	HIBADH
Q0ZGT2	NEXN	Q9H3R5	CENPH
Q92859	NEO1	P04843	RPN1
Q96QR8	PURB	Q9UKK9	NUDT5
O15169	AXIN1	P04637	TP53

P17931	LGALS3	P16402	HIST1H1D
Q8N128	FAM177A1	P17931	LGALS3
Q92574	TSC1	P0DMV9	HSPA1B; HSPA1A
P16402	HIST1H1D	Q6P5R6	RPL22L1
P04843	RPN1	Q86Y56	HEATR2; DNAAF5
Q13049	TRIM32	Q8IYU8	EFHA1; MICU2
Q6P5R6	RPL22L1	Q96CM8	ACSF2
Q6P6B1	C8orf47; ERICH5	P56381	ATP5E
Q9H9J4	USP42	O75794	CDC123
Q9NWQ8	PAG1	O95671	ASMTL
P39210	MPV17	P16104	H2AFX
P82909	MRPS36	Q99805	TM9SF2
Q9UK58	CCNL1	P61803	DAD1
P62072	TIMM10	P58107	EPPK1
O43464	HTRA2	Q9Y5V3	MAGED1
P61803	DAD1	Q01804	OTUD4
Q9NRZ7	AGPAT3	Q8N0U8	VKORC1L1
Q9Y241	HIGD1A	Q9BQE5	APOL2
Q9H3K2	GHITM	P67936	TPM4
Q7L9B9	EEPD1	Q9UBB4	ATXN10
Q8NCB2	CAMKV	Q9BPX6	MICU1
O95235	KIF20A	Q6RW13	AGTRAP
Q13099	IFT88	Q9HAS0	C17orf75
Q8TB36	GDAP1	O14967	CLGN
Q9Y4D1	DAAM1	Q96T17	MAP7D2
Q13501	SQSTM1	Q9H900	ZWILCH
Q96F86	EDC3	P08243	ASNS
Q2PZI1	DPY19L1	P36871	PGM1
P07197	NEFM	Q9BVM2	DPCD
Q9NPL8	TIMMDC1	Q8IWB7	WDFY1
Q16352	INA	P49748	ACADVL
Q9BQC3	DPH2	Q9NRG1	PRTFDC1
Q8IX15	HOMEZ	Q96NU1	SAMD11
P31323	PRKAR2B	O75531	BANF1
Q9UBC3	DNMT3B	P00918	CA2
P56181	NDUFV3	O95562	SFT2D2
Q9UIU6	SIX4	P50579	METAP2
O94766	B3GAT3	A6NCE7	MAP1LC3B2
Q6ZU80	CEP128	Q969E8	TSR2
Q8NHG7	SVIP	Q92597	NDRG1
Q3SY17	SLC25A52	Q99439	CNN2

Q8N999	C12orf29	P05455	SSB
Q9NRP0	OSTC	Q3KQV9	UAP1L1
Q96E52	OMA1	P09622	DLD
Q99504	EYA3	Q8WUM9	SLC20A1
Q9BPZ3	PAIP2	Q3SY69	ALDH1L2
Q86TB9	PATL1	P07339	CTSD
Q9UKA9	PTBP2	O43768	ENSA
P17026	ZNF22	P32929	CTH
P12109	COL6A1	Q9BVC6	TMEM109
P22492	HIST1H1T	Q9NZE8	MRPL35
Q969Z3	MARC2	Q16822	PCK2
Q9HAP2	MLXIP	Q14315	FLNC
Q9H300	PARL	P06737	PYGL
Q69YU5	C12orf73	Q13325	IFIT5
Q9HC62	SENP2	Q13641	TPBG
Q03112	MECOM	Q9BX68	HINT2
Q92466	DDB2	Q96FV2	SCRN2
Q2TB10	ZNF800	O60934	NBN
Q96BW1	UPRT	Q96GA7	SDSL
Q99417	MYCBP	P12532	CKMT1B; CKMT1A
Q96IX5	USMG5	P51798	CLCN7
Q8IY95	TMEM192	Q5TDH0	DDI2
P83111	LACTB	Q9Y4J8	DTNA
Q9H845	ACAD9	Q9Y5J9	TIMM8B
P20265	POU3F2	P07108	DBI
Q01831	XPC	O43741	LOC101060511; PRKAB2
Q9H7Z7	PTGES2	Q9H0F7	ARL6
Q9BX40	LSM14B	O94788	ALDH1A2
Q9BUR5	APOO	Q9UK45	LSM7
Q6IQ32	ADNP2	Q5JRX3	PITRM1
O94832	MYO1D	P83876	TXNL4A
Q8N2F6	ARMC10	Q9UNF1	MAGED2
Q8ND56	LSM14A	P46821	MAP1B
Q9NRY2	INIP	Q99808	SLC29A1
Q96II8	LRCH3	Q9BUE6	ISCA1
P39656	DDOST	P36405	ARL3
Q9H9Y4	GPN2	Q9H6E4	CCDC134
O94916	NFAT5	Q8TDB4	MGARP
Q8TCJ2	STT3B	P39656	DDOST
Q5BJF6	ODF2	Q99523	SORT1
Q96C92	SDCCAG3	Q9Y5M8	SRPRB

Q5GLZ8	HERC4	Q8TCJ2	STT3B
Q8N9M1	C19orf47	Q92692	PVRL2; NECTIN2
Q8NDV7	TNRC6A	Q02252	ALDH6A1
Q9H2C0	GAN	Q0VDF9	HSPA14
Q96NB2	SFXN2	Q8NCF5	NFATC2IP
Q86UP3	ZFHX4	P00966	ASS1
Q7L590	MCM10	Q86YN1	DOLPP1
P26196	DDX6	O00115	DNASE2
Q7Z2K8	GPRIN1	P09936	UCHL1
P07305	H1F0	Q8NDV7	TNRC6A
Q13268	DHRS2	Q9Y244	POMP
P98194	ATP2C1	P05026	ATP1B1
Q8IZH2	XRN1	Q8IZH2	XRN1
Q16777	HIST2H2AC	Q92540	SMG7
Q86SQ0	PHLDB2	Q92805	GOLGA1
Q9NXS2	QPCTL	Q16777	HIST2H2AC
Q9H9Q4	NHEJ1	P46977	STT3A
P69905	HBA2; HBA1	Q9BRT3	MIEN1
Q8IXM6	NRM	Q05639	EEF1A2
P18847	ATF3	P58546	LUZP6; MTPN
P78364	PHC1	Q8NHQ8	RASSF8
Q96RR1	C10orf2; TWNK	P29373	CRABP2
Q9Y4P8	WIPI2	Q9H2C2	ARV1
P05412	JUN	Q13636	RAB31
Q6SZW1	SARM1	Q9Y624	F11R
P41208	CETN2	Q9H008	LHPP
Q9NZ45	CISD1	Q5T440	IBA57
P19086	GNAZ	Q86WW8	COA5
Q9H0U3	MAGT1	Q99543	DNAJC2
Q8IUX1	TMEM126B	Q9NVG8	TBC1D13
A3KMH1	VWA8	Q96EL2	MRPS24
O94986	CEP152	Q96EL3	MRPL53
Q96GN5	CDCA7L	Q9P0V9	SEPT10
P49006	MARCKSL1	Q9NRZ9	HELLS
Q9P253	VPS18	Q3LXA3	DAK; TKFC
Q13310	PABPC4	Q6XQN6	NAPRT1; NAPRT
Q8WVJ2	NUDCD2	Q8IUE6	HIST2H2AB
Q9H0L4	CSTF2T	Q96BW5	PTER
Q8WVM7	STAG1	Q9NZ45	CISD1
Q9UPN4	AZI1; CEP131	Q9H0U3	MAGT1
Q8ND76	CCNY	Q14527	HLTF

P16401	HIST1H1B	Q92900	UPF1
Q93075	TATDN2	Q5VVQ6	YOD1
Q8N5U6	RNF10	Q01813	PFKP
Q658Y4	FAM91A1	Q13310	PABPC4
P62341	SELT; SELENOT	Q8IY31	IFT20
P07196	NEFL	Q9Y2Q3	GSTK1
Q99933	BAG1	Q9NP80	PNPLA8
P63218	GNG5	Q8N5Y8	PARP16
Q9H0Z9	RBM38	Q96AY3	FKBP10
Q709F0	ACAD11	P05114	HMGN1
Q16890	TPD52L1	P01023	A2M
P04844	RPN2	Q9Y2G5	POFUT2
Q9Y2D5	AKAP2; PALM2-AKAP2	Q8NBN3	TMEM87A
Q7Z589	C11orf30; EMSY	Q9Y2H6	FNDC3A
O43677	NDUFC1	O95834	EML2
Q8WTV0	SCARB1	P47712	PLA2G4A
A8MT69	STRA13; CENPX	Q99538	LGMN
Q9NPI6	DCP1A	Q8N5U6	RNF10
Q9NRA8	EIF4ENIF1	O15484	CAPN5
		Q99933	BAG1
		P15529	CD46
		Q9Y2S6	TMA7
		Q709F0	ACAD11
		P51956	NEK3
		P04844	RPN2
		Q7L2Z9	CENPQ
		Q6PI48	DARS2
		P05204	HMGN2

Table 2.3 Primer and custom siRNA sequences

Primer name	Primer sequence
Fwd B1 muSOX	GGGGACAACTTTGTACAAAAAAGTTGGCatggaagggtcgattattctgg
Rev B2 muSOX	GGGGACAACTTTGTACAAGAAAGTTGGGTAttattaaagtaattaaagc
Fwd Thy1.1 muSOX	ATTAGCTAGCATGGGTATGAACCCAGCC
Rev Thy1.1 muSOX	TAATCCGCGGTGGGCCCAGGGTTGGACTCGACGTCTCCGGCAAGCTTAAGAAG GTCGAAGTTCAGAGAAATGAAGTCCAGGGC
Fwd QC musox D219A	GAATTTTTGGAGTTTCCCTGGCCACTGCTTTCAATGTGTTTAC
Rev QC musox D219A	GTAAACACATTGAAAGCAGTGGCCAGGGAAACTCCAAAAATTC

Fwd F2A GFP	GGGCCCTTGGGAATTCCAATGGTGAGCAAGGGC
Rev F2A GFP	TAGATCCGGTGGATCCCCTACACATTGATCC
Xrn1 sgRNA	GCAAAAATGAACCAGCAGCG
Fwd Gapdh prom	TACTAGCGGTTTTACGGGCG
Rev Gapdh prom	TCGAACAGGAGGAGCAGAGACCGA
Fwd Rplp0 prom	AGGACTCCATGTTCCCAAAG
Rev Rplp0 prom	CGCAGCCAATAGACAGGAG
PABPC1 siRNA #1	GAAAGGAGCTCAATGGAAA
PABPC1 siRNA #2	GGACAAATCCATTGATAAT
PABPC4 siRNA #1	AGGAGAGAAUUAGUCGAUAUCAGGG
PABPC4 siRNA #2	GGAAUUCAACUCAAGGUUUGAAGAC
Fwd Thy1.1 Nsp1	GGGCCCTTGGGaattgagaaggggAGCGGCCG
Rev Thy1.1 Nsp1	TAGATCCGGTGGATCttaacctccattgagctcacgagt
Fwd Thy1.1 D10	GACAAGGGGgcggccgcCGCAATGAACTTTTACAGATCTAGTATAATTAGT
Rev Thy1.1 D10	GTCGAAGTTgcggccCCTGCATCATCCTC

Materials and Methods

Plasmids

Primers used for cloning are listed in Table S5. MHV68 muSOX was cloned into the Gateway entry vector pDON207 (Invitrogen), and then transferred into the Gateway-compatible peGFP-C1 destination vector to generate GFP-muSOX. Thy1.1-muSOX was generated by Infusion cloning (Clontech) of Thy1.1 (CD90.1) followed by a self-cleaving 2A peptide from foot-and-mouth disease virus in place of GFP into the Nhe1 and SacII restriction enzyme sites of GFP-muSOX. The D219A muSOX mutant was made using Quikchange site-directed mutagenesis (Agilent). Thy1.1-GFP was created with Infusion cloning to insert GFP back into the vector with the BamHI and EcoRI restriction enzyme sites to replace muSOX with GFP. pCDEF3-Flag-PABPC1 was described previously (Kumar, 2010). The Cas9 (lentiCas9-Blast) and sgRNA (lentiGuide-Puro) viral vectors were made as previously described (Sanjana et al., 2014; Shalem et al., 2014). The Xrn1 sgRNA was chosen using the Broad sgRNA design website (Doench et al., 2014).

Cells and transfections

NIH3T3 cells and HEK293T cells, both from ATCC and obtained through the UC Berkeley Tissue Culture Facility, were maintained in DMEM (Invitrogen) supplemented with 10% fetal bovine serum. Cell lines were authenticated by STR analysis, and determined to be free of mycoplasma by PCR screening. DNA transfections were carried out in HEK293T cells at 70% confluency in 15cm plates with 25μg DNA using PolyJet (SignaGen) for 24h. For small

interfering RNA (siRNA) transfections, HEK293T cells were transfected twice over 48h with 100μM siRNA using Lipofectomine RNAiMAX (Thermo Fisher), whereupon the cells were transfected with the indicated DNA plasmid for an additional 24h. Non-targeting scramble siRNAs, LARP4, MSI1, CHD3, and TRIM32 siRNAs were obtained from Dharmacon (Scramble: D-001206-13-50, LARP4: M-016523-00-0020, MSI1: M-011338-01-0010, CHD3: M-023015-01-0020, TRIM32: M-006950-01-0010). PABPC1 and PABPC4 siRNAs have been previously described and are listed in Table S5. (Kumar, 2010; Lee, 2009).

The Xrn1 knockout clone and control Cas9-expressing cells were made by transducing HEK293T cells as previously described (Sanjana et al., 2014; Shalem et al., 2014). Briefly, lenti-Cas9-blast lentivirus was spinfected onto a monolayer of HEK293T cells, which were then incubated with 20μg/ml blasticidin to remove non-transduced cells. These Cas9-expressing HEK293T cells were then spinfected with lentivirus made from lentiGuide-Puro containing the Xrn1 sgRNA sequence and selected with 1μg/ml puromycin. The pool of Xrn1 knockout cells was then single-cell cloned in 96-well plates and individual clones were screened by western blot to determine knockout efficiency.

Pure populations of cells expressing muSOX were generated using the Miltenyi Biotec MACS cell separation system. HEK293T cells were transfected with either Thy1.1-GFP, Thy1.1-muSOX, or Thy1.1-muSOX D219A for 24h, whereupon cells were washed twice with PBS and cell pellets were resuspended in 95μl auto-MACS rinsing buffer supplemented with 0.5% FBS and incubated with 3μl anti-CD90.1 microbeads on ice for 10-15 min, and mixed by flicking the tube every 5 min. Cells were then magnetically separated according to the manufacturer's instructions. Thy1.1 positive cells were used in all downstream experiments unless otherwise stated.

Viruses and infections

The MHV68 bacterial artificial chromosome (BAC), and the construction of the R443I muSOX mutant were previously described (Adler et al., 2000; Richner et al., 2011). MHV68 was produced by transfecting NIH3T3 cells in 6-well plates with 2.5μg BAC DNA using Mirus TransIT-X2 (Mirus Bio) for 24h, whereupon the cells were split into a 10cm dish and harvested after 5-7 days, once all the cells were green and dead. Virus was amplified in NIH 3T12 cells and titered by plaque assay. Cells were infected with MHV68 at an MOI of 5 for 24h.

Immunofluorescence assays

Cells were plated on coverslips coated with 100ug/mL poly-L-lysine and transfected at 70% confluency with either GFP or GFP-muSOX for 24h. Transfected cells were fixed in 4% formaldehyde, permeabilized with ice-cold methanol, and incubated with blocking buffer [1% Triton X-100, 0.5% Tween-20, 3% Bovine Serum Albumin] prior to incubation with mouse monoclonal PABPC diluted 1:25 (Santa Cruz Biotechnologies, 10E10) or rabbit polyclonal LARP4 diluted 1:200 (Thermo Fisher) in blocking buffer at 4°C overnight, followed by incubation with Alexa Fluor 594-conjugated goat anti-mouse, or anti-rabbit secondary antibody (Thermo Fisher, 1:1000) and DAPI (Pierce, 1:1000). Coverslips were mounted on slides using Vectashield hard-set mounting medium (VectorLabs) and imaged by confocal microscopy on a Zeiss LSM 710 AxioObserver microscope.

Subcellular Fractionation

HEK293T cells were fractionated using the REAP method (Nabbi and Riabowol, 2015). Briefly, cells were washed twice with ice-cold PBS and the cell pellet was lysed in 0.1% NP-40 PBS lysis buffer. The nuclei were then isolated by differential centrifugation at 10,000 x *g* for 10

sec and the supernatant retained as the cytoplasmic fraction. For western blotting, the nuclei were sonicated in 0.1% NP-40 PBS lysis buffer.

Complete lysis and protein digestion

WT Cas9-HEK293T cells were transfected with Thy1.1-GFP, Thy1.1-muSOX, or Thy1.1-muSOX D219A. Xrn1 knockout HEK293T cells were transfected with Thy1.1-GFP or Thy1.1-muSOX for 24h, followed by Thy1.1 separation. Separated cells were then fractionated as described above, and nuclear pellets were snap-frozen in liquid nitrogen. Cytoplasmic fractions were concentrated using an Amicon ultra filtration unit with a molecular weight cutoff of 3kDa (Millipore) and exchanged into a 50mM NH_4HCO_3, 2% Deoxycholate buffer and then snap frozen in liquid nitrogen. The nuclear pellets were lysed in 200µL of 100mM Tris-HCl, pH 8.0, 4% SDS, 1mM EDTA preheated to 70°C. Cytoplasmic fractions were thawed and adjusted to 1% SDS with a 10% SDS solution. Complete lysis of samples was achieved via five successive rounds of heating at 95°C for 3 min followed by sonication for 10 sec in a cup horn sonicator set on 1 sec pulses at medium output. Protein amounts were assessed by BCA protein assay (Pierce) and 50 µg of protein from each sample was simultaneously reduced and alkylated with 20mM tris(2-carboxyethyl)phosphine (Pierce) and chloroacetamide respectively for 20 min at 70°C. Protein samples were then cleaned up by methanol-chloroform precipitation (Wessel et al., 1984; Federspiel and Cristea, 2018). LC-MS grade methanol, chloroform, and water (at a 4:1:3 ratio) were added to the sample with vortexing following each addition. The samples were spun at 2,000 × *g* for 5 min at room temperature and the top phase was removed. Three volumes of cold methanol were then added and the samples were spun at 9,000 × *g* for 2 min at 4°C. All liquid was removed and the protein pellets were washed with five volumes of cold methanol and then spun at 9,000 × *g* for 2 min at 4°C. All liquid was removed again and the dried protein pellets were resuspended in 50mM HEPES pH 8.5 at a 0.5µg/µL concentration. Trypsin (Pierce) was added at a 1:50 trypsin:protein ratio and the samples were incubated at 37°C overnight.

TMT labeling

Digested samples were concentrated by speed vac to one half the original volume prior to labeling and adjusted to 20% acetonitrile (ACN). All three biological replicates were labeled concurrently with a 10-plex TMT kit (Thermo Fisher Scientific) as in (Sauls et al., 2018). The TMT reagents (0.8mg per channel) were dissolved in 42µL of anhydrous ACN and 14µL of this was added to each sample following the scheme in Figure 1A and allowed to react at RT for 1h. The labeling was quenched by the addition of hydroxylamine to a final 0.5% (v/v) concentration followed by incubation at RT for 15 min. Labeled peptides were pooled at equal peptide amounts thereby generating three 10-plex experiments, each of which was an individual biological replicate. An initial test mix for each replicate was analyzed, and the apparent peptide ratios were determined. Mixing ratios were adjusted using the information from the test mix to correct for sample losses and generate mixes with equal peptide amounts per channel.

Peptide fractionation

Pooled peptides were acidified and fractionated by 2D StageTip (Sauls et al., 2018). Peptides were first desalted via C18 StageTips to remove unreacted TMT reagent by washing the bound peptides with 5% ACN, 0.5% formic acid (FA) and then eluting the peptides in 70% ACN, 0.5% FA. The eluted peptides were then bound to SCX StageTips and eluted in four fractions with sequential elution (100µL) as follows: (1) 0.05 M ammonium formate/20% ACN, (2) 0.05 M ammonium acetate/20% ACN, (3) 0.05 M ammonium bicarbonate/20% ACN, and (4) 0.1% ammonium hydroxide/20% ACN. Each of these fractions were diluted 1:1 with 1% trifluoroacetic acid and further fractionated by SDB-RPS StageTips with sequential elution

(50µL) into three fractions as follows: (1) 0.2 M ammonium formate/0.5% FA/60% ACN, (2) 0.2 M ammonium acetate/0.5% FA/60% ACN, (3) 5% ammonium hydroxide/80% ACN. The resulting 12 fractions for each 10-plex experiment were dried *in vacuo* and resuspended in 5µL of 1% FA, 1% ACN in water.

LC-MS/MS analysis

Peptides (2µL) were analyzed by LC-MS/MS using a Dionex Ultimate 3000 UPLC coupled online to an EASYSpray ion source and Q Exactive HF. Peptides were separated on an EASYSpray C18 column (75µm x 50cm) heated to 50°C using a linear gradient of 5% ACN to 42% ACN in 0.1% FA over 150min at a flow rate of 250nL/min and ionized at 1.7kv. MS/MS analysis was performed as follows: an MS1 scan was performed from 400 to 1800 m/z at 120,000 resolution with an automatic gain control (AGC) setting of 3e6 and a maximum injection time (MIT) of 30ms recorded in profile. The top 18 precursors were then selected for fragmentation and MS2 scans were acquired at a resolution of 60,000 with an AGC setting of 2e5, a MIT of 105ms, an isolation window of 0.8 m/z, a fixed first mass of 100 m/z, normalized collision energy of 34, intensity threshold of 1e5, peptide match set to preferred, and a dynamic exclusion of 45s recorded in profile.

Informatic analysis of TMT data

MS/MS data were analyzed by Proteome Discoverer (Thermo Fisher Scientific, v2.2.0.388). The nuclear channels (126-128C) and cytoplasmic channels (129N-131) were analyzed in separate Proteome Discoverer studies to not bias the quantitation due to the expected protein expression differences between these two compartments. The Spectrum Files RC node was utilized to perform post-acquisition mass recalibration and the recalibrated spectra were passed to Sequest HT where two successive rounds of searching were employed against a Uniprot human database appended with common contaminants (2016-04, 22,349 sequences). Both search rounds required 5ppm accuracy on the precursor and 0.02Da accuracy on the fragments and included static carbamidomethyl modifications to cysteine, static TMT additions to peptide N-termini and lysine residues, dynamic oxidation of methionine, dynamic deamidation of asparagine, and dynamic methionine loss and acetylation of protein n-termini. The first Sequest HT search was for fully tryptic peptides only and any unmatched spectra were sent to a second Sequest HT search, which allowed semi-tryptic peptide matches. All matched spectra were scored by Percolator and reporter ion signal-to-noise (S/N) values were extracted (The et al., 2016). The resulting peptide spectrum matches were parsimoniously assembled into a set of identified peptide and protein identifications with a false discovery rate of less than 1% for both the peptide and protein level and at least 2 unique peptides identified per protein. TMT reporter ion quantification was performed for unique and razor peptides with an average S/N of at least 10 and a precursor co-isolation threshold of less than 30% which did not contain a variable modification. Reporter ion values were normalized to the total detected signal in each channel and protein abundances were calculated as the sum of all normalized reporter ion values for each channel in each protein. Missing values were input using the low abundance resampling algorithm. The reporter ion values for the empty vector WT samples (channels 126 and 129N) were set as 100 and the other channels were scaled to this value. Statistically differential proteins were assessed via a background based ANOVA analysis implemented in Proteome Discoverer. Proteins and associated TMT reporter ion abundances and adjusted p-values from the ANOVA analysis were exported to Excel for further analysis. The mass spectrometry proteomics data reported in this paper have been deposited at the ProteomeXchange Consortium via the PRIDE partner repository (Vizcaíno et al., 2014). The PRIDE accession number is PXD009487.

Gene Ontology analysis and informatic software used

Differential proteins (adjusted p-value ≤ 0.05) were analyzed via over representation analysis (www.pantherdb.org) for associated gene ontology enrichments (Mi et al., 2016). Example proteins of different classes, along with all heatmaps, were graphed in GraphPad Prism v7.

Western blotting

Nuclear, cytoplasmic, and whole cell lysates were quantified by Bradford assay and resolved by SDS-PAGE and western blotted with antibodies against PABPC (Cell Signaling, 1:1000), PABPC4 (Bethyl, 1:1000), LARP4 (Thermo Fisher, 1:1000), Gapdh (Abcam, 1:3000), Histone H3 (Cell Signaling, 1:2000), LYRIC (Abcam, 1:1000), RRBP1 (Bethyl, 1:1000), MSI1 (Abcam, 1:1000), Lin28b (Abcam, 1:1000), CHD3 (Cell Signaling, 1:1000), RPP20 (Novus, 1:1000), THOC6 (Life Technologies, 1:1000), PNN (Life Technologies, 1:1000), EXO4 (rabbit polyclonal produced using recombinant EXO4 with an MBP tag, 1:1000), NPM (Abcam, 1:1000), GW182 (Abcam, 1:1000), DDX6 (Bethyl, 1:1000), DCP2 (Bethyl, 1:1000), TRIM32 (Abcam, 1:1000), RNAPII Rpb1 (BioLegend, 1:2000), TBP (Abcam, 1:2000).

Chromatin immunoprecipitation (ChIP)

ChIP was performed on 15 cm plates of HEK293T cells transfected twice 4 h apart with the indicated plasmid DNA. 24 h after the first transfection, cells were crosslinked in 1% formaldehyde in PBS for 10 min at room temperature, quenched in 0.125 M glycine, and washed twice with ice-cold PBS. Crosslinked cell pellets were mixed with 1 ml ice-cold ChIP lysis buffer (5mM PIPES pH 8.0, 85mM KCl, 0.5% NP-40) and incubated on ice for 10 min, whereupon the lysate was dounce homogenized to release nuclei and spun at 1.5 x *g* for 5 min at 4°C. Nuclei were then resuspended in 500 µl of nuclei lysis buffer (50mM Tris-HCl pH 8.0, 0.3% SDS, 10mM EDTA) and rotated for 10 min at 4°C followed by sonication using a QSonica Ultrasonicator with a cup horn set to 75 amps for 20 min total (5 min on, 5 min off). Chromatin was spun at 16,000 x *g* for 10 min at 4°C and the pellet was discarded. 100µl of chromatin was diluted 1:5 in ChIP dilution buffer (16.7 mM Tris-HCl pH 8.0, 1.1% Triton X-100, 1.2 mM EDTA, 167 mM NaCl) and incubated with 10 µg mouse monoclonal anti-RNAPII (BioLegend, 8WG16), rabbit IgG (Fisher Scientific), rabbit polyclonal anti-RNAPII phospho S5 (Abcam ab5131), rabbit polyclonal anti-RNAPII phospho S2 (Abcam ab5095), rabbit polyclonal anti-TBP (Abcam ab28175), or rabbit polyclonal anti-POLR3A (Abcam ab96328) overnight, whereupon samples were rotated with 20 µl protein G dynabeads (with mouse antibodies), or 20µl mixed protein G and A dynabeads (with rabbit antibodies) (Thermofisher) for 2 h at 4°C. Beads were washed with low salt immune complex (20 mM Tris pH 8.0, 1% Triton-x-100, 2 mM EDTA, 150 mM NaCl, 0.1% SDS), high salt immune complex (20 mM Tris pH 8.0, 1% Triton-x-100, 2 mM EDTA, 500 mM NaCl, 0.1% SDS), lithium chloride immune complex (10mM Tris pH 8.0, 0.25 M LiCl, 1% NP-40, 1% Deoxycholic acid, 1 mM EDTA), and Tris-EDTA for 5 min each at 4°C with rotation. DNA was eluted from the beads using 100 µl of elution buffer (150 mM NaCl, 50 µg/ml proteinase K) and incubated at 50°C for 2h, then 65°C overnight. DNA was purified using a Zymo Oligo Clean & Concentrator kit. Purified DNA was quantified by qPCR using iTaq Universal SYBR Mastermix (BioRad) with the indicated primers (Table S5). Each sample was normalized to its own input.

Replicates

In this study, individual biological replicates are experiments performed separately on biologically distinct samples representing identical conditions and/or time points. For cell

culture-based assays, this means that the cells are maintained in different flasks. Technical replicates are experiments performed on the same biological sample multiple times. See **Figure Legends** for the number of experimental replicates performed for each experiment. No outliers were encountered in this study. Criteria for the inclusion of data was based on the performance of positive and negative controls within each experiment.

Chapter 3: Characterization of the function of nuclear PABPC in the mRNA decay-transcription feedback loop

Introduction

Viruses manipulate host gene expression in a variety of ways in order to co-opt cellular machinery for viral gene expression and replication. A common example of this occurs post-transcriptionally through accelerated RNA turnover, a process called host shutoff. This can be both an efficient method of liberating translational machinery and can allow transcriptome wide targeting. Gammaherpesviruses do this through expression of a single virally-encoded mRNA endonuclease that causes acceleration of mRNA decay in the cytoplasm of infected cells through the use of the cellular exonucleases Xrn1 and Dis3L2 or the exosome. We recently uncovered a pathway which connects accelerated mRNA decay and transcription in cells infected with the gammaherpesvirus Kaposi's sarcoma-associated herpesvirus (KSHV) as well as with the murine homolog MHV68 (Abernathy et al., 2015). In this system, infected cells, or cells expressing the viral endonuclease, have accelerated cytoplasmic mRNA decay that leads to repression of RNA polymerase II (RNAPII) promoter occupancy. This repression depends on the cellular exonucleases, where depletion of either Xrn1 or Dis3L2 blocks RNAPII repression. Furthermore, accelerated cytoplasmic mRNA decay drives nuclear translocation of many RNA binding proteins (RBPs) (Gilbertson et al., 2018). Many of these RBPs depend on Xrn1 for translocation, with striking movement RBPs that bind the 3'end of mRNAs.

These data were found using the viral endonuclease muSOX in human cells, which recapitulates the mRNA decay-transcription feedback pathway without infection. However, we sought to address how host shutoff in infected cells alters the landscape of RBPs. Here, we characterize global protein subcellular localization in mouse cells infected with either WT MHV68, or the point mutant R443I that renders the virus defective for host shutoff. We found only a small number of shuttling proteins in common between this infection system and those from muSOX-expressing human cells, which importantly, included PABPC. In contrast, however, other transcription-related proteins were also found to be enriched in the nucleus, including seven subunits of RNA polymerase III.

As PABPC nuclear translocation is critical for the connection between mRNA decay and transcription and also displays the same shuttling behavior in infected cells, we sought to address the mechanism by which PABPC represses transcription. To do this, we identified PABPC protein-protein interactions in the nucleus of cells expressing muSOX. We found important interactions with the ubiquitin E3 ligases makorin 1 (MKRN1) and MKRN2. Like PABPC, these proteins were critical for the repression of RNAPII during accelerated mRNA decay. With these data, we uncovered a new set of proteins that, together with nuclear PABPC, may repress the recruitment of RNAPII to promoters.

Results

Transcription-related proteins, and RNA binding proteins, translocate from the cytoplasm to the nucleus during MHV68 infection in a host-shutoff dependent manner.

To further explore mRNA decay-driven movement of proteins between the cytoplasm and the nucleus, we used the same quantitative liquid chromatography/tandem mass spectrometry (LC/MS-MS)-based approach used in Chapter 1 during gammaherpesvirus infection. Specifically, proteins from nuclear and cytoplasmic fractions of MHV68-infected NIH3T3 fibroblasts were labeled with isobaric tandem mass tags (TMT). Three biological replicates of mock infected, WT MHV68, or the R443I MHV68 infected cells were separated into nuclear and cytoplasmic fractions, and trypsin-digested proteins from each fraction were differentially TMT labeled prior to LC/MS-MS.

Among the 6,289 total quantifiable nuclear proteins (detected in at least two replicates), 155 displayed significant nuclear enrichment (adjusted P value of ≤ 0.05) in WT MHV68 infected cells relative to mock infection (**Figure 3.1A**). We then removed from further analysis proteins that were simultaneously increased in the cytoplasm in WT MHV68 infection to remove proteins that increase in overall abundance. These filtering steps yielded a final list of 12 proteins that were differentially enriched in the nucleus during infection (**Figure 3.1B, Table 3.1**). Interestingly, 4 of the 12 proteins (33%) are annotated as DNA-dependent transcription-related proteins (Pantherdb), and this group of proteins was statistically overrepresented in the group (p= .000428). We did the same analysis with the R443I-MHV68 infection compared to mock, and found that 9 proteins were significantly enriched in the nucleus compared to mock infection. Of these 9 proteins, 3 were also enriched in WT infection. Removing these 3 proteins gave a final group of 9 proteins that displayed significant nuclear enrichment in WT infection only, and therefore we considered dependent on accelerated mRNA decay for translocation (**Table 3.1**). However, a number of these proteins still appeared to translocate to the nucleus in R443I-MHV68 infected cells, despite the statistics (**Figure 3.1B, MLX and E2F5**). Also, noteworthy was the absence of PABPC, as well as other RNA binding proteins from this list, despite our extensive previous data showing it robustly translocated to the nucleus during infection in a manner dependent on mRNA decay (Gilbertson et al., 2018; Kumar and Glaunsinger, 2010; Kumar et al., 2011; Lee and Glaunsinger, 2009). In this analysis, PABPC displayed only a 10% enrichment in the nucleus of WT infected cells compared to R443I infection, which was not considered statistically significant (**Figure 3.1C**). Since it appeared we were not capturing relocalization of at least one known event with our current analysis, we performed additional analyses to identify RNA binding proteins that showed at least a 10% enrichment in the nucleus of WT infected cells compared to R443I infection. This identified 18 additional RNA binding proteins that showed a 10% enrichment in the nucleus, similar to PABPC (**Figure 3.1C, Table 3.2**). This identified LARP4, in addition to PABPC, as being the only proteins to shuttle to the nucleus both during infection, and transfection of muSOX. As an independent validation of these results, we evaluated 7 of the top hits by western blotting of fractionated cell lysates in mock, WT, or R443I MHV68 infection, 5 of which recapitulated the MS/MS results (**Figure 3.1D**).

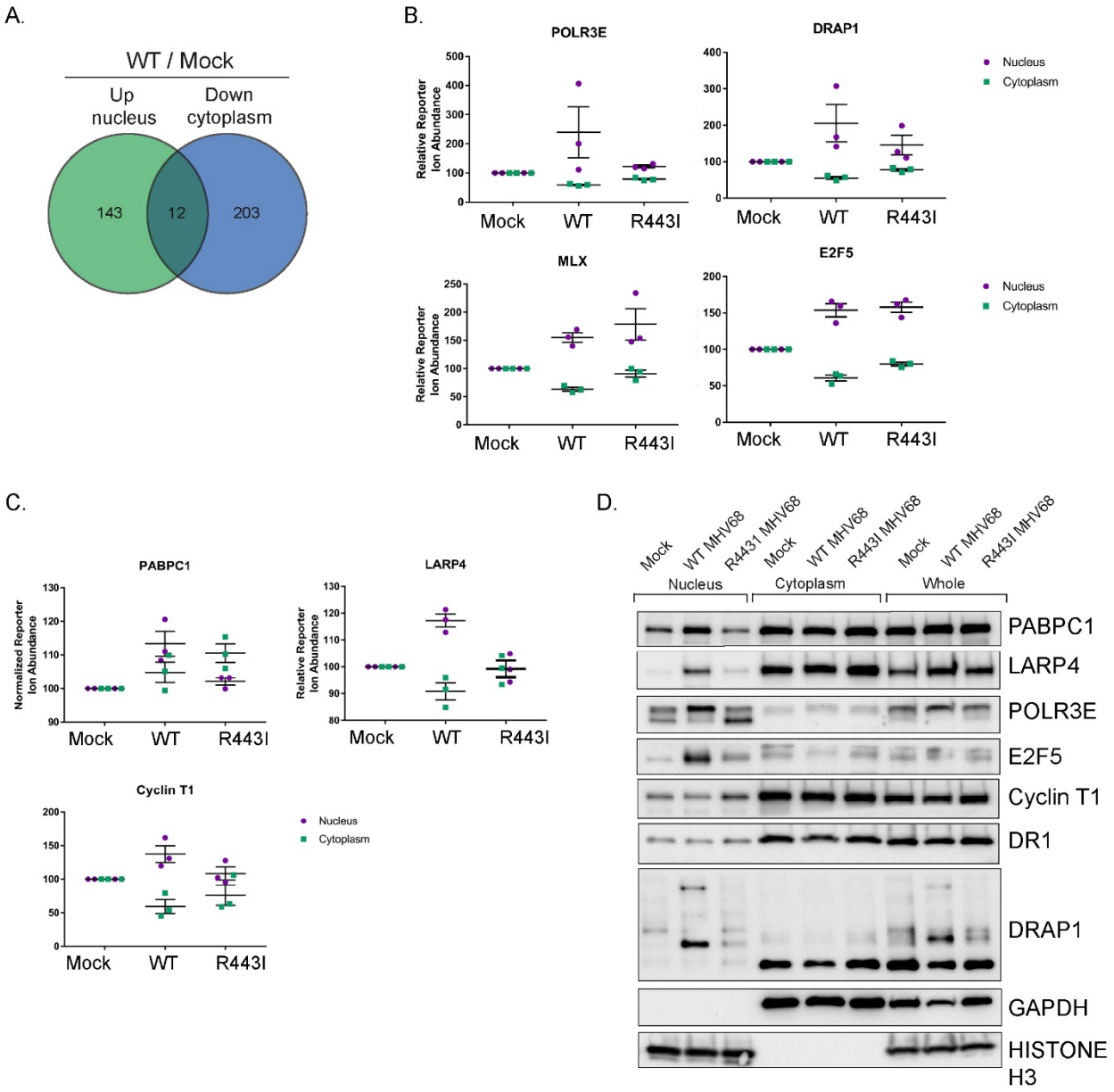

Figure 3.1. Transcription-related proteins, and RNA binding proteins, translocate from the cytoplasm to the nucleus during MHV68 infection in a host-shutoff dependent manner. (A) Venn diagram of nuclear proteins that are specifically and significantly ($p < 0.05$) enriched in WT MHV68 infection compared to mock infection that also show a decrease in cytoplasmic abundance. (B) Graphs showing the nuclear and cytoplasmic distribution of 4 of the top 12 hits from the TMT-MS/MS data. Graphs display the mean with SEM of all three biological replicates. (C) Graphs showing the nuclear and cytoplasmic distribution of 3 of the 18 RNA binding protein hits from the TMT-MS/MS data. Graphs display the mean with SEM of all three biological replicates. (D) Western blots of nuclear, cytoplasmic, and whole cell fractions of NIH3T3 cells infected with either mock, WT MHV68, or R443I MHV68. GAPDH and histone H3 serve as fractionation and loading controls.

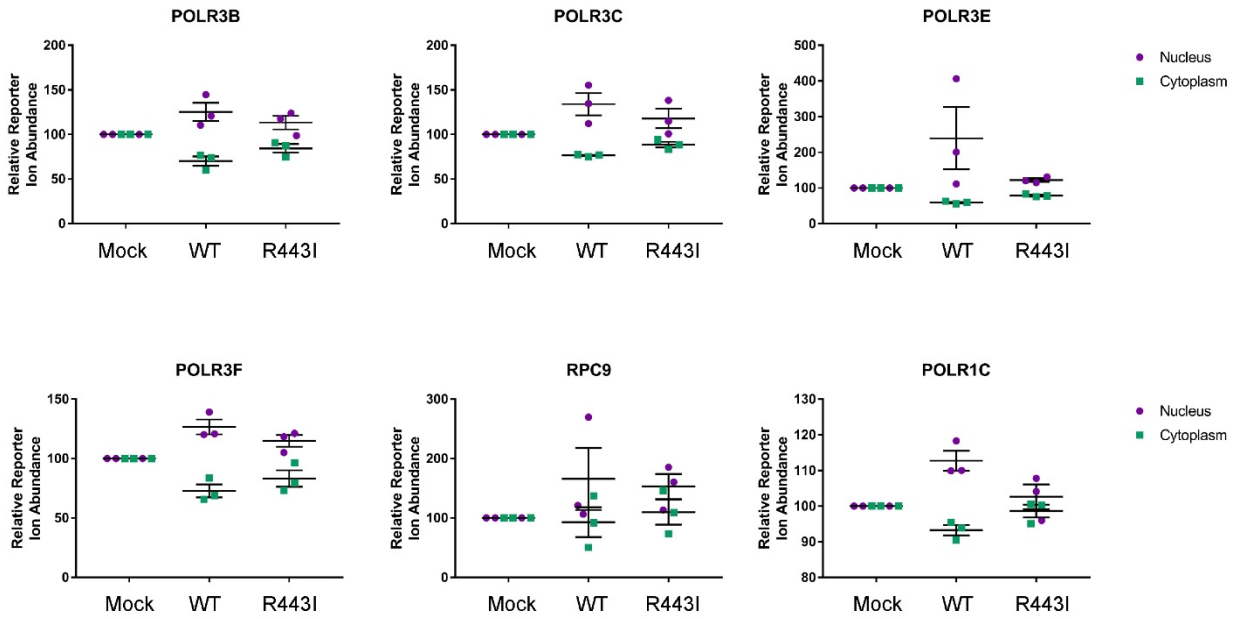

Figure 3.2. RNA polymerase III subunits translocate to the nucleus during MHV68 infection. Graphs showing the nuclear and cytoplasmic distribution of 6 subunits of RNA polymerase III from the TMT-MS/MS data. Graphs display the mean with SEM of all three biological replicates.

RNA polymerase III subunits translocate to the nucleus during MHV68 infection.

An intriguing finding in this analysis was that 5 subunits of RNA polymerase III were among the 18 RNA binding proteins enriched in the nucleus: POLR3E, POLR3C, POLR3D, POLR3B, and POLR3F (peptides corresponding to POLR3D were only identified in 1 replicate). Looking further, the trend continued with RPC9, as well as the shared subunit from RNA polymerase I, POLR1C, for a total of 7 subunits with enrichment in the nucleus (**Figure 3.2**). Some of the subunits showed a dependence on host shutoff for their nuclear enrichment, such as POLR3E, but not all, suggesting that RNA polymerase III relocalization may not be an important factor in the mRNA decay-transcription feedback pathway.

Nuclear PABPC interacts with proteins involved in the ubiquitin-proteasome system.

Two proteins, PABPC and LARP4, translocated to the nucleus in both muSOX expression and MHV68 infection. Having only two proteins in common between these two datasets underscored our model that nuclear translocation of PABPC is critical for the connection between cytoplasm mRNA decay and transcription. To explore the mechanism of RNAPII repression by nuclear PABPC, we used a combination of subcellular fractionation and co-immunoprecipitation (Co-IP) with mass spectrometry to identify PABPC protein-protein interactions in the nucleus. Cells transfected with either empty vector or muSOX were fractionated into the nucleus and cytoplasm, and lysates from each fraction were treated with RNase I to degrade RNA, following immunoprecipitation with either a PABPC1 antibody, or an IgG control, and elutions were analyzed by tandem mass spectrometry (MS/MS). RNase I treatment was used to identify only direct protein-protein interactions, and remove RNA-dependent PABPC interactions from our analysis.

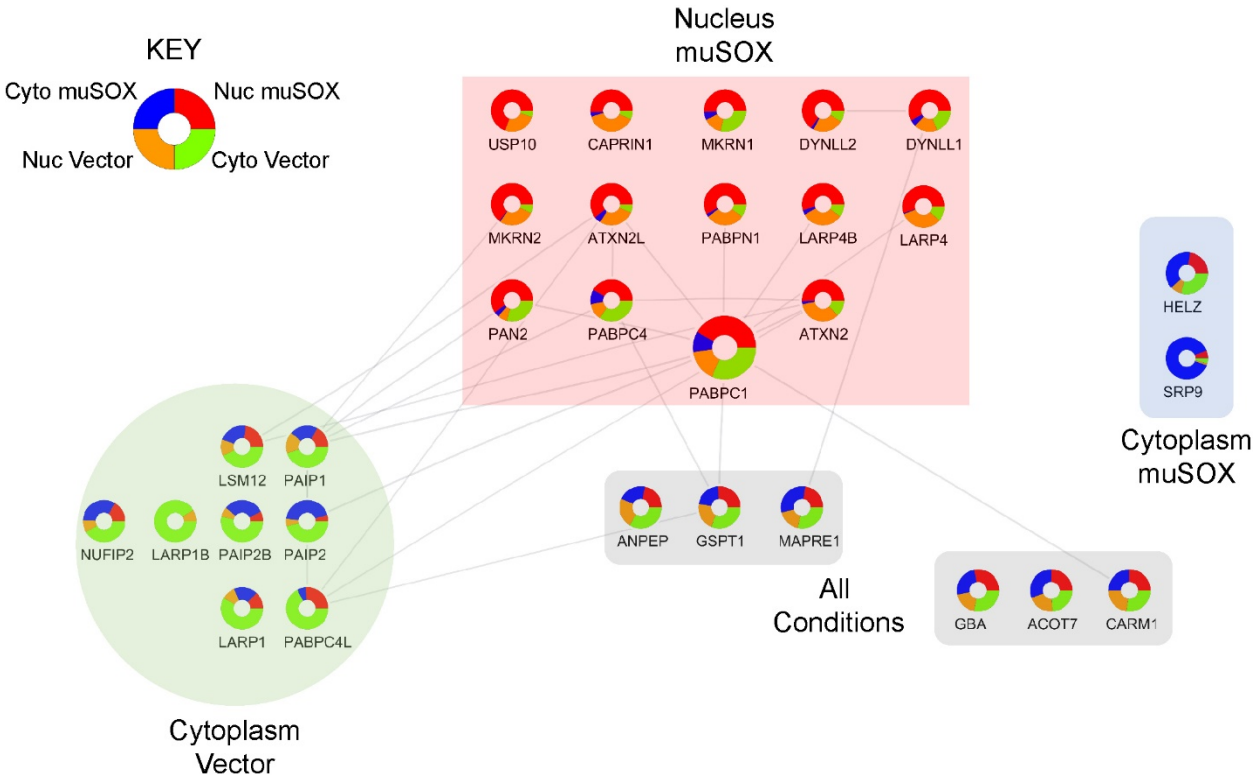

Figure 3.3. Nuclear PABPC1 interacts with proteins involved in the ubiquitin-proteasome system. STRING network of PABPC1 protein-protein interactions from the Co-IP-MS/MS data. The network is grouped to show proteins that are higher in association with PABPC1 in a given condition. Each protein is shown as a circle graph with proportional MS1 abundances for that protein in each condition (see key for color meanings). Edges, shown in grey, connecting proteins indicate known interactions from the STRING database.

We used SAINTexpress (Significance Analysis of INTeractome) to determine the specificity of the interactions (Teo et al., 2014). Using a SAINT score threshold of 0.7, we identified 30 proteins across all conditions that passed the specificity filter. The abundance of each interaction is depicted for each condition (**Figure 3.3**). Of note were the proteins that showed an increase in interaction with PABPC following its translocation to the nucleus in muSOX expressing cells (**Figure 3.3, red box**). We confirmed a number of known PABPC interactions (as listed in the STRING database) in addition to new ones. Interestingly, among these interactions were three proteins involved in the ubiquitin-proteasome system. USP10, a deubiquitinase, and two related E3 ubiquitin ligases, MKRN1 and 2. Proteasome-mediated degradation plays an important role in transcription. Whether these interactions with PABPC were involved in the repression of RNAPII transcription following accelerated mRNA decay was unknown.

Depletion of the E3 ubiquitin ligases MKRN1 and MKRN2 restores RNAPII promoter occupancy during muSOX expression.

To begin to address the role of these PABPC interacting proteins in the mRNA decay-transcription feedback loop, we first confirmed the interactions from the MS/MS data by Co-IP western blot. We validated these interactions and confirmed the known cytoplasmic interaction

with LARP4, and found that it also occurred in the nucleus in muSOX-expressing cells (**Figure 3.4A**). We next analyzed USP10 and MKRN1 for validation of their PABPC interactions (**Figure 3.4B**). We found a strong interaction with MKRN1 and MKRN2 (MKRN2 data not shown). However, there was very little evidence of an interaction with USP10. This validation was done as a single replicate, and bears repeating. Little is known about the function of MKRN2. However, an interaction between MKRN1 and PABPC has been previously reported to exist in rat brain tissue, where a short-form of the protein regulates protein synthesis (Miroci et al., 2012). Furthermore, MKRN1 has been suggested to be involved in regulating RNAPII activity both positively and negatively in a way that is not dependent on its ubiquitin ligase activity (Omwancha et al., 2006).

We used a knockdown approach to explore whether MKRN1 or MKRN2 were involved in mRNA decay-induced RNAPII repression. We depleted both MKRN1 and MKRN2 using siRNAs and analyzed RNAPII promoter occupancy following muSOX expression by ChIP (**Figure 3.4C**). Co-depletion of these two factors resulted in a restoration of RNAPII promoter occupancy. This suggests that like PABPC, one or both of these factors is required for repression of RNAPII promoter recruitment. Further experiments, including single knockdown of these factors, is required to delineate their role and whether the interaction with PABPC is important in this pathway.

Discussion

We characterized the subcellular landscape of proteins during gammaherpesvirus infection. We found that PABPC and LARP4 were the only proteins to translocate to the nucleus in both MHV68 infection that also did so during transfection with muSOX. While it was initially surprising that the majority of shuttling proteins were not shared in infection, there could be a few reasons for this. First, while the R443I MHV68 mutant is 'defective' for host shutoff, it is not a catalytic mutant and therefore it is not totally inactive. Second, there could be differences between the human 293T cells used previously and the murine NIH3T3 cells used here that may not be representative of the commonalities between muSOX expression alone and infection. Ideally, muSOX expression in NIH3T3 cells could overcome this issue, however these cells are difficult to transfect with plasmids. Lastly, there may be differences in the level of infection among the three replicates used here that would lead to proteins dropping out of the significance list. In fact, this may be the reason that PABPC was not captured in the initial analysis, and is highlighted in the differences between replicates as graphed in the reporter ion abundances from the TMT-MS/MS data (**Figure 3.1B, C**). While the same preparation of virus was used for each replicate, and it was titered correctly using a plaque-assay, de novo infection often leads to variability in the intensity of each infection.

Despite these differences, interesting results were found with the nuclear translocation of subunits of RNAPIII. Seven subunits showed enrichment in the nucleus during infection. Some of these depended on host shutoff for translocation, but the majority did not. This suggests that the shift in RNAPIII may be involved in a different process than mRNA decay-transcription feedback pathway. It has recently been shown that RNAPIII may be an innate immune sensor for cytoplasmic foreign nucleic acids, such as those present during viral infection (Ablasser et al., 2009; Chiu et al., 2009; Koo et al., 2015; Ogunjimi et al., 2017). While this has not been shown to be the case for gammaherpesvirus infection, it is interesting to consider whether these viruses alter the localization of RNAPIII in order to prevent the sensing of cytoplasmic nucleic acids. It will be important to address this question with future work.

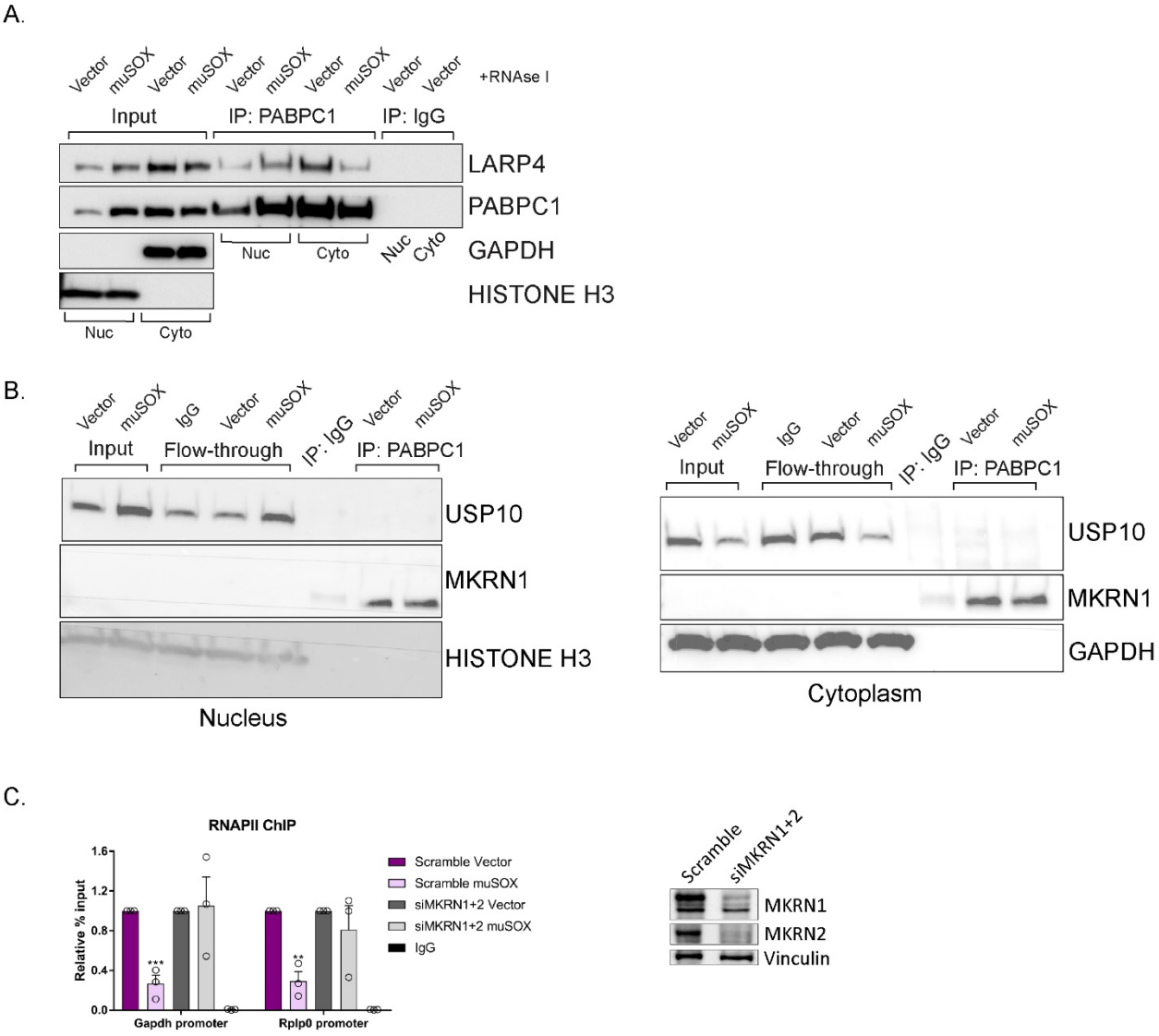

Figure 3.4. Depletion of the E3 ubiquitin ligases MKRN1 and MKRN2 restores RNAPII promoter occupancy during muSOX expression. (A) Western blots from PABPC1 or control IgG co-immunoprecipitations (Co-IPs) from nuclear and cytoplasmic fractions of either vector transfected, or muSOX transfected HEK293Ts. GAPDH and HISTONE H3 in the input samples serve as fractionation controls. (B) Western blots from PABPC1 or control IgG co-immunoprecipitations (Co-IPs) from nuclear (left panel) and cytoplasmic (right panel) fractions of either vector transfected, or muSOX transfected HEK293Ts. GAPDH and HISTONE H3 in the input samples serve as fractionation controls. (C) HEK293T cells treated with siRNAs targeting MKRN1 and MKRN2, or non-targeting scramble siRNAs were subsequently transfected with either empty vector or muSOX, then subjected to chromatin immunoprecipitation (ChIP) using antibodies to RNAPII or IgG. Purified chromatin was quantified by RT-qPCR. Western blots showing protein levels after siRNA depletion are shown, along with a loading control. Graph displays individual biological replicates as dots, with the mean and SEM. Statistical significance was determined using Student's t test *p <0.05 **p <0.005 ***p <0.0005.

As PABPC was a top hit both during infection and muSOX expression, we began to explore the function of nuclear PABPC to gain insight into the mechanism of transcriptional repression. We analyzed the nuclear specific protein-protein interactions of PABPC during muSOX expression. Importantly, PABPC did not make interactions with any subunits of RNAPII, or other general transcription factors, and therefore does not directly alter transcription by binding these factors. We did find, however, important hits with proteins in the ubiquitin proteasome system, including the deubiquitinase USP10, and the E3 ubiquitin ligases MKRN1 and MKRN2. Depletion of MKRN1 and MKRN2 together restored muSOX induced repression of RNAPII promoter occupancy. PABPC is the only other factor to be required for RNAPII repression. This suggests that the interaction between these proteins may be critical to initiate repression. It remains unclear whether the E3 ligase activity of MKRN1 and MKRN2 are involved. Future work will further delineate their contributions to this pathway, especially experiments which disrupt their E3 ligase activity, or their interaction with PABPC.

Table 3.1 Proteins enriched in the nucleus during WT MHV68 and R443I MHV68 infection. Proteins significantly ($p < 0.05$) enriched in the nucleus of cells infected with either WT MHV68 or R443I MHV68 compared to mock infection, that did not also display an increase in cytoplasmic abundance.

WT MHV68 / mock		R443I MHV68 / mock	
Accession number	**Gene symbol**	**Accession number**	**Gene symbol**
Q9CZT4	Polr3e	P63158	Hmgb1
P63158	Hmgb1	P23475	Xrcc6
P23475	Xrcc6	O54879	Hmgb3
O54879	Hmgb3	Q7TQJ8	Wtip
Q9D6N5	Drap1	P23927	Cryab
P27641	Xrcc5	Q91V64	Isoc1
Q91WV0	Dr1	Q80TM6	R3hdm2
O08609	Mlx	P04184	Tk1
Q64092	Tfe3	Q9JJ66	Cdc20
Q61502	E2f5		
Q9ESE1	Lrba		
B7ZNG0	Kif7		

Table 3.2 RNA binding proteins with a 10% increase in nuclear abundance in cells infected with WT MHV68 compared to R443I MHV68.

WT MHV68 / R443I MHV68	
Accession number	**Gene symbol**
Q9CZT4	Polr3e
Q9QWV9	Cyclin-T1
Q8K3Z9	POM121
Q8BG81	Poldip3
Q8BWW4	Larp4
Q64339	ISG15

Q9DBG7	Srpra
Q9D483	Polr3c
Q9D6S7	Mrrf
O70305	Atxn2
Q9CQS2	Nop10
Q9CY66	Gar1
Q8BYM8	Cars2
Q6DFW4	Nop58
Q91WD1	Polr3d
P59470	Polr3b
Q9JJL8	Sars2
Q921X6	Polr3f

Materials and Methods

Plasmids

See Chapter 2 Materials and Methods for the construction of the muSOX plasmid.

Cells and Transfections

NIH3T3 cells and HEK293T cells, both from ATCC and obtained through the UC Berkeley Tissue Culture Facility, were maintained in DMEM (Invitrogen) supplemented with 10% fetal bovine serum. Cell lines were authenticated by STR analysis, and determined to be free of mycoplasma by PCR screening. DNA transfections were carried out in HEK293T cells at 70% confluency in 15cm plates with 25μg DNA using PolyJet (SignaGen) for 24h. For small interfering RNA (siRNA) transfections, HEK293T cells were transfected twice over 48h with 100μM siRNA using Lipofectomine RNAiMAX (Thermo Fisher), whereupon the cells were transfected with the indicated DNA plasmid for an additional 24h. Non-targeting scramble siRNAs, MKRN1, and MKRN2 siRNAs were obtained from Dharmacon (Scramble: D-001206-13-50, MKRN1: M-006959-00-0020, MKRN2: M-006960-01-0020).

Viruses and infections

The MHV68 bacterial artificial chromosome (BAC), and the construction of the R443I muSOX mutant were previously described (Adler et al., 2000; Richner et al., 2011). MHV68 was produced by transfecting NIH3T3 cells in 6-well plates with 2.5μg BAC DNA using Mirus TransIT-X2 (Mirus Bio) for 24h, whereupon the cells were split into a 10cm dish and harvested after 5-7 days, once all the cells were green and dead. Virus was amplified in NIH 3T12 cells and titered by plaque assay. Cells were infected with MHV68 at an MOI of 5 for 24h.

Subcellular Fractionation

HEK293T and NIH3T3 cells were fractionated using the REAP method (Nabbi and Riabowol, 2015). Briefly, cells were washed twice with ice-cold PBS and the cell pellet was lysed in 0.1% NP-40 PBS lysis buffer. The nuclei were then isolated by differential centrifugation at 10,000 x *g* for 10 sec and the supernatant retained as the cytoplasmic fraction. For western blotting, the nuclei were sonicated in 0.1% NP-40 PBS lysis buffer.

Complete lysis and protein digestion

NIH3T3 cells were infected with either mock, WT MHV68, or R443I MHV68 for 24h prior to subcellular fractionation as described above. Nuclear pellets were snap-frozen in liquid nitrogen. Cytoplasmic fractions were concentrated using an Amicon ultra filtration unit with a

molecular weight cutoff of 3kDa (Millipore) and exchanged into a 50mM NH_4HCO_3, 2% Deoxycholate buffer and then snap frozen in liquid nitrogen. The nuclear pellets were lysed in 200µL of 100mM Tris-HCl, pH 8.0, 4% SDS, 1mM EDTA preheated to 70°C. Cytoplasmic fractions were thawed and adjusted to 1% SDS. Complete lysis of samples was achieved via five successive rounds of heating at 95°C for 3 min followed by sonication for 10 sec in a cup horn sonicator set on 1 sec pulses at medium output. Protein amounts were assessed by BCA protein assay (Pierce) and 50 µg of protein from each sample was simultaneously reduced and alkylated with 20mM tris(2-carboxyethyl)phosphine (Pierce) and chloroacetamide respectively for 20 min at 70°C. Protein samples were then cleaned up by methanol-chloroform precipitation (Wessel et al., 1984; Federspiel and Cristea, 2018). LC-MS grade methanol, chloroform, and water (at a 4:1:3 ratio) were added to the sample with vortexing following each addition. The samples were spun at 2,000 × *g* for 5 min at room temperature and the top phase was removed. Three volumes of cold methanol were then added and the samples were spun at 9,000 × *g* for 2 min at 4°C. All liquid was removed and the protein pellets were washed with five volumes of cold methanol and then spun at 9,000 × *g* for 2 min at 4°C. All liquid was removed again and the dried protein pellets were resuspended in 50mM HEPES pH 8.5 at a 0.5µg/µL concentration. Trypsin (Pierce) was added at a 1:50 trypsin:protein ratio and the samples were incubated at 37°C overnight.

TMT labeling

Digested samples were concentrated by speed vac to one half the original volume prior to labeling and adjusted to 20% acetonitrile (ACN). All three biological replicates were labeled concurrently with a 10-plex TMT kit (Thermo Fisher Scientific) as in (Sauls et al., 2018). The TMT reagents (0.8mg per channel) were dissolved in 42µL of anhydrous ACN and 14µL of this was added to each sample following the scheme in Figure 1A and allowed to react at RT for 1h. The labeling was quenched by the addition of hydroxylamine to a final 0.5% (v/v) concentration followed by incubation at RT for 15 min. Labeled peptides were pooled at equal peptide amounts thereby generating three 10-plex experiments, each of which was an individual biological replicate. An initial test mix for each replicate was analyzed, and the apparent peptide ratios were determined. Mixing ratios were adjusted using the information from the test mix to correct for sample losses and generate mixes with equal peptide amounts per channel.

Peptide fractionation

Pooled peptides were acidified and fractionated by 2D StageTip (Sauls et al., 2018). Peptides were first desalted via C18 StageTips to remove unreacted TMT reagent by washing the bound peptides with 5% ACN, 0.5% formic acid (FA) and then eluting the peptides in 70% ACN, 0.5% FA. The eluted peptides were then bound to SCX StageTips and eluted in four fractions with sequential elution (100µL) as follows: (1) 0.05 M ammonium formate/20% ACN, (2) 0.05 M ammonium acetate/20% ACN, (3) 0.05 M ammonium bicarbonate/20% ACN, and (4) 0.1% ammonium hydroxide/20% ACN. Each of these fractions were diluted 1:1 with 1% trifluoroacetic acid and further fractionated by SDB-RPS StageTips with sequential elution (50µL) into three fractions as follows: (1) 0.2 M ammonium formate/0.5% FA/60% ACN, (2) 0.2 M ammonium acetate/0.5% FA/60% ACN, (3) 5% ammonium hydroxide/80% ACN. The resulting 12 fractions for each 10-plex experiment were dried *in vacuo* and resuspended in 5µL of 1% FA, 1% ACN in water.

LC-MS/MS analysis

Peptides (2µL) were analyzed by LC-MS/MS using a Dionex Ultimate 3000 UPLC coupled online to an EASYSpray ion source and Q Exactive HF. Peptides were separated on an EASYSpray C18 column (75µm x 50cm) heated to 50°C using a linear gradient of 5% ACN to

42% ACN in 0.1% FA over 150min at a flow rate of 250nL/min and ionized at 1.7kv. MS/MS analysis was performed as follows: an MS1 scan was performed from 400 to 1800 m/z at 120,000 resolution with an automatic gain control (AGC) setting of 3e6 and a maximum injection time (MIT) of 30ms recorded in profile. The top 18 precursors were then selected for fragmentation and MS2 scans were acquired at a resolution of 60,000 with an AGC setting of 2e5, a MIT of 105ms, an isolation window of 0.8 m/z, a fixed first mass of 100 m/z, normalized collision energy of 34, intensity threshold of 1e5, peptide match set to preferred, and a dynamic exclusion of 45s recorded in profile.

Informatic analysis of TMT data

MS/MS data were analyzed by Proteome Discoverer (Thermo Fisher Scientific, v2.2.0.388). The nuclear channels (126-128C) and cytoplasmic channels (129N-131) were analyzed in separate Proteome Discoverer studies to not bias the quantitation due to the expected protein expression differences between these two compartments. The Spectrum Files RC node was utilized to perform post-acquisition mass recalibration and the recalibrated spectra were passed to Sequest HT where two successive rounds of searching were employed against a Uniprot murine database appended with common contaminants (2016-04, 22,349 sequences). Both search rounds required 5ppm accuracy on the precursor and 0.02Da accuracy on the fragments and included static carbamidomethyl modifications to cysteine, static TMT additions to peptide N-termini and lysine residues, dynamic oxidation of methionine, dynamic deamidation of asparagine, and dynamic methionine loss and acetylation of protein n-termini. The first Sequest HT search was for fully tryptic peptides only and any unmatched spectra were sent to a second Sequest HT search, which allowed semi-tryptic peptide matches. All matched spectra were scored by Percolator and reporter ion signal-to-noise (S/N) values were extracted (The et al., 2016). The resulting peptide spectrum matches were parsimoniously assembled into a set of identified peptide and protein identifications with a false discovery rate of less than 1% for both the peptide and protein level and at least 2 unique peptides identified per protein. TMT reporter ion quantification was performed for unique and razor peptides with an average S/N of at least 10 and a precursor co-isolation threshold of less than 30% which did not contain a variable modification. Reporter ion values were normalized to the total detected signal in each channel and protein abundances were calculated as the sum of all normalized reporter ion values for each channel in each protein. Missing values were input using the low abundance resampling algorithm. The reporter ion values for the empty vector WT samples (channels 126 and 129N) were set as 100 and the other channels were scaled to this value. Statistically differential proteins were assessed via a background based ANOVA analysis implemented in Proteome Discoverer. Proteins and associated TMT reporter ion abundances and adjusted p-values from the ANOVA analysis were exported to Excel for further analysis.

Gene Ontology analysis and informatic software used

Differential proteins (adjusted p-value ≤ 0.05) were analyzed via over representation analysis (www.pantherdb.org) for associated gene ontology enrichments (Mi et al., 2016). Example proteins of different classes were graphed in GraphPad Prism v7.

Co-immunoprecipitation (Co-IP)

Co-IP was performed on 15 cm plates of HEK293T cells transfected twice 4 h apart with the indicated plasmid DNA. 24 h after the first transfection, nuclear and cytoplasmic fractions of harvested cells were brought to 1% NP-40, and sonicated for 10 min at 75 amps using a QSonica Ultrasonicator with a cup horn. Fractions were incubated at 4°C for 1h with 10 units of RNase I (Epicenter, N6901K). Fractions were then centrifuged at 10,000 x *g* for 10 min, whereupon the

pellet was discarded. Fractions were quantified using a Bradford assay, and an equal amount of protein from each fraction were diluted to 1mg/ml and 5µl was set aside for inputs. Diluted fractions were then incubated for 1h at 4°C with either 20µl of mixed protein A and protein G dynabeads (Thermofisher), cross-linked with 5µg rabbit polyclonal PABPC1 (Abcam, ab21060) or rabbit polyclonal IgG (Thermofisher, OB11101). Immunoprecipitated fractions were washed 3X at 4°C rotated for 5 min with IP wash buffer (50mM Tris pH 7.4, 150mM NaCl, 1mM EDTA, 0.05% NP-40). Beads were captured on a magnet, and keeping the tubes on the magnet, the last wash was aspirated, with addition of PBS without detergent. Tubes were not mixed, and PBS was aspirated, followed by elution in 500µl freshly made aqueous 0.5N NH4OH, 0.5mM EDTA with shaking at room temperature for 20 min. Tubes were placed back on the magnet and supernatant was collected and snap frozen in liquid nitrogen. Frozen elutions were dried by speed vac for 3 hours and frozen at -80°C.

Mass spectrometry

Elutions were resuspended in 1X TEL buffer and digested by FASP. Samples were fractionated into three peptide fractions by SDB-RPS, and each fraction was analyzed on an Orbitrap Velos mass spectrometer with a 150 minute gradient, with a total of 54 fractions analyzed. Samples were randomized with standard runs in between each run to mitigate carryover effects.

Data search and assembly

MS/MS data were searched with a Sequest HT in Proteome Discoverer 2.2. MS1 tolerance was 4ppm and MS2 tolerance was 0.3Da. Modifications allowed were oxidized M, phosphorylated STY, and Deamidated N. 2 peptides per protein were required for identification. MS1 quantitation was used in addition to spectral counting for analyses. For the MS1 quant, the PD2.2 matching algorithm was used to decrease missing values.

Western blotting

Nuclear, cytoplasmic, and whole cell lysates were quantified by Bradford assay and resolved by SDS-PAGE and western blotted with antibodies against PABPC (Cell Signaling, 1:1000), LARP4 (Thermo Fisher, 1:1000), Gapdh (Abcam, 1:3000), Histone H3 (Cell Signaling, 1:2000), POLR3E (Sigma, 1:200), E2F5 (Novus, 1:1000), Cyclin T1 (Abcam, 1:1000), DR1 (Abcam, 1:100), DRAP1 (Abcam, 1:100), USP10 (Abcam, 1:500), MKRN1 (Bethyl, 1:200), MKRN2 (Bethyl, 1:200), Vinculin (Abcam, 1:1000).

Chromatin immunoprecipitation (ChIP)

ChIP was performed as described in the Chapter 2 materials and methods, using antibodies to RNAPII (BioLegend, 8WG16), or IgG (Thermofisher).

Replicates

In this study, individual biological replicates are experiments performed separately on biologically distinct samples representing identical conditions and/or time points. For cell culture-based assays, this means that the cells are maintained in different flasks. Technical replicates are experiments performed on the same biological sample multiple times. See **Figure Legends** for the number of experimental replicates performed for each experiment. No outliers were encountered in this study. Criteria for the inclusion of data was based on the performance of positive and negative controls within each experiment.

Chapter 4: PABPC nuclear translocation is not sufficient to repress production of RNA polymerase II transcripts

Introduction

The mRNA decay-transcription feedback loop has been established during infection with gammaherpesviruses, and expression of herpesviral endonucleases. In these systems, host shutoff is initiated through cleavage of cytoplasmic mRNAs, leading to their degradation by the cellular exonucleases Xrn1 and Dis3L2. Exonuclease degradation of the 3'fragment by Xrn1 leads to liberation of bound cytoplasmic poly(A) binding protein (PABPC) from the poly(A) tail. The nuclear localization signal within the PABPC RNA recognition motifs becomes unmasked, directing PABPC nuclear localization through direct interaction with the nuclear import machinery. Ultimately, PABPC nuclear relocalization leads to repression of RNAPII promoter occupancy, through reduction in TBP binding. However, while it has been shown that accelerated cytoplasmic mRNA decay by other routes also leads to PABPC nuclear accumulation, transcriptional repression through other endonucleases has not been shown.

In addition, the role of Dis3L2 in the feedback loop remains an outstanding question in the field. It was shown previously that depletion of Dis3L2, similar to depletion of Xrn1, disrupts the feedback loop and restores RNAPII occupancy at promoters. However, since it appeared that PABPC nuclear translocation was the critical step connecting transcription and mRNA decay, it is unclear how Dis3L2 activity on the 5'fragment following muSOX cleavage would contribute to PABPC movement.

To address these questions, we compared accelerated mRNA decay by the diverse viral endonucleases and decapping enzymes SOX, muSOX, vhs, nsp1, and D10. We found that nascent transcript production is repressed similarly in all cases suggesting they follow the same pathway. Further experiments comparing muSOX and D10 find that Xrn1 P-body localization is disrupted, shedding light on how the extra turnover burden affects the main site of mRNA degradation. P-bodies are cytoplasmic ribonucleoprotein granules composed of mRNAs in complex with proteins involved with translational repression and mRNA decay (Beckham and Parker, 2008; Cougot et al., 2013; Eulalio et al., 2007; Hubstenberger et al., 2017; Luo et al., 2018; Parker and Sheth, 2007). It is hypothesized that P-bodies serve as sights of repressed mRNAs and mRNA decay enzymes that are not in immediate need by the cell. Similar to muSOX, D10 mediated mRNA turnover also drove PABPC nuclear translocation and required Xrn1 to repress transcription.

In contrast, we found that Dis3L2 was dispensable for D10 induced transcriptional repression, emphasizing that Dis3L2 is only required for degradation when a 5'fragment is created. Surprisingly, however, when we examined PABPC relocalization during muSOX expression in Dis3L2 knockdown cells, we found that PABPC translocation was maintained. This was the first example in which PABPC accumulated in the nucleus without RNAPII repression. Furthermore, we reveal that artificially driving PABPC into the nucleus is not sufficient to repress nascent mRNA production, despite being able repress RNAPII promoter occupancy.

Results

Accelerated mRNA decay by diverse viral endonucleases results in transcriptional repression.

mRNA decay induced by the herpesviral endonucleases SOX, muSOX, and vhs was previously shown to drive repression of RNAPII transcription (Abernathy et al., 2015). While SOX and muSOX are closely related endonucleases from gammaherpesviruses, vhs from the alphaherpesvirus HSV-1 is a non-homologous yet similarly broad acting cytoplasmic endonuclease. We further explored whether any source of mRNA decay is sufficient to drive transcriptional repression using unrelated viral factors. In addition to SOX, muSOX, and vhs, mRNA decay was initiated using the Nsp1 protein from SARS coronavirus and the mRNA decapping endonuclease D10 from vaccinia virus (**Figure 4.1**). Unlike the other viral factors, Nsp1 is not an endonuclease, yet it recruits an unknown cellular endonuclease to the 5' end of transcripts. Like SOX, muSOX, and vhs, accelerated mRNA decay using Nsp1 repressed nascent transcription of the two cellular *gapdh* and *actB* as measured by 4-thiouridine (4sU) incorporation (**Figure 4.1D**). Similarly, removal of mRNA 5' caps by the viral factor D10 also results in repression of nascent transcription (**Figure 4.1E**). These data suggest that this repression responds to accelerated mRNA decay in a manner that is not dependent on the mechanism by which it is initiated.

Accelerated mRNA decay disrupts Xrn1 localization in P-bodies.

To further explore the downstream consequences of enhanced cytoplasmic mRNA decay, we examined the localization of the major 5'-3' exonuclease Xrn1. Xrn1 is required for the full degradation of the cleaved mRNAs from each of these viral proteins (Burgess and Mohr, 2015; Gaglia et al., 2012), and is therefore a central component mediating the downstream transcriptional repression. We used immunofluorescence and confocal microscopy to monitor Xrn1 localization in cells expressing GFP-muSOX, or the host shutoff defective GFP-muSOX-R443I single point mutant (**Figure 4.2A**). In untransfected cells, Xrn1 localized to the cytoplasm in small punctae corresponding to the RNA-protein granules called P-bodies. Xrn1-stained P-bodies in untransfected cells, or cells expressing GFP-muSOX-R443I were more numerous than in cells expressing WT GFP-muSOX, where there was a reduction in these punctae. In addition, cells expressing D10 also had a reduction in the number of Xrn1-stained punctae, compared to vector transfected cells (**Figure 4.2B**). This disruption, therefore, is not dependent on the mechanism by which enhanced cytoplasmic mRNA decay is initiated, and it occurred with accelerated endonucleolytic cleavage of mRNAs by muSOX, or by decapping of mRNAs. Whether this disruption occurred by either specifically altering Xrn1 localization, or generally disrupting P-body structure, was unclear.

To distinguish between these two scenarios, we tested the localization of another P-body-associated factor, EDC4. EDC4, along with EDC3, promotes decapping complex formation and is known to localize to P-bodies. If P-body structure is disrupted, this factor would be dispersed in the cytoplasm. In cells transfected with empty vector, EDC4 colocalized with Xrn1 in the small cytoplasmic punctae, as expected (**Figure 4.3A**). Unlike Xrn1, however, EDC4 remained in these punctae in cells expressing GFP-muSOX, and was not disperse (**Figure 4.3B**). This would suggest that the overall structure of P-bodies remained intact during accelerated mRNA decay, and that it specifically caused disruption of Xrn1 localization.

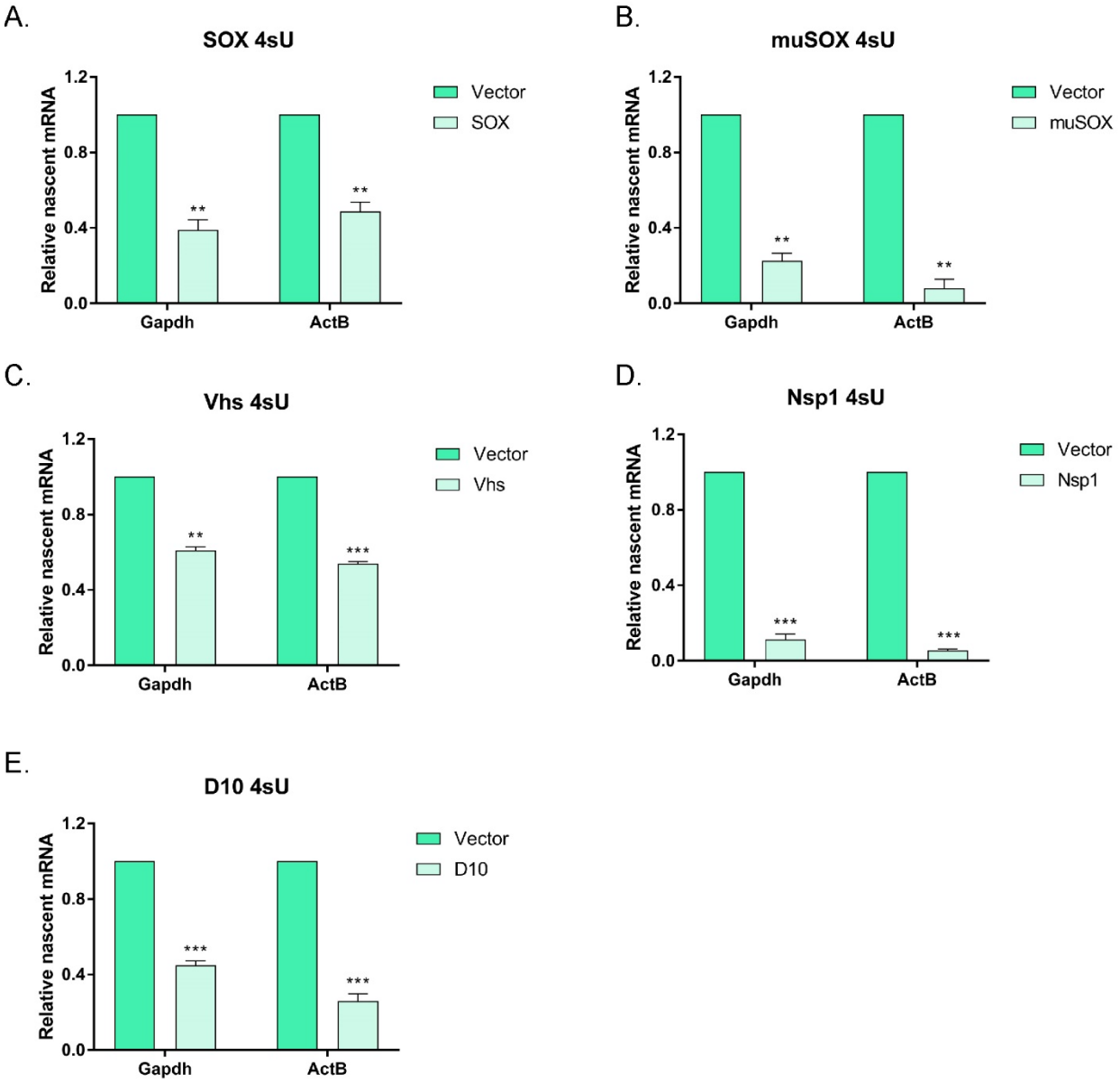

Figure 4.1. Accelerated mRNA decay by diverse viral endonucleases results in transcriptional repression. (A-E) 293T cells were transfected with empty vector or a plasmid expressing SOX (A) muSOX (B) Vhs (C) Nsp1 (D) or D10 (E), and nascent RNA was analyzed by 4-thiouridine (4sU) pulse labeling and purification, followed by quantification by RT-qPCR. All graphs display the mean with SEM of at least 2 biological replicates. Statistical significance was determined using Student's t test *p <0.05 **p <0.005 ***p <0.0005.

Transcriptional repression by mRNA decapping-induced mRNA decay requires Xrn1 catalytic activity, and results in PABPC nuclear translocation.

PABPC nuclear translocation is a result of Xrn1-mediated mRNA degradation during MHV68 infection, and/or muSOX expression, where it appears to be critical for repression of RNAPII promoter recruitment. Repression of RNAPII transcription also occurs during

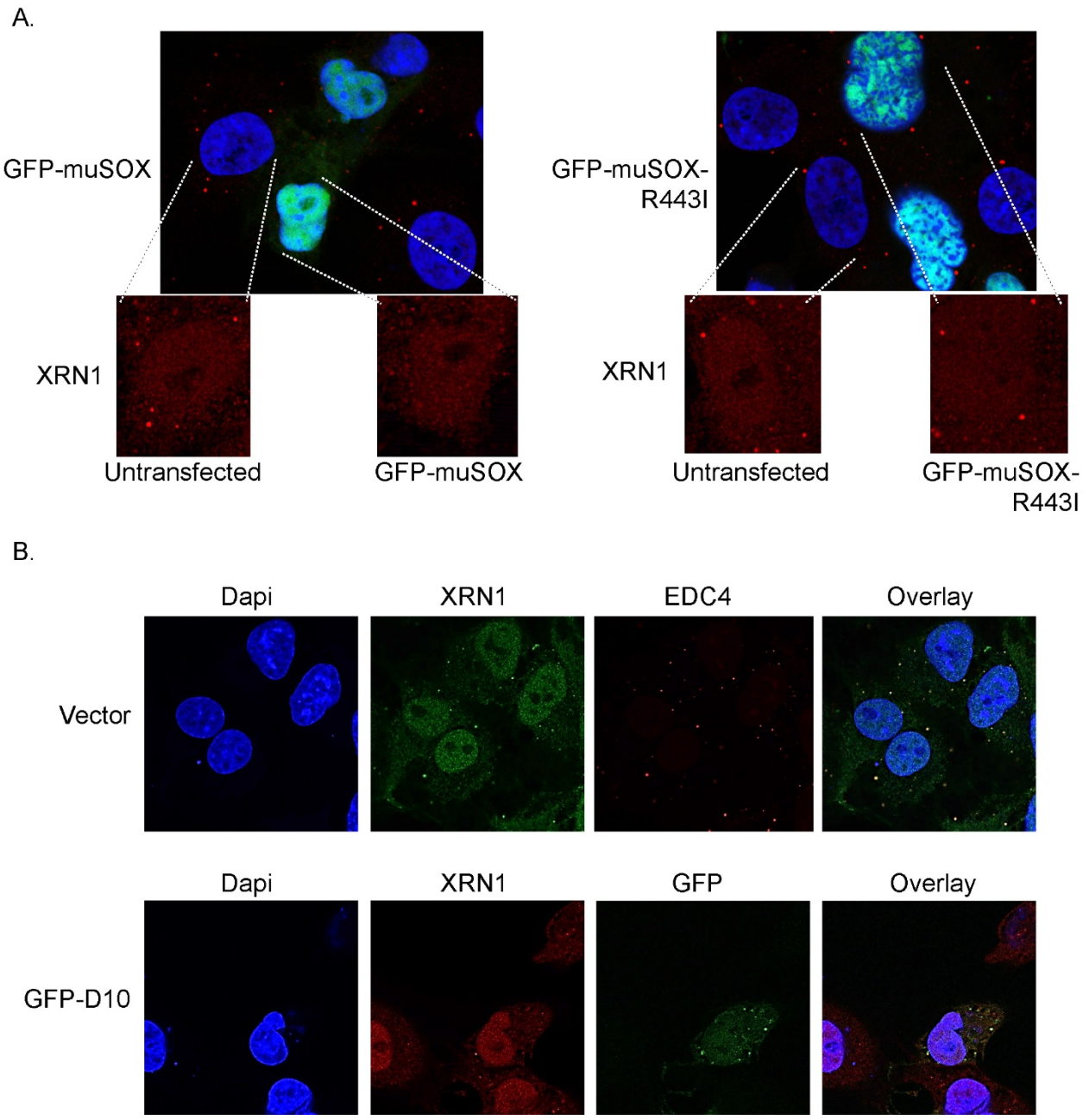

Figure 4.2. Accelerated mRNA decay disrupts Xrn1 localization in P-bodies. (A) Confocal microscopy of Cos-7 cells transfected with either GFP-muSOX (left panel) or the host shutoff defective GFP-muSOX-R443I point mutant (right panel) showing overlaid signals of DAPI (blue), Xrn1 (red), and GFP (green). Insets display zoomed-in Xrn1 signal for characteristic cells. (B) Confocal microscopy of Cos-7 cells transfected with empty vector (top panel) or GFP-D10 (bottom panel). Top panel shows signals for DAPI (blue), Xrn1 (green), EDC4 (red), and overlay. Bottom panel shows signals for DAPI (blue), Xrn1 (red), GFP (green), and overlay.

expression other viral endonucleases such as D10. We therefore explored whether PABPC translocated to the nucleus upon D10 expression. Indeed, PABPC as well as LARP4 are both enriched in the nucleus of cells expressing D10 (**Figure 4.4A**). This suggests that the repression

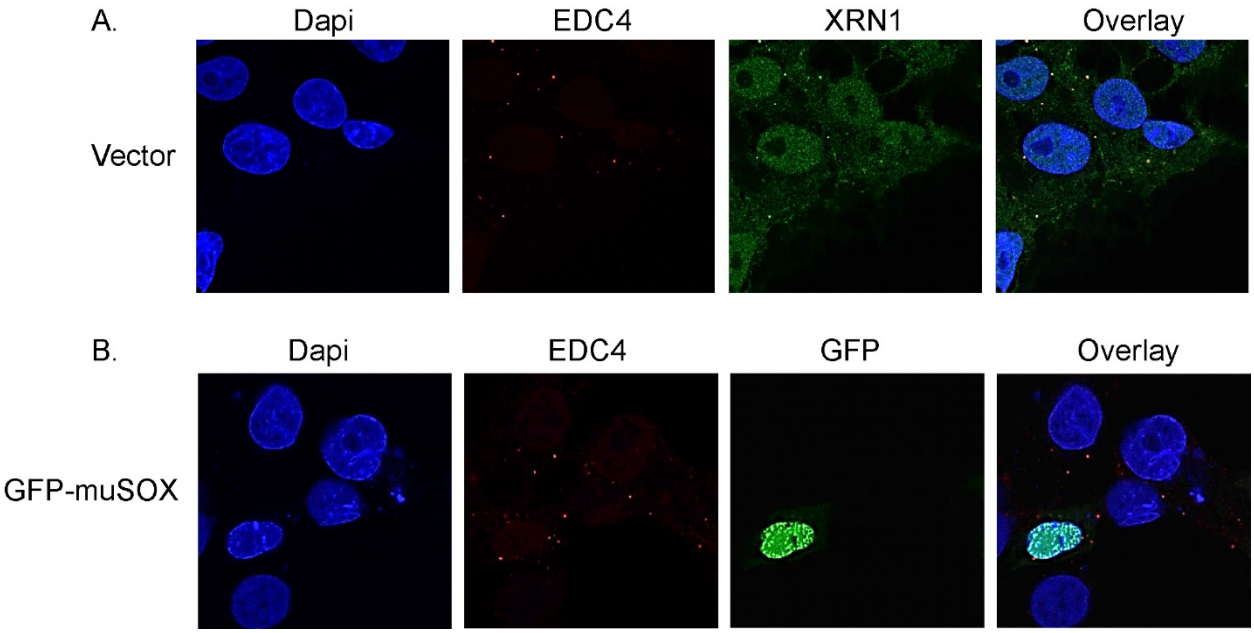

Figure 4.3. P-bodies remain stable during accelerated mRNA decay. (A) Confocal microscopy of Cos-7 cells transfected with empty vector, and showing signals for DAPI (blue), EDC4 (red), Xrn1 (green), and overlay. (B) Confocal microscopy of Cos-7 cells transfected with GFP-muSOX showing signals for DAPI (blue), EDC4 (red), GFP (green), and overlay.

of RNAPII as a result of accelerated mRNA decay is carried out through a similar PABPC-related mechanism. To address this, we used 293T cells with a doxycycline (dox)-inducible Xrn1-specific shRNA to deplete Xrn1 and monitor nascent mRNA production by 4sU. In cells expressing D10, there was a significant reduction in nascent transcription of *gapdh* and *actB* (**Figure 4.4B**). However, in cells depleted of Xrn1, nascent transcript levels were restored when D10 was expressed (**Figure 4.4B**). This suggests that indeed, Xrn1-mediated degradation of decapped mRNAs is required for downstream PABPC nuclear translocation and RNAPII repression. Alternately, when the 3'-5' exonuclease Dis3L2 was depleted from cells using a similar system, it was dispensable for D10-mediated transcriptional repression (**Figure 4.4C**). This result supports the fact that decapped mRNAs are not a substrate for Dis3L2, and its depletion would not affect Xrn1 activity and its ability to displace PABPC from poly(A) tails.

To further address whether Xrn1 exonucleolytic activity was required, and not some other function of Xrn1, we complemented Xrn1 knockout cells expressing D10, with either WT Xrn1 or Xrn1 truncated at the C-terminus (Xrn1dC). The C-terminal domain has previously been shown to be dispensable for exonuclease activity *in vitro* (Jinek et al., 2011). Xrn1 knockout cells expressing D10 did not have a reduction in nascent transcription as expected (**Figure 4.4D**). When D10-expressing Xrn1 knockout cells were complemented with a plasmid expressing either WT Xrn1, or Xrn1dC, transcriptional repression was restored (**Figure 4.4D**). Xrn1's catalytic activity has been shown to be disrupted by three different mutations to the catalytic active site, D208A, H41A, and R100/101A, all of which destroy its exonuclease activity (Jinek et al., 2011). When D10-expressing Xrn1 knockout cells were complemented with these Xrn1 catalytic mutants, all mutants failed to complement the Xrn1 knockout, and nascent transcription was not repressed (**Figure 4.4E**). This supports our model in which Xrn1 exonucleolytic degradation of decapped mRNAs, and not another function of Xrn1, is required for transcriptional repression.

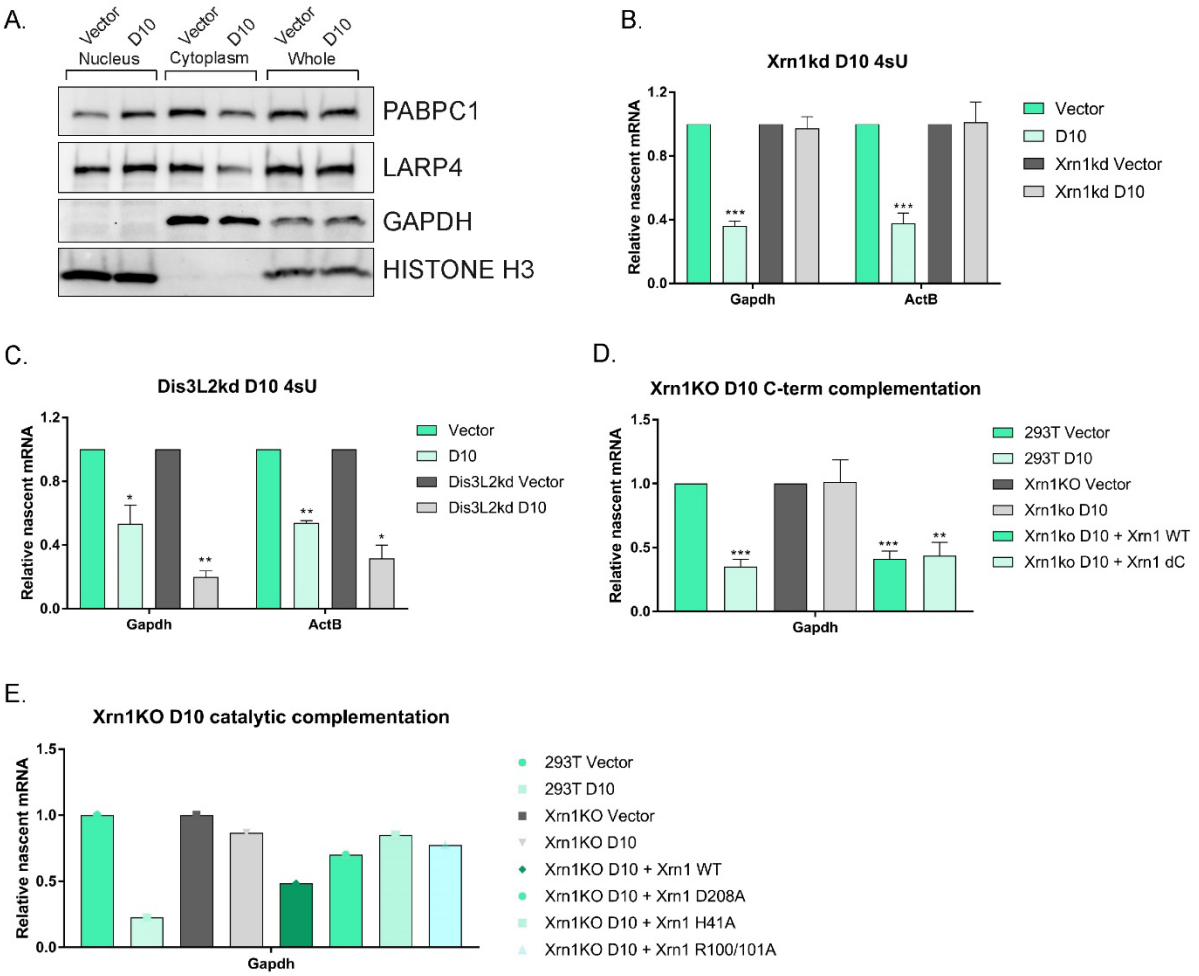

Figure 4.4. Transcriptional repression due to mRNA decapping-induced mRNA decay requires Xrn1 catalytic activity, and results in PABPC nuclear translocation. (A) Western blots of nuclear, cytoplasmic, and whole cell fractions from cells transfected with either empty vector or D10. GAPDH and HISTONE H3 serve as fractionation and loading controls. (B) 293T cells with a dox-inducible Xrn1-specific shRNA were transfected with empty vector or D10, and nascent RNA was analyzed by 4-thiouridine (4sU) pulse labeling and purification, followed by quantification by RT-qPCR. (C) Same as (B) but with a Dis3L2-specific shRNA. (D, E) WT or Xrn1 knockout (KO) cells were transfected with either empty vector, D10, or D10 complemented with the indicated Xrn1 plasmid. Nascent RNA was analyzed by 4-thiouridine (4sU) pulse labeling and purification, followed by quantification by RT-qPCR. All graphs display the mean with SEM of at least 3 biological replicates, with the exception of (E) which displays 1 replicate. Where possible, statistical significance was determined using Student's t test *p <0.05 **p <0.005 ***p <0.0005.

PABPC nuclear translocation alone is not sufficient to repress transcript production.

Dis3L2 is not involved in the degradation of decapped mRNAs and the above data confirm that it did not play a role in the downstream transcriptional responses, unlike during muSOX mediated mRNA decay. With muSOX, Dis3L2 has been shown previously to be required to repress RNAPII promoter recruitment. While Dis3L2 would indeed have a role in

degrading the 5' mRNA fragment following muSOX cleavage, it remained unclear how degradation of this fragment might influence the poly(A) binding state of PABPC or PABPC nuclear translocation. It is therefore unknown how Dis3L2 may affect RNAPII transcription. To address these questions, we analyzed PABPC localization using subcellular fractionation in muSOX-expressing cells depleted of Dis3L2 using a dox-inducible shRNA. Interestingly, depletion of Dis3L2 did not affect PABPC nuclear enrichment during muSOX expression (**Figure 4.5A**). This result isn't unexpected given the directionality of Dis3L2 activity. However, it suggests that nuclear translocation of PABPC may not be sufficient to repress RNAPII promoter recruitment. RNAPII promoter occupancy is restored in muSOX-expressing Dis3L2 knockdown cells, yet these results provide evidence that PABPC is enriched in the nucleus. This conflicts with our previous data showing that overexpression of PABPC alone, and its ensuing nuclear enrichment, is sufficient to repress RNAPII occupancy. One possibility is that overexpression of PABPC results in a higher level of nuclear enrichment than translocation of endogenous PABPC during accelerated mRNA decay. This 'over-abundance' of nuclear PABPC may overcome the absence of other factor(s), causing reduced RNAPII occupancy alone.

It was also unclear how nascent mRNA production was affected by an over-abundance of nuclear PABPC, during which promoter occupancy of RNAPII is reduced. To address this, we monitored nascent RNA production during PABPC transfection by 4sU. Surprisingly, PABPC expression, and its ensuing nuclear translocation, did not repress the levels of the *gapdh* or *actB* transcripts (**Figure 4.5B**). This suggests that despite the reduced RNAPII promoter occupancy, additional factor(s) may be required to disrupt the transcriptional output.

Discussion

Proteins that bind the 3'UTR of mRNAs, including PABPC, serve as indicators of cellular mRNA abundance and convey this information between subcellular compartments. These proteins translocate to the nucleus during accelerated cytoplasmic mRNA decay, and in the case of PABPC, serve to further restrict gene expression. In this work we show that accelerated cytoplasmic mRNA decay by diverse viral endonucleases and decapping enzymes drives transcriptional repression. We show with the decapping enzyme D10 from vaccinia virus that PABPC translocates to the nucleus where nascent mRNA synthesis by RNAPII is disrupted in an Xrn1-dependent manner. This is similar to the effects driven by herpesviral endonucleases and underscores the importance of mRNA turnover on cellular gene expression.

Xrn1 and other proteins involved in mRNA turnover are localized to cytoplasmic foci called P-bodies (Beckham and Parker, 2008; Eulalio et al., 2007; Luo et al., 2018; Parker and Sheth, 2007). P-bodies are nonmembraneous RNA-protein granules that regulate the availability of mRNAs for translation and repression, as well as serving to enclose the proteins involved in mRNA turnover. Many viruses have been shown to disrupt P-body structure during infection (Chahar et al., 2013; Dougherty et al., 2011; Pérez-Vilaró et al., 2015; Reineke and Lloyd, 2013). RNA viruses especially need to disrupt the mRNA turnover machinery within P-bodies in order to prevent degradation of the viral genome. Gammaherpesvirus host shutoff creates an abundance of mRNA fragments and it is unclear how this increase in mRNA turnover and use of cellular degradation machinery affects P-body structure and composition. Interestingly, we found that increased mRNA turnover by muSOX and the decapping enzyme D10 led to Xrn1 dispersal from P-bodies. However, not all components are dispersed and P-bodies appear to remain intact, as the decapping-related factor EDC4 remained localized to these foci. This suggests that

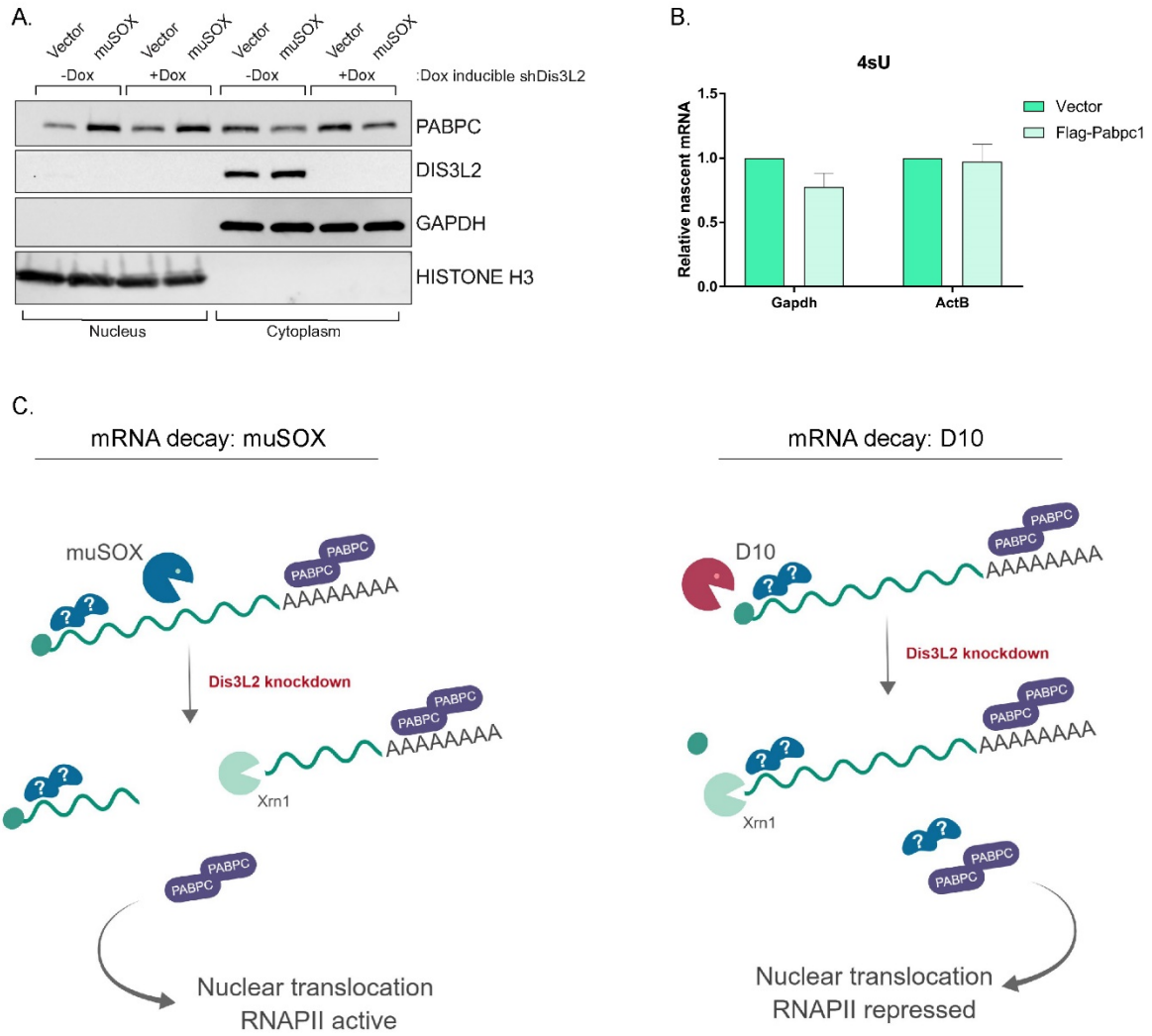

Figure 4.5. PABPC nuclear translocation alone is not sufficient to repress transcript production. (A) Western blots of nuclear and cytoplasmic fractions from 293T cells with a dox-inducible Dis3L2 specific shRNA that were transfected with either empty vector or muSOX. GAPDH and HISTONE H3 serve as fractionation and loading controls. (B) 293T cells were transfected with either empty vector or FLAG-PABPC1, and nascent RNA was analyzed by 4-thiouridine (4sU) pulse labeling and purification, followed by quantification by RT-qPCR. The graph displays the mean with SEM of 3 biological replicates, with no statistically significant differences observed. (C) Model summarizing the downstream effects of muSOX- versus D10-mediated mRNA decay in Dis3L2 knockdown cells. See text for details.

degradation of these mRNA fragments, which does not require decapping, specifically alters Xrn1 localization while maintaining other P-body factors within the structure.

We further analyzed the role of Dis3L2 in the feedback loop. Using the decapping enzyme D10, we found that Dis3L2 was dispensable for the ensuing repression of RNAPII mRNA synthesis, in contrast to muSOX where Dis3L2 is required. Removal of the 5'cap would

create a single fragment with an unprotected 5'end, which would be degraded by Xrn1 without the need for Dis3L2. Therefore, Dis3L2 activity is only required when a 5'fragment is created which needs degradation. However, the degradation of a 5'fragment does not affect PABPC nuclear translocation, because we found that PABPC shuttling was not disrupted in Dis3L2 knockdown cells with muSOX. At first, these data did not seem to support the fact that PABPC nuclear enrichment is sufficient to repress RNAPII promoter occupancy. However, in that experiment, when PABPC is artificially enriched in the nucleus, it is enriched at much higher levels than endogenous PABPC enrichment by mRNA decay (although not shown on the same blot, compare **Figures 2.4A** and **2.10A**). We hypothesized that these higher levels of nuclear PABPC may overwhelm the system, allowing it to appear sufficient to repress RNAPII. Yet under conditions of endogenous PABPC shuttling, other factor(s) may be required. This hypothesis is supported by the fact that artificial PABPC nuclear enrichment did not repress nascent mRNA synthesis by RNAPII, despite the repression of RNAPII promoter recruitment. Together these data support a model in which accelerated cytoplasmic mRNA decay and the ensuing translocation of PABPC and another unknown factor together are required to fully repress transcription by RNAPII (**Figure 4.5C**). The unknown factor presumably shuttles to the nucleus in a Dis3L2-dependent manner in muSOX-expressing cells and is therefore likely an RBP that binds the 5'end of mRNAs. Important future experiments will be needed to identify this factor.

Materials and Methods

Plasmids

Primers used for cloning are listed in Table 2.3. MHV68 muSOX was cloned into the Gateway entry vector pDON207 (Invitrogen), and then transferred into the Gateway-compatible peGFP-C1 destination vector to generate GFP-muSOX. Thy1.1-muSOX was generated by Infusion cloning (Clontech) of Thy1.1 (CD90.1) followed by a self-cleaving 2A peptide from foot-and-mouth disease virus in place of GFP into the Nhe1 and SacII restriction enzyme sites of GFP-muSOX. An ECORI site was added and used with BAMHI to remove muSOX and replace with either of the following viral endonucleases: SOX, muSOX, vhs, D10, and Nsp1. pCDEF3-Flag-PABPC1 was described previously (Kumar, 2010). GFP-D10 was kindly provided by the Mohr lab.

Cells and Transfections

HEK293T cells and Cos-7 cells, both from ATCC and obtained through the UC Berkeley Tissue Culture Facility, were maintained in DMEM (Invitrogen) supplemented with 10% fetal bovine serum. Cell lines were authenticated by STR analysis, and determined to be free of mycoplasma by PCR screening. DNA transfections were carried out in HEK293T cells at 70% confluency in 15cm plates with 25µg DNA using PolyJet (SignaGen) for 24h. Doxycycline-inducible shRNA HEK293T stable cells were described previously (Abernathy et al, 2015).

Pure populations of cells expressing SOX, muSOX, vhs, Nsp1, or D10 were generated using the Miltenyi Biotec MACS cell separation system. HEK293T cells were transfected with either Thy1.1-GFP, or a Thy1.1-expressing viral endonuclease, for 24h, whereupon cells were washed twice with PBS and cell pellets were resuspended in 95µl auto-MACS rinsing buffer supplemented with 0.5% FBS and incubated with 3µl anti-CD90.1 microbeads on ice for 10-15 min, and mixed by flicking the tube every 5 min. Cells were then magnetically separated

according to the manufacturer's instructions. Thy1.1 positive cells were used in all downstream experiments unless otherwise stated.

4-thiouridine (4sU) labeling

HEK293T cells transfected with the indicated plasmid, were pulsed with 500μM 4sU for 10 minutes prior to harvest. Total RNA was purified using TRIzol (Thermofisher) and quantified by nanodrop. 50μg total RNA was incubated with 5μg (50μl) of 100μg/ml MTSEA-biotin in DMF, 50ml 5X biotinylation buffer (50mM Hepes pH 7.5, 5mM EDTA), and RNase-free nanopore water to 250μl. An extra control sample was prepared using DMF without MTSEA-biotin. Samples were incubated with rotating at room temperature in the dark for 30 min, whereupon RNA was extracted using phenol/chloroform and resuspended in 100μl RNase-free nanopore water, whereupon RNA was heated to 65°C for 5 min, followed by incubation on ice for 5 min. To purify nascent RNA, samples were mixed with 50ml dynabeads MyOne streptactavidin-C1 (Thermofisher) beads for 2h in the dark at room temperature with rotation. Beads captured using a magnet and were washed prior to incubation 2X with 4sU wash buffer (100mM Tris pH 7.5, 10mM EDTA, 1M NaCl, 0.1% Tween-20) for 5 min at room temperature with rotation. Beads were washed 2X with 4sU wash buffer at 65°C, and 2X with room temperature 4sU wash buffer, whereupon nascent RNA was eluted using 100μl of freshly prepared 100mM DTT, incubated for 5 minutes at room temperature. The beads were discarded and RNA was isolated using ethanol precipitation and resuspended in 20μl RNase-free nanopore water. Nascent RNA was quantified by RT-qPCR using iTaq Universal SYBR Mastermix (BioRad) with either Gapdh primers (F- CAACGGATTTGGTCGTATTGG; R- GCAACAATATCCACTTTACCAGAGTTAA) or ActB primers (F- CATGTACGTTGCTATCCAGGC; R- CTCCTTAATGTCACGCACGAT), and normalized to 18S.

Subcellular Fractionation

HEK293T cells were fractionated using the REAP method (Nabbi and Riabowol, 2015). Briefly, cells were washed twice with ice-cold PBS and the cell pellet was lysed in 0.1% NP-40 PBS lysis buffer. The nuclei were then isolated by differential centrifugation at 10,000 x *g* for 10 sec and the supernatant retained as the cytoplasmic fraction. For western blotting, the nuclei were sonicated in 0.1% NP-40 PBS lysis buffer.

Western blotting

Nuclear, cytoplasmic, and whole cell lysates were quantified by Bradford assay and resolved by SDS-PAGE and western blotted with antibodies against PABPC (Cell Signaling, 1:1000), LARP4 (Thermo Fisher, 1:1000), Gapdh (Abcam, 1:3000), Histone H3 (Cell Signaling, 1:2000), Dis3L2 (Novus, 1:500).

Immunofluorescence assays

Cells were plated on coverslips coated with 100ug/mL poly-L-lysine and transfected at 70% confluency with either GFP, GFP-muSOX, or GFP-D10 for 24h. Transfected cells were fixed in 4% formaldehyde, permeabilized with ice-cold methanol, and incubated with blocking buffer [1% Triton X-100, 0.5% Tween-20, 3% Bovine Serum Albumin] prior to incubation with rabbit polyclonal Xrn1 diluted 1:200 (Sigma, SAB42000-28) or rabbit polyclonal EDC4 diluted 1:200 (Santa Cruz Biotechnologies, sc-374211) in blocking buffer at 4°C overnight, followed by incubation with Alexa Fluor 594-conjugated goat anti-rabbit secondary antibody (Thermo Fisher, 1:1000) and DAPI (Pierce, 1:1000). Coverslips were

mounted on slides using Vectashield hard-set mounting medium (VectorLabs) and imaged by confocal microscopy on a Zeiss LSM 710 AxioObserver microscope.

Replicates

In this study, individual biological replicates are experiments performed separately on biologically distinct samples representing identical conditions and/or time points. For cell culture-based assays, this means that the cells are maintained in different flasks. Technical replicates are experiments performed on the same biological sample multiple times. See **Figure Legends** for the number of experimental replicates performed for each experiment. No outliers were encountered in this study. Criteria for the inclusion of data was based on the performance of positive and negative controls within each experiment.

Chapter 5: Perspectives and concluding remarks

In this work we present and characterize the nature of the signal connecting mRNA decay and transcription in mammalian cells. We find that large changes in mRNA abundance, driven by herpesviral endonucleases, is conveyed between the cytoplasm and nucleus through the nuclear translocation of RNA binding proteins, especially those that bind the 3'end of mRNAs. Specifically, we find that when PABPC accumulates in the nucleus, it restricts gene expression by repressing transcription of RNAPII genes, in addition to its known role in blocking nascent mRNA export. Interactions between PABPC and two E3 ubiquitin ligases appears to direct the repression of RNAPII. In addition, we reveal that RNAPII is repressed due to a decrease in TBP promoter occupancy. TBP serves as the critical first step in RNAPII pre-initiation complex formation, and a reduction in this step would explain the defect in RNAPII transcription. This is the first description of this pathway in any system, uncovering how these physically separated events are connected.

RNA binding proteins as indicators of cytoplasmic mRNA abundance

mRNA abundance has been shown to be broadly altered in response to a number of cellular stresses, including bacterial infection, viral infection, and early apoptosis (Abernathy and Glaunsinger, 2015; Barry et al., 2017; Thomas et al., 2015). Proteins that bind the poly(A) tail are ideal indicators of mRNA abundance due to the universal presence of the poly(A) tail on mRNAs. As such, it is not surprising that PABPC has arisen as critical in the mRNA decay-transcription feedback pathway. The presence of a hidden NLS within the PABPC RNA recognition motif (RRM) ensures that its subcellular localization is coupled to its poly(A) binding state. Release from poly(A) tails by events such as accelerated mRNA depletion guarantees nuclear accumulation through exposure of the previously masked NLS. Once in the nucleus, we found that PABPC is a critical factor for repression of RNAPII. Overexpression of PABPC causes it to translocate to the nucleus as well, a tool we used throughout this work. In this system, expression of PABPC beyond endogenous levels leads to exposure of the NLS of the excess, unbound PABPC and corresponding nuclear translocation. This system was useful to analyze the result of PABPC nuclear accumulation alone without accelerated mRNA decay. We found that surprisingly, while nuclear PABPC enrichment alone is sufficient to repress RNAPII promoter recruitment, it was not enough to repress nascent mRNA synthesis. While it remains unclear how reduced promoter-bound RNAPII does not lead to reduced overall transcriptional

output in this system, it suggests that another unknown factor is required to repress transcription in totality.

It is possible that this factor is contained within the TMT-MS/MS data, but was missed in the analysis. For example, we found that Dis3L2 knockdown restores RNAPII transcription during muSOX expression, yet in this system, Dis3L2 knockdown does not alter PABPC nuclear accumulation. If the role of Dis3L2 during muSOX expression is to degrade the 5'fragment, then it may be that the missing factor would bind mRNAs at the 5'end. Since our proteomics experiment compared WT and Xrn1 knockout cells with muSOX, this factor would not be captured. However, the factor may be hidden within the data if it in fact shuttles to the nucleus during muSOX expression and is not dependent on Xrn1. With that in mind, a few possible candidates arise, displaying similar nuclear accumulation in WT and Xrn1 knockout cells with muSOX: ATXN2, PTBP3, PUM2, and MBNL1 are all RBPs that display this pattern. ATXN2 is particularly interesting as it also appears in the infection TMT-MS/MS and is known to bind PABPC. It is interesting to speculate that ATXN2 and PABPC could interact through the mRNA closed-loop, and that upon endonucleolytic cleavage, this interaction is disrupted and ATXN2 is left at the 5'end. Future experiments will be needed to confirm or deny this model.

Similarities and differences with the yeast mRNA decay-transcription feedback loop

An mRNA-transcription feedback loop has also been discovered in yeast, suggesting that connections such as this between different stages of gene expression serve an essential function in eukaryotic cells (Haimovich et al., 2013; Sun et al., 2013). However, the connection between mRNA decay and transcription in yeast operates differently than it does in mammalian cells. Overall mRNA abundance is 'buffered' to maintain steady-state transcript levels. Decreases in transcription rates are compensated by comparable adjustments to global mRNA degradation, and vice versa. While the details of this pathway have not yet been described, Xrn1 was found to be a critical factor. Xrn1 is also critical for the mammalian feedback loop, however that remains the only known similarity between these systems. It is likely that RBPs such as poly(A) binding proteins may be involved in the yeast pathway as well, as these factors are ideal indicators of mRNA abundance information. Future experiments, such as the ones performed in this work, are needed to shed light on the pathway in yeast. Until then, it is interesting to imagine why these systems operate differently. For example, why is it that yeast cells increase transcription in the face of widespread mRNA loss? In contrast, why do mammalian cells continue the shutdown of gene expression without attempting to repopulate cytoplasmic mRNAs? We hypothesize that there was an evolutionary divergence in which unicellular eukaryotes buffer their overall gene expression for continued maintenance of the organism. On the other hand, multicellular eukaryotes like mammals have established global mRNA decay (which is induced by numerous pathogens) as a stress signal, and the ensuing response is thus geared towards shutdown of major cellular programs.

Chapter 6: References

Abernathy, E., and Glaunsinger, B. (2015). Emerging roles for RNA degradation in viral replication and antiviral defense. Virology *479–480*, 600–608.

Abernathy, E., Clyde, K., Yeasmin, R., Krug, L.T., Burlingame, A., Coscoy, L., and Glaunsinger, B. (2014). Gammaherpesviral Gene Expression and Virion Composition Are Broadly Controlled by Accelerated mRNA Degradation. PLoS Pathogens *10*, e1003882.

Abernathy, E., Gilbertson, S., Alla, R., and Glaunsinger, B. (2015). Viral Nucleases Induce an mRNA Degradation-Transcription Feedback Loop in Mammalian Cells. Cell Host & Microbe *18*, 243–253.

Ablasser, A., Bauernfeind, F., Hartmann, G., Latz, E., Fitzgerald, K.A., and Hornung, V. (2009). RIG-I-dependent sensing of poly(dA:dT) through the induction of an RNA polymerase III-transcribed RNA intermediate. Nature Immunology *10*, 1065–1072.

Bablanian, R., Goswami, S.K., M, M., Banerjee, A.K., and Merrick, W.C. (1991). Mechanism of selective translation of vaccinia virus mRNAs: differential role of poly (A) and initiation factors in the translation of viral and cellular mRNAs. Journal of Virology *65*.

Barry, K.C., Ingolia, N.T., and Vance, R.E. (2017). Global analysis of gene expression reveals mRNA superinduction is required for the inducible immune response to a bacterial pathogen. ELife *6*.

Beckham, C.J., and Parker, R. (2008). P Bodies, Stress Granules, and Viral Life Cycles. Cell Host & Microbe *3*, 206–212.

Beltran, P.M., Mathias, R.A., and Cristea, I.M. (2016). A Portrait of the Human Organelle Proteome In Space and Time during Cytomegalovirus Infection. Cell Systems *3*, 361-373.e6.

Beltran, P.M., Federspiel, J.D., Sheng, X., and Cristea, I.M. (2017). Proteomics and integrative omic approaches for understanding host-pathogen interactions and infectious diseases. Molecular Systems Biology *13*, 922.

Borah, S., Nichols, L.A., Hassman, L.M., Kedes, D.H., and Steitz, J.A. (2012). Tracking expression and subcellular localization of RNA and protein species using high-throughput single cell imaging flow cytometry. RNA *18*, 1573–1579.

Braun, K.A., and Young, E.T. (2014). Coupling mRNA Synthesis and Decay. Molecular and Cellular Biology *34*, 4078–4087.

Braun, J.E., Huntzinger, E., Fauser, M., and Izaurralde, E. (2011). GW182 proteins directly recruit cytoplasmic deadenylase complexes to miRNA targets. Molecular Cell *44*, 120–133.

Burgess, H.M., and Gray, N.K. (2010). mRNA-specific regulation of translation by poly(A)-binding proteins. Biochemical Society Transactions *38*, 1517–1522.

Burgess, H.M., and Mohr, I. (2015). Cellular 5'-3' mRNA exonuclease Xrn1 controls double-stranded RNA accumulation and anti-viral responses. Cell Host & Microbe *17*, 332–344.

Chahar, H.S., Chen, S., and Manjunath, N. (2013). P-body components LSM1, GW182, DDX3, DDX6 and XRN1 are recruited to WNV replication sites and positively regulate viral replication. Virology *436*, 1–7.

Chapman, E.G., Costantino, D.A., Rabe, J.L., Moon, S.L., Wilusz, J., Nix, J.C., and Kieft, J.S. (2014). The structural basis of pathogenic subgenomic flavivirus RNA (sfRNA) production. Science (New York, N.Y.) *344*, 307–310.

Chen, C.-Y.A., and Shyu, A.-B.B. (2011). Mechanisms of deadenylation-dependent decay. Wiley Interdisciplinary Reviews. RNA *2*, 167–183.

Chiu, Y.-H.H., Macmillan, J.B., and Chen, Z.J. (2009). RNA polymerase III detects cytosolic DNA and induces type I interferons through the RIG-I pathway. Cell *138*, 576–591.

Cougot, N., Molza, A.-E., Giudice, E., Cavalier, A., Thomas, D., and Gillet, R. (2013). Structural organization of the polysomes adjacent to mammalian processing bodies (P-bodies). RNA Biology *10*, 314–320.

Covarrubias, S., Richner, J.M., Clyde, K., Lee, Y.J., and Glaunsinger, B.A. (2009). Host Shutoff Is a Conserved Phenotype of Gammaherpesvirus Infection and Is Orchestrated Exclusively from the Cytoplasm. Journal of Virology *83*, 9554–9566.

Covarrubias, S., Gaglia, M.M., Kumar, G., Wong, W., Jackson, A.O., and Glaunsinger, B.A. (2011). Coordinated destruction of cellular messages in translation complexes by the gammaherpesvirus host shutoff factor and the mammalian exonuclease Xrn1. PLoS Pathogens *7*, e1002339.

Darzacq, X., Shav-Tal, Y., de Turris, V., Brody, Y., enoy, S., Phair, R.D., and Singer, R.H. (2007). In vivo dynamics of RNA polymerase II transcription. Nature Structural & Molecular Biology *14*, 796–806.

Dougherty, J.D., White, J.P., and Lloyd, R.E. (2011). Poliovirus-mediated disruption of cytoplasmic processing bodies. Journal of Virology *85*, 64–75.

Eulalio, A., Behm-Ansmant, I., and Izaurralde, E. (2007). P bodies: at the crossroads of post-transcriptional pathways. Nature Reviews Molecular Cell Biology *8*, 9–22.

Feng, P., Everly, D.N., and Read, G. (2005). mRNA decay during herpes simplex virus (HSV) infections: protein-protein interactions involving the HSV virion host shutoff protein and translation factors eIF4H and eIF4A. Journal of Virology *79*, 9651–9664.

Gaglia, M.M., and Glaunsinger, B.A. (2010). Viruses and the cellular RNA decay machinery. Wiley Interdisciplinary Reviews. RNA *1*, 47–59.

Gaglia, M.M., Covarrubias, S., Wong, W., and Glaunsinger, B.A. (2012). A common strategy for host RNA degradation by divergent viruses. Journal of Virology *86*, 9527–9530.

Gaglia, M.M., Rycroft, C.H., and Glaunsinger, B.A. (2015). Transcriptome-Wide Cleavage Site Mapping on Cellular mRNAs Reveals Features Underlying Sequence-Specific Cleavage by the Viral Ribonuclease SOX. PLoS Pathogens *11*, e1005305.

Gerstberger, S., Hafner, M., and Tuschl, T. (2014). A census of human RNA-binding proteins. Nature Reviews Genetics *15*, 829–845.

Gilbertson, S., Federspiel, J.D., Hartenian, E., Cristea, I.M., and Glaunsinger, B. (2018). Changes in mRNA abundance drive shuttling of RNA binding proteins, linking cytoplasmic RNA degradation to transcription. ELife *7*.

Haimovich, G., Medina, D.A., Causse, S.Z., Garber, M., Millán-Zambrano, G., Barkai, O., Chávez, S., Pérez-Ortín, J.E., Darzacq, X., and Choder, M. (2013). Gene Expression Is Circular: Factors for mRNA Degradation Also Foster mRNA Synthesis. Cell *153*, 1000–1011.

Harb, M., Becker, M.M., Vitour, D., Baron, C.H., Vende, P., Brown, S.C., Bolte, S., Arold, S.T., and Poncet, D. (2008). Nuclear Localization of Cytoplasmic Poly(A)-Binding Protein upon Rotavirus Infection Involves the Interaction of NSP3 with eIF4G and RoXaN. Journal of Virology *82*, 11283–11293.

Heidemann, M., Hintermair, C., Voß, K., and Eick, D. (2013). Dynamic phosphorylation patterns of RNA polymerase II CTD during transcription. Biochimica et Biophysica Acta *1829*, 55–62.

Huang, C., Lokugamage, K.G., Rozovics, J.M., Narayanan, K., Semler, B.L., and Makino, S. (2011). SARS coronavirus nsp1 protein induces template-dependent endonucleolytic cleavage of mRNAs: viral mRNAs are resistant to nsp1-induced RNA cleavage. PLoS Pathogens *7*, e1002433.

Hubstenberger, A., Courel, M., Bénard, M., Souquere, S., Ernoult-Lange, M., Chouaib, R., Yi, Z., Morlot, J.-B., Munier, A., Fradet, M., et al. (2017). P-Body Purification Reveals the Condensation of Repressed mRNA Regulons. Molecular Cell *68*, 144-157.e5.

Kawahara, H., Imai, T., Imataka, H., Tsujimoto, M., Matsumoto, K., and Okano, H. (2008). Neural RNA-binding protein Musashi1 inhibits translation initiation by competing with eIF4G for PABP. The Journal of Cell Biology *181*, 639–653.

Khaperskyy, D.A., Emara, M.M., Johnston, B.P., Anderson, P., Hatchette, T.F., and McCormick, C. (2014). Influenza a virus host shutoff disables antiviral stress-induced translation arrest. PLoS Pathog. 10, e1004217.

Khaperskyy, D.A., Schmaling, S., Larkins-Ford, J., McCormick, C., and Gaglia, M.M. (2016). Selective Degradation of Host RNA Polymerase II Transcripts by Influenza A Virus PA-X Host Shutoff Protein. Plos Pathog *12*, e1005427.

Koo, C.X., Kobiyama, K., Shen, Y.J., LeBert, N., Ahmad, S., Khatoo, M., Aoshi, T., Gasser, S.,

and Ishii, K.J. (2015). RNA polymerase III regulates cytosolic RNA:DNA hybrids and intracellular microRNA expression. The Journal of Biological Chemistry *290*, 7463–7473.

Kumar, R.G., and Glaunsinger, B.A. (2010). Nuclear Import of Cytoplasmic Poly(A) Binding Protein Restricts Gene Expression via Hyperadenylation and Nuclear Retention of mRNA. Molecular and Cellular Biology *30*, 4996–5008.

Kumar, R.G., Shum, L., and Glaunsinger, B.A. (2011). Importin α-Mediated Nuclear Import of Cytoplasmic Poly(A) Binding Protein Occurs as a Direct Consequence of Cytoplasmic mRNA Depletion. Molecular and Cellular Biology *31*, 3113–3125.

Łabno, A., Tomecki, R., and Dziembowski, A. (2016). Cytoplasmic RNA decay pathways - Enzymes and mechanisms. Biochimica et Biophysica Acta *1863*, 3125–3147.

Larimer, F., and Stevens, A. (1990). Disruption of the gene XRN1, coding for a 5'----3' exoribonuclease, restricts yeast cell growth. Gene *95*, 85–90.

Lee, Y.J., and Glaunsinger, B.A. (2009). Aberrant Herpesvirus-Induced Polyadenylation Correlates With Cellular Messenger RNA Destruction. PLoS Biology *7*, e1000107.

Louder, R.K., He, Y., López-Blanco, J.R., Fang, J., Chacón, P., and Nogales, E. (2016). Structure of promoter-bound TFIID and model of human pre-initiation complex assembly. Nature *531*, 604–609.

Lubas, M., Damgaard, C.K., Tomecki, R., Cysewski, D., Jensen, T., and Dziembowski, A. (2013). Exonuclease hDIS3L2 specifies an exosome-independent 3′-5′ degradation pathway of human cytoplasmic mRNA. The EMBO Journal *32*, 1855–1868.

Luo, Y., Na, Z., and Slavoff, S.A. (2018). P-Bodies: Composition, Properties, and Functions. Biochemistry *57*, 2424–2431.

Lykke-Andersen, S., Chen, Y., Ardal, B.R., Lilje, B., Waage, J., Sandelin, A., and Jensen, T. (2014). Human nonsense-mediated RNA decay initiates widely by endonucleolysis and targets snoRNA host genes. Gene Dev *28*, 2498–2517.

Marceau, C.D., Puschnik, A.S., Majzoub, K., Ooi, Y.S., Brewer, S.M., Fuchs, G., Swaminathan, K., Mata, M.A., Elias, J.E., Sarnow, P., et al. (2016). Genetic dissection of Flaviviridae host factors through genome-scale CRISPR screens. Nature *535*, 159–163.

Mattijssen, S., Arimbasseri, A.G., Iben, J.R., Gaidamakov, S., Lee, J., Hafner, M., and Maraia, R.J. (2017). LARP4 mRNA codon-tRNA match contributes to LARP4 activity for ribosomal protein mRNA poly(A) tail length protection. Elife *6*, e28889.

McAlister, G.C., Huttlin, E.L., Haas, W., Ting, L., Jedrychowski, M.P., Rogers, J.C., Kuhn, K., Pike, I., Grothe, R.A., Blethrow, J.D., et al. (2012). Increasing the Multiplexing Capacity of

TMTs Using Reporter Ion Isotopologues with Isobaric Masses. Analytical Chemistry *84*, 7469–7478.

Mendez, A.S., Vogt, C., Bohne, J., and Glaunsinger, B.A. (2018). Site specific target binding controls RNA cleavage efficiency by the Kaposi's sarcoma-associated herpesvirus endonuclease SOX. Nucleic Acids Res

Miroci, H., Schob, C., Kindler, S., Ölschläger-Schütt, J., Fehr, S., Jungenitz, T., Schwarzacher, S.W., Bagni, C., and Mohr, E. (2012). Makorin Ring Zinc Finger Protein 1 (MKRN1), a Novel Poly(A)-binding Protein-interacting Protein, Stimulates Translation in Nerve Cells. J Biol Chem *287*, 1322–1334.

Mitchell, S.F., and Parker, R. (2014). Principles and properties of eukaryotic mRNPs. Molecular Cell *54*, 547–558.

Moon, S.L., Anderson, J.R., Kumagai, Y., Wilusz, C.J., Akira, S., Khromykh, A.A., and Wilusz, J. (2012). A noncoding RNA produced by arthropod-borne flaviviruses inhibits the cellular exoribonuclease XRN1 and alters host mRNA stability. RNA *18*, 2029–2040.

Müller-McNicoll, M., and Neugebauer, K.M. (2013). How cells get the message: dynamic assembly and function of mRNA–protein complexes. Nature Reviews Genetics *14*, nrg3434.

Neto, O.P., Standart, N., and Sa, C. (1995). Autoregulation of poly (A)-binding protein synthesis in vitro. Nucleic Acids Research *23*, 2198–2205.

Ogunjimi, B., Zhang, S.-Y.Y., Sørensen, K.B., Skipper, K.A., Carter-Timofte, M., Kerner, G., Luecke, S., Prabakaran, T., Cai, Y., Meester, J., et al. (2017). Inborn errors in RNA polymerase III underlie severe varicella zoster virus infections. The Journal of Clinical Investigation *127*, 3543–3556.

Omwancha, J., Zhou, X.-F., Chen, S.-Y., Baslan, T., Fisher, C.J., Zheng, Z., Cai, C., and Shemshedini, L. (2006). Makorin RING Finger Protein 1 (MKRN1) Has Negative and Positive Effects on RNA Polymerase II-Dependent Transcription. Endocrine *29*, 363–374.

Page, H.G., and Read, G. (2010). The virion host shutoff endonuclease (UL41) of herpes simplex virus interacts with the cellular cap-binding complex eIF4F. Journal of Virology *84*, 6886–6890.

Park, R., El-Guindy, A., Heston, L., Lin, S.-F., Yu, K.-P., Nagy, M., Borah, S., Delecluse, H.-J., Steitz, J., and Miller, G. (2014). Nuclear Translocation and Regulation of Intranuclear Distribution of Cytoplasmic Poly(A)-Binding Protein Are Distinct Processes Mediated by Two Epstein Barr Virus Proteins. PLoS ONE *9*, e92593.

Parker, R., and Sheth, U. (2007). P Bodies and the Control of mRNA Translation and Degradation. Molecular Cell *25*, 635–646.

Parrish, S., and Moss, B. (2007). Characterization of a second vaccinia virus mRNA-decapping

enzyme conserved in poxviruses. Journal of Virology *81*, 12973–12978.

Parrish, S., Resch, W., and Moss, B. (2007). Vaccinia virus D10 protein has mRNA decapping activity, providing a mechanism for control of host and viral gene expression. Proceedings of the National Academy of Sciences of the United States of America *104*, 2139–2144.

Pérez-Vilaró, G., Fernández-Carrillo, C., Mensa, L., Miquel, R., Sanjuan, X., Forns, X., Pérez-del-Pulgar, S., and Díez, J. (2015). Hepatitis C virus infection inhibits P-body granule formation in human livers. Journal of Hepatology *62*, 785–790.

Piron, M., Vende, P., Cohen, J., and Poncet, D. (1998). Rotavirus RNA-binding protein NSP3 interacts with eIF4GI and evicts the poly(A) binding protein from eIF4F. The EMBO Journal *17*, 5811–5821.

Puschnik, A.S., Marceau, C.D., Ooi, Y.S., Majzoub, K., Rinis, N., Contessa, J.N., and Carette, J.E. (2017). A Small-Molecule Oligosaccharyltransferase Inhibitor with Pan-flaviviral Activity. Cell Reports *21*, 3032–3039.

Reineke, L.C., and Lloyd, R.E. (2013). Diversion of stress granules and P-bodies during viral infection. Virology *436*, 255–267.

Reuter, M.L., Meinel, D.M., and Sträßer, K. (2015). The poly(A)-binding protein Nab2 functions in RNA polymerase III transcription. Genes & Development *29*, 1565–1575.

Richner, J.M., Clyde, K., Pezda, A.C., Cheng, B., Wang, T., Kumar, R.G., Covarrubias, S., Coscoy, L., and Glaunsinger, B. (2011). Global mRNA Degradation during Lytic Gammaherpesvirus Infection Contributes to Establishment of Viral Latency. PLoS Pathogens *7*, e1002150.

Rivas, H., Schmaling, S., and Gaglia, M. (2016). Shutoff of host gene expression in influenza A virus and herpesviruses: similar mechanisms and common themes. Viruses.

Salaun, C., MacDonald, A., Larralde, O., Howard, L., Lochtie, K., Burgess, H., Brook, M., Malik, P., Gray, N., and Graham, S. (2010). Poly(A)-binding protein 1 partially relocalizes to the nucleus during herpes simplex virus type 1 infection in an ICP27-independent manner and does not inhibit virus replication. Journal of Virology *84*, 8539–8548.

Schoenberg, D.R., and Maquat, L.E. (2012). Regulation of cytoplasmic mRNA decay. Nature Reviews Genetics *13*, 246–259.

Shoemaker, C.J., and Green, R. (2012). Translation drives mRNA quality control. Nature Structural & Molecular Biology *19*, 594–601.

Singh, G., Pratt, G., Yeo, G.W., and Moore, M.J. (2015). The Clothes Make the mRNA: Past and Present Trends in mRNP Fashion. Annual Review of Biochemistry *84*, 325–354.

Stubbs, M.T., and Wahle, E. (2014). Deadenylation-a piece of PANcake. The EMBO Journal *33*, 1503–1505.

Sun, M., Schwalb, B., Pirkl, N., Maier, K.C., Schenk, A., Failmezger, H., Tresch, A., and Cramer, P. (2013). Global Analysis of Eukaryotic mRNA Degradation Reveals Xrn1-Dependent Buffering of Transcript Levels. Molecular Cell *52*, 52–62.

Sutherland, J.M., Sobinoff, A.P., Fraser, B.A., Redgrove, K.A., Davidson, T.-L., Siddall, N.A., Koopman, P., Hime, G.R., and McLaughlin, E.A. (2015). RNA binding protein Musashi-1 directly targets Msi2 and Erh during early testis germ cell development and interacts with IPO5 upon translocation to the nucleus. The FASEB Journal *29*, 2759–2768.

Teo, G., Liu, G., Zhang, J., Nesvizhskii, A.I., Gingras, A.-C., and Choi, H. (2014). SAINTexpress: Improvements and additional features in Significance Analysis of INTeractome software. J Proteomics *100*, 37–43.

Thomas, M.P., Liu, X., Whangbo, J., McCrossan, G., Sanborn, K.B., Basar, E., Walch, M., and Lieberman, J. (2015). Apoptosis Triggers Specific, Rapid, and Global mRNA Decay with 3' Uridylated Intermediates Degraded by DIS3L2. Cell Reports *11*, 1079–1089.

Wolf, J., and Passmore, L.A. (2014). mRNA deadenylation by Pan2–Pan3. Biochemical Society Transactions *42*, 184–187.

Wu, J., and Bag, J. (1998). Negative Control of the Poly(A)-binding Protein mRNA Translation Is Mediated by the Adenine-rich Region of Its 5′-Untranslated Region. Journal of Biological Chemistry *273*, 34535–34542.

Yang, R., Gaidamakov, S.A., Xie, J., Lee, J., Martino, L., Kozlov, G., Crawford, A.K., Russo, A.N., Conte, M.R., Gehring, K., et al. (2011). La-related protein 4 binds poly(A), interacts with the poly(A)-binding protein MLLE domain via a variant PAM2w motif, and can promote mRNA stability. Molecular and Cellular Biology *31*, 542–556.